PRODUCTION OF ORBITAL (EYE) IMPLANT FROM HYDROXYAPATITE

by

Buğra Bayraktar

B.S. in Metallurgy and Materials Science Eng.,
Yıldız Teknik University, 2002

Submitted to the Institute of Biomedical Engineering
in partial fulfillment of the requirements
for the degree of
Master of Science
in

Biomedical Engineering

Boğaziçi University
June, 2006

ACKNOWLEDGEMENTS

I would like to express my sincere gratitude to my thesis supervisor Prof. Dr. Sabri ALTINTAŞ for his suggestions and guidance broadening my horizon. I believe that his point of view will help me through my life.

I would like to thank Dr. Gürsel Turgut for his guidance which encouraged us to be interested in this thessis subject.

I am so much indebted to Necati Güleç for his help throughout this study.

I would also like to thank Önder Albayrak, Nazım Mahmutyazıcıoğlu, Mehmet İpekoğlu from Department of Mechanical Engineering, the staff of Türkiye Atom Enerjisi Institution, Prof. Dr. Hamza Yılmaz from Ankara University, Bülent Bostan from Gazi University and the staff of TOFAŞ (Bursa) for their help.

Finally and most importantly, I would like to thank my parents, my brother and my little sister for their support, help and tolerance through this study.

ABSTRACT

PRODUCTION OF ORBITAL IMPLANT FROM HYDROXYAPATITE

When an eye was lost due to trauma or in the events that require to remove eye globe from the orbit, spherically shaped orbital implants were used in order to fill the cavity, to protect the area from infection and to preserve the structure of orbit. In recent years, hydroxyapatite has gained wide acceptance as an orbital implant material due to its biocompatibility and its porous structure allowing tissue ingrowth.

In this study, it is intended to manufacture porous orbital implant by a novel and simple process. The amount of porosity and pore size of implant is tried to be controlled through varying amount of naphthalene addition. Here, it is proposed to make the implants light in weight as well as suitable for rapid vascularization after implantation. Characterization of the implants with respect to phase purity was performed by X-ray diffraction (XRD) and Infra-red spectrometer (IR) so as to compare this characteristic of the final product to that of starting material. Based on these investigations, no sign of decomposition phases, impurities and the trace of naphthalene were detected in the sintered samples. The pore morphology and pore size distribution of the samples were investigated by scanning electron microscope (SEM) and the results were compared with respect to variables. Besides, weight, bulk density, rate of contraction and porosity of implants were measured. As a mechanical test, compressive strength of the specimens prepared for this purpose was investigated. All results were evaluated and compared to each other.

As far as the mechanical strength, weight, pore size distribution in terms of micro macropores and interconnectivity concerned, the best results were achieved from %45 naphthalene added implant specimen.

Keywords: Hydroxyapatite, porous implant, orbital implant, eye implant

ÖZET

HİDROKSİLAPATİTTEN ORBİTAL İMPLANT ÜRETİMİ

Göz kayıplarında yada göz küresinin orbitten (göz çukuru) çıkarılmasını gerektiren durumlarda bu boşluğu doldurmak, enfeksiyon riskinden korumak ve orbit yapısını koruyabilmek için küre biçiminde orbital implantlar kullanılmaktadır. Son zamanlarda hidroksilapatit (HAp), biyouyumluluğu ve doku iç büyümesine olanak veren yapısı nedeniyle orbital implant malzemesi olarak büyük kabul gördü.

Bu çalışmada HAp tozundan, yeni ve basit bir metotla poroz orbital implant üretilmeye çalışıldı. İmplantın porozite (gözenek) miktarı ve gözenek büyüklükleri farklı miktarda naftalin eklentisi ile kontrol edilmeye çalışıldı. Burada amaç implantın daha hafif olması ve doku iç büyümesine olanak vermesini sağlamaktı. X ışını kırınımı (XRD) ve kızılötesi (IR) spektrum analizi vasıtasıyla sinterleme işlemi öncesi ve sonrası faz ve bileşim değişimi karakterize edildi. Bu analizlere gore, sinterlenmiş numunelerde bozunum fazları, empürite ve naftalin kalıntısına rastlanmadı. Gözenek morfolojisi ve gözenek dağılımı tarama elektron mikroskobu (SEM) vasıtasıyla incelendi ve eklentilere bağlı olarak karşılaştırıldı. Ayrıca implantların ağırlık, yoğunluk, büzülme miktarı ve porozite ölçümleri yapıldı. Mekanik test olarak, hazırlanan numunelerin basma dayanımları ölçüldü. Tüm sonuçlar değerlendirildi ve karşılaştırıldı.

Mekanik dayanım, ağırlık, gözenek morfolojisi, gözeneklerin dağılımı ve gözenekler arası bağlantı dikkate alındığında en iyi sonuçlar %45 naftalin katkılı numuneden elde edildi.

Anahtar Sözcükler: Hidroksilapatit, poroz implant, orbital implant, göz implantı

TABLE OF CONTENTS

LIST OF FIGURES

LIST OF TABLES

1. INTRODUCTION

When an eye is removed, orbital implant (ocular implant) is used to replace the area in the orbit (bony cavity) that was occupied by the eye. This small, spherical implant maintains the natural structure of the orbit and provides support for the artificial eye. The implant itself is not visible however.

The ocular losses are embarrassing to the bearer becouse they commit the face which has the essential organs for the human relationship. The orbital implant fills in the ocular cavity simulating the facial growth and restoring its symmetry. Therefore, there are aesthetics anatomic and physiological improvement on the patient's face that allows him to be reinstated in society without being discriminated for his/her differences. With the help of implant the patient will be able to protect the area from infection and in a lot of cases it will help him psychologically. At the same time, it could be easier for the patient to be reinstated in the society.

An artificial eye (ocular prosthesis) is used to restore the natural appearance of the eye and surrounding tissues, and is the visible part of the surgical changes to the socket, artificial eyes are usually made of plastic or glass. Custom artificial eyes are handcrafted by highly skilled ocularists to precisely match the look of the natural eye.

While artificial eyes have been made for thousands of years, the first orbital implants were developed about 100 years ago. These small spheres of glass or gold were later replaced by acrylic or silicone spheres; but until recently, the basic design of these "first-generation" implants had changed little over the years.

The mineral part of bone and teeth is made of crystalline form of calcium phosphate similar to hydroxyapatite. Hydroxyapatite is known to be the most important bioceramic materials for its unique bioactivity and stability.

The modern age of integrated orbital implants began in 1989 when an implant made from hydroxyapatite received Food and Drug Administration approval [34]. The porous nature of this material allows fibrovascular ingrowth throughout the implant and permits insertion of a coupling device without the inflammation or infection associated with earlier types of nonintegrated implants. In a secondary procedure, an externalized, round-headed peg or screw is inserted into the implant. The prosthesis is modified to accommodate the peg, creating a ball-and-socket joint.

Porous polyethylene enucleation implants have been used since at least 1989. Polyethylene also becomes vascularized, allowing placement of a titanium motility post that joins the implant to the prosthesis in the same way that the peg is used for hydroxyapatite implants. The potential benefits of porous implants include improved prosthetic motility and a lower incidence of implant migration and extrusion. Porous enucleation implants currently are fabricated from a variety of materials including natural and synthetic hydroxyapatite, aluminum oxide, and polyethylene. Hydroxyapatite implants are spherical and made in a variety of sizes.

In recent years, among porous ocular implants, hydroxyapatite (HA) implants are widely accepted for reconstruction of the anopthalmic socket after enucleation and evisceration surgery [36].

2. CONCEPT AND DEFINITION OF BIOCOMPATIBILITY

Any material incorporated into a human organism has to comply with certain properties that will assure that there are no negative interactions with living tissue. Biomaterials by definition are inorganic compounds that are designed to replace a part or a function of the human body in a safe, reliable, economic, and physiologically and aesthetically acceptable manner [1].

Biocompatibility refers to the ability of a material to perform with an appropriate host response, in a specific application [2]. Hence biocompatibility is neither a single event nor a single phenomenon but is meant to be a collection of processes involving different but interdependent interaction mechanisms between material and living tissue. In increasing order of biocompatibility the interaction of biomaterials with living tissue can be defined as follows.

When a synthetic material is placed within the human body, tissue reacts towards the implant in a variety of ways depending on the material type. The mechanism of tissue interaction (if any) depends on the tissue response to the implant surface. In general, there are three terms in which a biomaterial may be described in or classified into representing the tissues responses. These are bioinert, bioresorbable, and bioactive [3].

Incompatible materials are materials that release to the body substances in toxic concentrations and/or trigger the formation of antigens that may cause immune reactions ranging from simple allergies to inflammation to septic rejection with the associated severe health consequences.

Biocompatible materials, in contrast, are those that also release substances but in non-toxic concentrations that may lead to only benign tissue reactions such as formation of a fibrous connective tissue capsule or weak immune reactions that cause formation of giant cells or phagocytes. These materials are often called **biotolerant** and include austenitic stainless steels or bone cement consisting of polymethylmethacrylate (PMMA).

Bioinert materials do not release any toxic constituents but also do not show positive interaction with living tissue. The term bioinert refers to any material that once placed in the human body has minimal interaction with its surrounding tissue; examples of these are stainless steel, titanium, alumina, partially stabilized zirconia, and ultra high molecular weight polyethylene. Generally a fibrous capsule might form around bioinert implants hence its biofunctionality relies on tissue integration through the implant [3].

Bioactive materials show a positive interaction with living tissue that includes also differentiation of immature cells towards bone cells. In contrast to bioinert materials there is chemical bonding to the bone along the interface, thought to be triggered by the adsorption of bone growth-mediating proteins at the biomaterials surface. Hence there will be a biochemically-mediated strong formation of bone. In addition to compressive forces, to some degree tensile and shear forces can also be transmitted through the interface ("bony ingrowth"). Typical bioactive materials are calcium phosphates and bioglasses, see Table 2.1. It is believed that bioactivity of calcium phosphates is associated with the formation of carbonate hydroxyapatite (CHA), similar to bone-like apatite [4].

Bioactive refers to a material, which upon being placed within the human body interacts with the surrounding bone and in some cases, even soft tissue. This occurs through a time dependent kinetic modification of the surface, triggered by their implantation within the living bone. An ion exchange reaction between the bioactive implant and surrounding body fluids results in the formation of a biologically active carbonate apatite (CHA) layer on the implant that is chemically and crystallographically equivalent to the mineral phase in bone. Prime examples of these materials are synthetic hydroxyapatite [$Ca_{10}(PO_4)_6(OH)_2$], glass ceramics and bioglass [3].

Bioresorbable materials Bioresorbable refers to a material that upon placement within the human body starts to dissolve (resorbed) and slowly replaced by advancing tissue (such as bone). Common examples of bioresorbable materials are tricalcium phosphate [$Ca_3(PO_4)_2$] and polylactic polyglycolic acid copolymers. Calcium oxide, calcium carbonate and gypsum are other common materials that have been utilized during the last three decades.

Table 2.1 Examples of biomaterials and their applications [5]

Material	Application	Biological behaviour
Stainless (austenitic) steel	Osteosynthesis (bone screws)	biotolerant
Bone cement (PMMA)	Fixation of implants	biotolerant
cp-titanium	Acetabular cups	bioinert
Ti6Al4V alloy	Shafts for hip implants, tibia	bioinert
CoCrMo alloy	Femoral balls and shafts, knee implants	bioinert (?)
Alumina	Femoral balls, inserts of acetabular cups	bioinert
Zirconia (Y-TZP)	Femoral balls	bioinert
HD-polyethylene	Articulation components	bioinert
Carbon (graphite)	Heart valve components	bioinert
CFRP	Inserts of acetabular cups	bioinert
Hydroxyapatite	Bone cavity fillings, coatings, ear implants, vertebrae replacement	bioactive
Tricalcium phosphate	Bone replacement	bioactive
Tetracalcium phosphate	Dental cement	bioactive
Bioglass	Bone replacement	bioactive

3. BIOCERAMICS

3.1 About Bioceramics

A biomaterial can be defined as "a material intended to interface with biological systems to evaluate, treat, augment, or replace any tissue, organ, or function of the body" [6]. There are three classes of biomaterial: metals, polymers and ceramics.

Bioceramics have become a diverse class of biomaterials presently including three basic types: bioinert high strength ceramics, bioactive ceramics which form direct chemical bonds with bone or even with soft tissue of a living organism; various bioresorbable ceramics that actively participate in the metabolic processes of an organism with the predictable results [7]. Alumina (Al_2O_3), Zirconia (ZrO_2) and carbon are termed bioinert. Bioglass and glass ceramics are bioactive.

Inert bioceramics, such as $A1_2O_3$ and ZrO_2 have inherently low levels of reactivity compared to other materials such as polymers and metals as well as surface reactive or resorbable ceramics (Figure.3.1) [8].

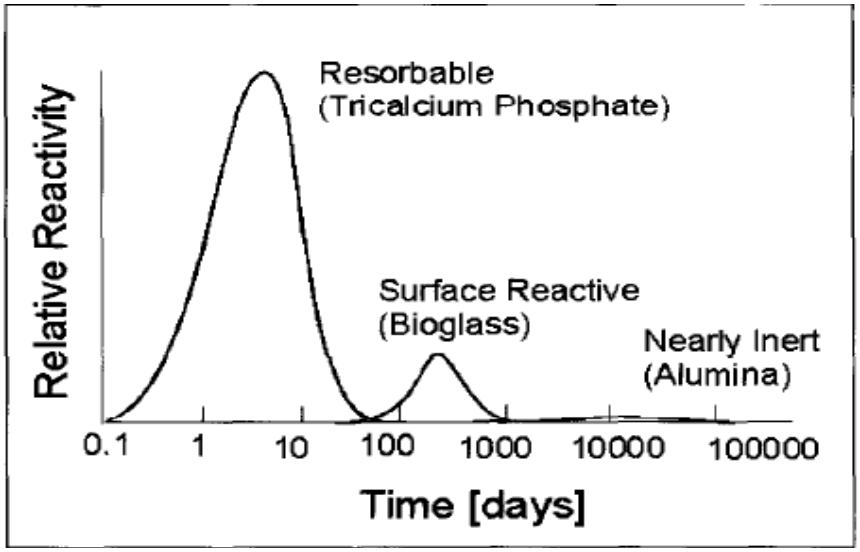

Figure 3.1 Three subgroups of bioceramics used in medical applications and classified by their reactivity Alumina and zirconia belong to the most inert materials used in medicine [8].

Calcium phosphate ceramics are categorized as bioresorbable. Bioceramics became an accepted group of materials for medical applications, mainly for implants in orthopedics, maxillofacial surgery and for dental implants. Table 3.1 elicits the biomedical applications of bioceramics [10].

Table 3.1: Biomedical Applications of Bioceramics [10]

Devices	Function	Biomaterial
Artificial total hip, knee, shoulder, elbow, wrist	Reconstruct arthritic or fractured joints	High-density alumina, metal bioglass coatings
Bone plates, screws, wires	Repair fractures	Bioglass-metal fiber composite, Polysulfone-carbon fiber composite
Intramedullary nails	Align fractures	Bioglass-metal fiber composite, Polysulfone-carbon fiber composite
Harrington rods	Correct chronic spinal curvature	Bioglass-metal fiber composite, Polysulfone-carbon fiber composite
Permanently implanted artificial limbs	Replace missing extremities	Bioglass-metal fiber composite, Polysulfone-carbon fiber composite
Vertebrae Spacers and extensors	Correct congenital deformity	Al_2O_3
Spinal fusion	Immobilize vertebrae to protect spinal cord	Bioglass
Alveolar bone replacements, mandibular reconstruction	Restore the alveolar ridge to improve denture fit	Polytetra fluro ethylene (PTFE) - carbon composite, Porous Al_2O_3, Bioglass, dense-apatite
End osseous tooth replacement implants	Replace diseased, damaged or loosened teeth	Al_2O_3, Bioglass, dense hydroxyapatite, vitreous carbon
Orthodontic anchors	Provide posts for stress application required to change deformities	Bioglass-coated Al_2O_3, Bioglass coated vitallium

3.2 Alumina (Al_2O_3)

Since 1975 alumina ceramic has proven its bioinertness. An alumina ceramic has characteristics of high hardness and high abrasion resistance. The reasons for the excellent wear and friction behavior of Al_2O_3 are associated with the surface energy and surface smoothness of this ceramic [9]. There is only one thermodynamically stable phase, i.e. Al_2O_3 that has a hexagonal structure with aluminum ions at the octahedral interstitial sites. The characteristic features of alumina are depicted in Table

3.2 [10]. Abrasion resistance, strength and chemical inertness of alumina have made it to be recognized as a ceramic for dental and bone implants.

Table 3.2 Properties of clinically utilized alumina ceramics [10].

Properties	**Aluminia**	**Aluminia ISO 6474**	**Aluminia new Iso norm**
Density [g/cm^3]	3.98	>3.90	>3.94
Al_2O_3 [%]	>99.7	>99.5	
SiO_2+Na_2O [%]	<0.02	<0.1	
SiO_2+Na_2O+CaO [%]			<0.1
Average grain size [µm]	3.6	<7	<4.5
Vickers hardness [HV0.1]	2400	>2000	
E modulus [GPa]	380-420	.	.
Compressive strength [GPa]	4-5		
Tensile strength [MPa]	350		
Flexural strength [MPa]	400-560	>400	>450
Fracture toughness [MN m$^{-3/2}$]	4-6		

3.3 Zirconia (ZrO_2)

Zirconia is a biomaterial that has a bright future because of its high mechanical strength and fracture toughness. Zirconia ceramics have several advantages over other ceramic materials due to the transformation toughening mechanisms operating in their microstructure that can be manifested in components made out of them. The research on the use of zirconia ceramics as biomaterials started about twenty years ago and now zirconia is in clinical use in total hip replacement (THR) but developments are in progress for application in other medical devices. Today's main application of zirconia ceramics is in THR ball heads [10].

3.4 Bioglass & Glass Ceramic

Bioglasses are interesting versatile class of materials and structurally all silica-based glasses have the same basic building block $SiO44^-$. Glasses of various compositions can be obtained and they show very different properties. Bioglasses have also found a place in prosthetics. These bioglasses are embedded in a biomaterial support to form prosthetics for hard tissues. Such prosthetics are biocompatible, show excellent mechanical properties and are useful for orthopedic and dental prosthetics [10].

Bioactive glass ceramic materials were the first to actively interact with tissues and induce their intrinsic repair and regenerative potential which involves control over the cell cycle, molecular frame work that controls cell proliferation and differentiation. Depending upon the rate of resorption and release of ions they can create chemical gradients with specific biological actions over cells and tissues [11]. Glass ceramics for use as a biomaterial comprises CaO-34.6-54.6, SiO_2-24.2-44.8, P_2O_5-0-8.0, CaF_2-0.1-1.0 and MgO-1.0-10.0 weight percentage and the composition has a primary crystal phase and a secondary apatite crystal phase. The glass ceramic has superior mechanical properties, good biocompatibility, bioactivity and no toxicity making it useful as a biomaterial in artificial bone and dental implants [12].

3.5 Calcium Phosphate Ceramics

Calcium phosphate biomaterials are polycrystalline ceramics deriving from individual crystals of a highly oxidized substance that have been fused together. The two most important are tricalcium phosphate $Ca_3(PO_4)_2$, or ß-whitlockite, and hydroxyapatite $Ca_{10}(PO_4)_6(OH)_2$. Both materials are known to be biocompatible and osteoconductive and to bond directly to bone. The main difference between these two materials is that tricalcium phosphate (TCP) degrades much faster than HAp. The chemical structure of calcium ceramics resembles that of bone [12].

Calcium phosphate can be crystallized into salts, hydroxyapatite and ß-whitlockite depending on the Ca/P ratio, presence of water, impurities, and temperature (Figure 3.2). In wet environment and at lower temperature (<900 °C) it is more likely that the (hydroxyl or hydroxy) apatite will form, whereas in a dry atmosphere and higher temperature the ß-whitlockite will be formed [13].

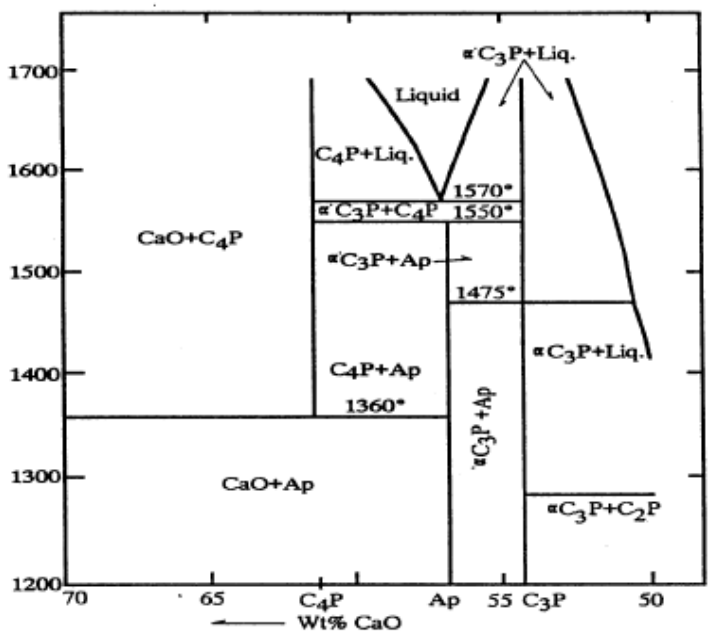

Figure 3.2 Phase diagram of the quasi-binary system $CaO-P_2O_5-H_2O$ at a water partial pressure of 65.5 kPa [4]

It has been known for more than twenty years that ceramics made of calcium phosphate salts can be used successfully for replacing and augmenting bone tissue. The most widely used calcium phosphate based bioceramics are hydroxyapatite (HAp) and β-tricalcium phosphate (β-TCP) [10]. β-tricalcium phosphate (β-TCP) is represented by the chemical formula $Ca_3(PO4)_2$, the Ca/P ratio being 1.5. β-TCP shows an X ray pattern consistent with a pure hexagonal crystal structure, although the related α-TCP is monoclinic. Single-phase TCP powders have also been synthesized successfully by many researchers. β-TCP turns into α-TCP around 1200°C; the latter phase is considered to be stable in the range 700 to 1200°C. β-TCP is highly soluble in body fluid. HAp is formed on exposed surfaces of TCP by the following reaction.

$$4Ca_3(PO4)_2(s) + 2H_2O \rightarrow Ca_{10}(PO4)_6(OH)_2(surface) + Ca^{2+} + 2HPO_4^{2-}$$

Thus, the solubility of a TCP surface approaches the solubility of HAp and decreases the pH of the solution, which further increases the solubility of TCP and enhances resorption. Many studies have indicated that the dissolution of HAp in the human body after implantation is too low to achieve the optimal results. On the other hand, the dissolution rate of β-TCP ceramic is too fast for bone bonding. To achieve an optimum resorbability of the material, studies have mainly focused on the biphasic calcium phosphate ceramics composed of HAp and TCP. Several results suggest that the resorbability of biphasic ceramics is largely determined by the HAp/TCP ratio [14].

The most important properties of calcium phosphate biomaterials are their bioresorption and bioactivity. These phenomena are essentially dynamic and strongly depend on biological parameters. When calcium phosphate biomaterials are put in contact with living tissues, several interactions occur. As HAp and TCP have a lower solubility product than the calcium phosphate ionic product of body fluids, they induce the formation on their surface, a calcium phosphate apatite from ions present in the fluids. The first stage is the interaction with collagen and later accumulation of proteins and cells on the surface of the material followed by resorption of the material and bone formation. The composition of the crystals themselves is an important factor and there is generally a relationship between the resorption of biomaterials and their solubility. Tricalcium phosphate for instance is more easily resorbed than stoichiometric apatites [15].

3.5.1 Hyroxyapatite & Properties

The mineral part of bone and teeth is made of crystalline form of calcium phosphate similar to hydroxyapatite ($Ca_{10}(PO4)_6(OH)_2$). The apatite family of minerals, $A_{10}(BO_4)_6X_2$, crystallizes into hexagonal rhombic prisms and has a unit cell dimension a=9.432 A° and c=6.881 A. The atomic structure of hydroxyapatite projected down the c axis onto basal plane is given in Figure 3.3 [13].

The ideal Ca/P ratio of HAp is 10:6 and calculated density is 3.219 g/cm^3. It is interesting to note that the substitution of OH^- with F will give greater chemical stability due to closer coordination of F (symmetric shape) as compared to hydroxyl (nonsymmetric, two atoms) by nearest calcium. This is one of the reasons for better caries resistance of teeth following fluoridation [13].

Hydroxyapatite is the most important bioceramic materials for its unique bioactivity and stability. Naturally occurring and mostly available hydroxyapatite is hexagonal in structure with the chemical formula of one unit cell being $Ca_{10}(PO_4)_6(OH)_2$. Some of the calcium phosphate materials include, in order of solubility [16].

Tetracalcium Phosphate ($Ca_4P_2O_9$) > Amorphous calcium Phosphate > alpha-Tricalcium Phosphate ($Ca_3(PO_4)_2$) > beta- Tricalcium Phosphate ($Ca_3(PO_4)_2$) >> Hydroxyapatite ($Ca_{10}(PO_4)_6(OH)_2$).

Unlike the other calcium phosphates, hydroxyapatite does not break down under physiological conditions. In fact, it is thermodynamically stable at physiological pH and actively takes part in bone bonding, forming strong chemical bonds with surrounding bone. This property has been exploited for rapid bone repair after major trauma or surgery. While its mechanical properties have been found to be unsuitable for load-bearing applications such as orthopedics, it is used as a coating on load bearing implant materials such as titanium and titanium alloys or composites with other materials [15].

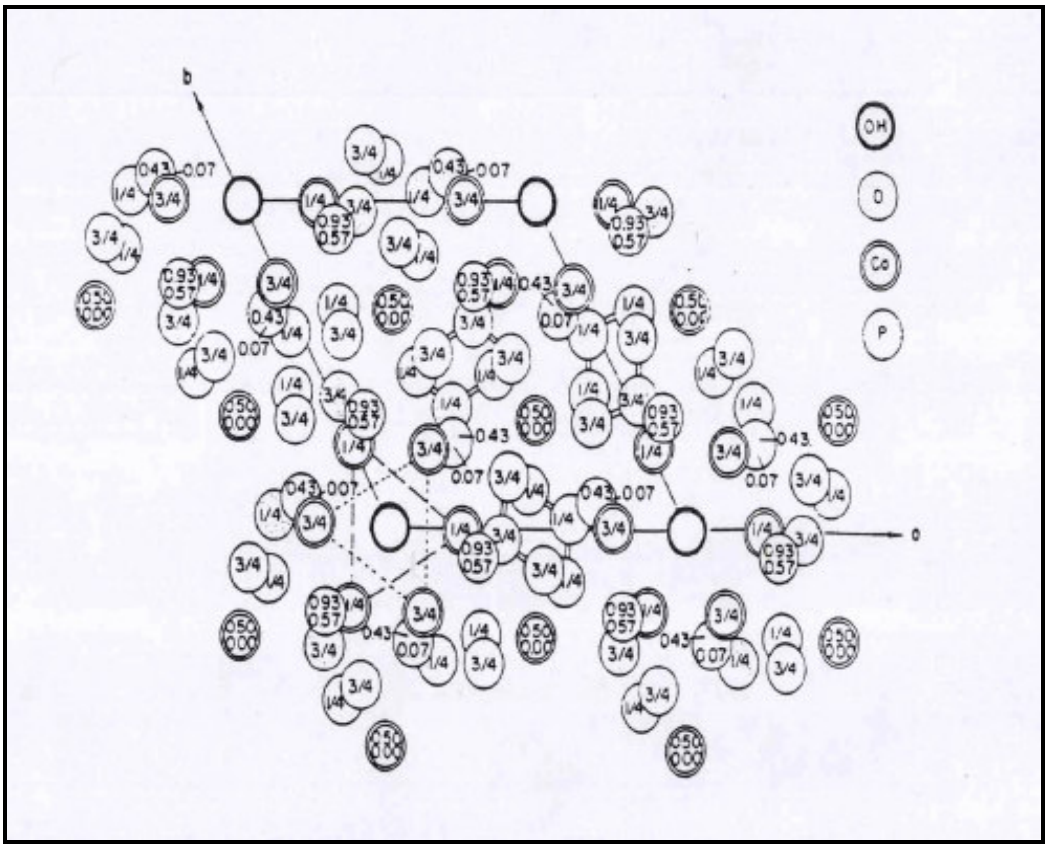

Figure 3.3 The atomic structure of hydroxyapatite projected down the c axis onto basal plane [13]

3.5.1.1 Coral derived HA & Calcium Carbonate Ceramics Calcium carbonate ($CaCO_3$) resembles hydroxyapatite in many respects. The material is biocompatible and osteoconductive but, like HAp, has no osteoinductive properties. The main difference to HAp is the resorption rate. Resorption seems to be clinically unimportant with HAp, but animal experiments have shown resorption rates of only a few weeks, when CC is used.

Coralline apatites can be derived from the sea coral. Coral is composed of calcium carbonate in the form of aragonite. Coral is a naturally occurring structure and has optimal strength and structural characteristics. The pore structure of coralline calcium phosphate produced by certain species is similar to human cancellous bone, making it a suitable material for bone graft applications (Figure 3.4) [3]. Choice of the appropriate species therefore enables a desired and constant implant structure to be achieved.

The porosity of the coral skeleton is around 50% and the mean size of the pore is 150μm, the pores are interconnecting with each other. Coral and converted coralline hydroxyapatite have been used as bone grafts and orbital implants since the 1980s, as the porous nature of the structure allows in-growth of blood vessels to supply blood for bone, which eventually infiltrates the implant [17,18].

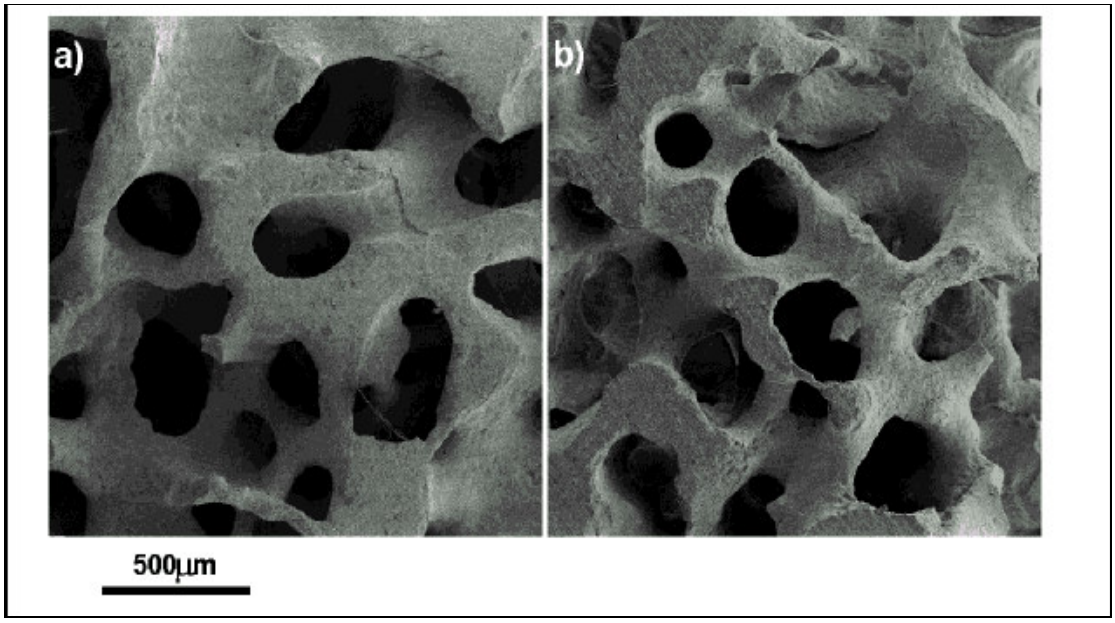

Figure 3.4 Comparison of the Australian coral (a) in original state and (b) after hydrothermal conversion [3].

The harvested coral is purified physically and chemically and the final implant material contains no proteins and less than 0.1% amino acids. The chemical composition of purified coral is like below [18]:

Calcium carbonate >97%

Trace elements 0.5-1%

Magnesium 0.05-0.2%

Sodium <1%

Potassium <0.03%

Phosphorus <0.05%

Water <0.5%

Hydrothermal treatment is required to convert aragonite ($CaCO_3$) to a complex calcium phosphate salt whilst preserving the porous structure. The following exchange takes place: [3]

$$10\ CaCO_3 + 6(NH_4)2HPO_4 + 2\ H_2O \rightarrow Ca_{10}\,(PO_4)_6\,(OH)_2 + 6(NH_4)2CO_3 + 4H_3CO_3$$

The resulting material is known as coralline hydroxyapatite, whether in the porous coralline structure or in powdered form.

3.5.2 Thermal Behavior and Sintering of Hydroxyapatite

The knowledge about the thermal behaviour of HAp is important since at high temperatures the HAp structure may be modified. The sintering mechanism of HAp in particular at elevated temperatures plays a significant role in order to evaluate the thermal stability of HAp in terms of phases present, densification behaviour, solubility and hardness.

Sintering of HAp in air is complicated by two processes namely dehydroxylation and decomposition of HAp, at elevated temperatures. The dehydroxylation reaction of HAp is given below in Eq. (1) [19],

$$Ca_{10}(PO_4)_6(OH)_2 \rightarrow Ca_{10}(PO_4)_6(OH)_{2-2X}\ O_X\square_X + XH_2O\uparrow \quad (1)$$

where $\square$ is vacancy and $x < 1$.

The hydroxyl ion deficient product obtained is known as oxyhydroxyapatite (OHA) [20]. In air OHA is formed at 900 °C and in water-free environment it is formed around 850 °C. Results from thermogravimetric analysis, X-ray diffraction and IR absorption analysis show the presence of two types of water, namely absorbed water and lattice water. Stoichiometric HAp contains constitutional water in the form of OH^- ions and this water can be driven off at high temperatures (~1200°C), by producing a partially dehydrated HAp which presumably contains one O_2^- ion of each water molecule that has been lost [21].

At high temperatures, HAp can be totally or partially dehydrated. Above 900°C a small weight loss is recorded. From 1200°C onwards the HAP may decompose according to the reaction given in Eq. (2).

$$Ca_{10}(PO_4)_6(OH)_2 \rightarrow 2Ca_3(PO_4)_2 + Ca_4P_2O_9 + H_2O \quad (2)$$

Sintering of HA is also complicated by the fact that HA is a hydrated phase which decomposes to anhydrous calcium phosphates such as tricalcium phosphate (TCP) at 1200–1450°C [20,23]. At temperatures higher than 1350°C, β-$Ca_3(PO_4)_2$ irreversibly transforms to α-$Ca_3(PO_4)_2$. The degradation occurs at varying degrees in the order of α-TCP > β-TCP >HA [19,20].

Decomposition of HAp must be avoided since it results in enhanced in vitro dissolution and the formation of other calcium phosphate phases [22]. Decomposition results from dehydroxylation beyond a critical point. For temperatures below the critical point, the HAp crystal structure is retained despite dehydroxylation and HAp rehydrates on cooling. If the critical point is exceeded, complete and irreversible dehydroxylation occurs, resulting in the collapse of the HAp structure and thus its decomposition. The critical point here is the decomposition temperature that corresponds to a temperature typically in the range 1200–1450 °C, the actual value depending on the characteristics of the HA powder [23]. After the critical point, α-TCP and β-TCP are often formed. In particular, the molecular volume increase that occurs in the β- TCP →α-TCP transformation seems to be the most deleterious phenomenon for mechanical properties [22].

3.5.3 Synthesis of Hydroxyapatite

Considering the numerous applications of hydroxyapatite in biomedical fields, numerous HAp synthesis techniques have been developed. The two most commonly known techniques for the formation of HAp powder are the organic method and the inorganic method. The organic method involves the preparation of HAp powders from organic sources like bones and teeth [24, 25, 26]. As a synthetic method, the most popular and widely researched route is solution precipitation. HAp nanoparticles can be prepared using microwave irradiation, Solgel and hydrothermal routes which are other important

routes for HAp synthesis [30]. Even HAp can be produced by mechanosynthesis route, in which case no heat treatment is required to produce crystalline nano HAp. There are also alternative techniques for preparation of HAp powders such as flux method, electrocrystallisation, spray pyrolysis, freeze-drying [27].

Wet methods in aqueous solutions both by simple precipitation method or hydrolysis of acidic calcium phosphate salts. Synthesis of HAp using wet method is very complicated and needs a special attention to control the Ca/P ratio as well as the crystallinity. The substitution of phosphate ions PO_4^{3-} by hydrogen phosphate HPO_4^{2-} allows a continuous variation of the Ca/P atomic ratio between 9/6 and 10/6. This leads to calcium-deficient hydroxyapatites, $Ca_{10-x}(PO_4)_{6-x}(HPO_4)_x(OH)_{2-x.}$ Calcium-deficient hydroxyapatite powders can be precipitated from conventional wet chemical methods and decomposed into a mixture of HA and tricalcium phosphate, $Ca_3(PO_4)_2$ (TCP) by thermal treatment above 700 °C. This allows a direct processing of biphasic calcium phosphate ceramics HA/TCP without the step of powder blending [28,29].

Both Ca^{2+} and PO_4^{3-} ions, as well as the OH^- group in HAp, can be replaced by other ions, several of them present in physiological surroundings. A well-known ion is fluoride, leading to fluorapatites.

$$Ca_{10}(PO_4)_6(OH)_{2-x}\,F$$

$$O<X<2$$

The carbonate ion, when incorporated into HAp yields carbonated apatites with various chemical formulae.

$$Ca_{10}(PO_4)_6(OH)_{2-2x}(CO_3)_x$$

$$\text{and } Ca_{10-x+y}(PO4)_{6-x}(CO3)_x(OH)_{2-x+2y}$$

$$O<X<2$$

$$O<Y<1/2X$$

For biomedical purposes, the carbonated apatite and fluorapatite are the materials of interest because of assumed similarity to bony apatite and decreased solubility in aqueous solutions respectively [29].

Mechanochemical powder synthesis is a solid-state synthesis method that takes advantage of the perturbation of surface-bonded species by pressure to enhance thermodynamic and kinetic reactions between solids [29,31]. The main advantages of mechanochemical synthesis of ceramic powders are simplicity and low cost, which make it a valuable method for industrial production of HAp powder. Equipments used for mechanochemcal synthesis are conventional milling equipment, such as ball mills and vibratory mills.

The pore size can be controlled and also complex shaped materials can be fabricated. Porous HAp can be manufactured in several ways. Homogenizing calcium phosphate powder with appropriately sized naphthalene particles results in macroporous material after the naphtalen has been removed. The final form is achieved after sintering at high temperatures (1100-1300°C). Another method relies on the decomposition of hydrogen peroxide to generate a pore-filled structure [30].

4. ANATOMY OF EYE

4.1 Parts of Eye Globe

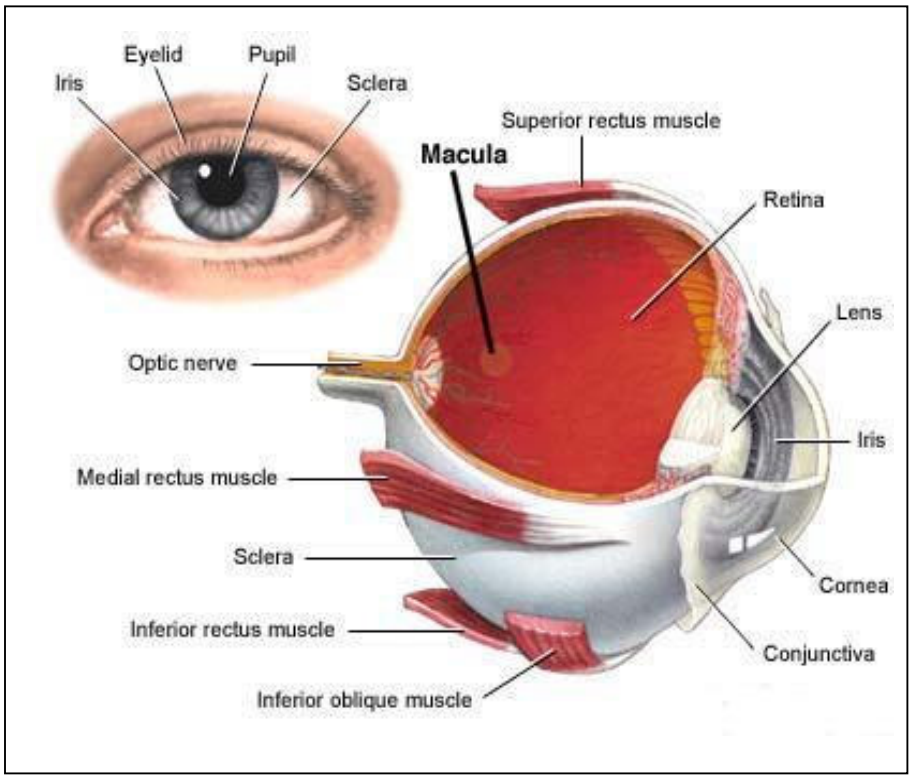

Figure 4.1 Major parts of eye globe (Medical Encyclopedia A.D.A.M)

The eye globe can be considered under four headings:

- The protective coat – cornea, sclera and conjunctiva.
- The vascular layer - iris, ciliary body, and choroid - together called the uvea.
- The visual layer - retina and optic nerve.
- The contents of the eye - aqueous, lens and vitreous.

Sclera: The sclera, commonly known as "the white of the eye," is the tough, opaque tissue that serves as the eye's protective outer coat (Figure 4.2).

Figure 4.2 The layers of eye globe (Medical Encyclopeida A.D.A.M.)

Cornea: The cornea is the transparent, dome-shaped window covering the front of the eye. It is a powerful refracting surface, providing 2/3 of the eye's focusing power.

Iris: The colored part of the eye is called the iris. It controls light levels inside the eye similar to the aperture on a camera. The round opening in the center of the iris is called the pupil. The iris is embedded with tiny muscles that dilate and constrict the pupil size.

Lens: The purpose of the lens is to focus light onto the back of the eye. The nucleus, the innermost part of the lens is surrounded by softer material called the cortex. The lens is encased in a capsular-like bag and suspended within the eye by tiny guy wires called zonules.

Conjunctiva: The conjunctiva is the thin, transparent tissue that covers the outer surface of the eye. It begins at the outer edge of the cornea, covers the visible part of the eye, and lines the inside of the eyelids. It is nourished by tiny blood vessels that are nearly invisible to the naked eye.

Vitreous: The vitreous is a thick, transparent substance that fills the center of the eye. It is composed mainly of water and comprises about 2/3 of the eye's volume, giving it form and shape.

Retina: The retina is a very thin layer of tissue that lines the inner part of the eye. It is responsible for capturing the light rays that enter the eye. Much like the film's role in photography. These light impulses are then sent to the brain for processing, via the optic nerve.

Macula: The macula is located roughly in the center of the retina, temporal to the optic nerve. It is a small and highly sensitive part of the retina responsible for detailed central vision. The fovea is the very center of the macula. The macula allows us to appreciate detail and perform tasks that require central vision such reading.

Optic Nerve: The optic nerve transmits electrical impulses from the retina to the brain. It connects to the back of the eye near the macula. The visible portion of the optic nerve is called the optic disc.

4.2 Eye Muscles & Movement

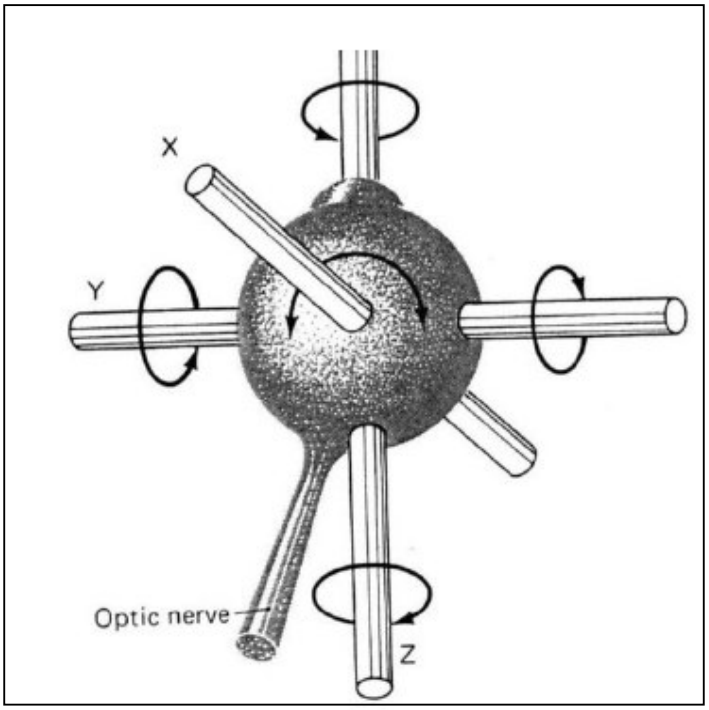

Figure 4.3 Three axes rotation of the eye globe [32]

The eye can be rotated around any axis. A three-dimensional model seen in Fig. 4.3 can be used to describe the movement of the eye. The eye can rotate from side to side around the x-axis. Rotation around the horizontal y-axis leads to eye movements that are directed upward or downward. Torsional eye movement occurs around the z-axis [32].

Three antagonistic pairs of muscles control natural eye movement: the lateral and medial recti, the superior and inferior oblique, and the superior and inferior recti, as shown in Fig. 4.4. Although, all of the extra ocular muscles contribute to some degree to all eye movement by contracting or relaxing, only two muscles in any one plane determine each movement. For example, the lateral and medial recti are chiefly responsible for moving the eyes horizontally. Both the superior and inferior oblique

and the superior and inferior recti can move the eye vertically as well as torsionally [33].

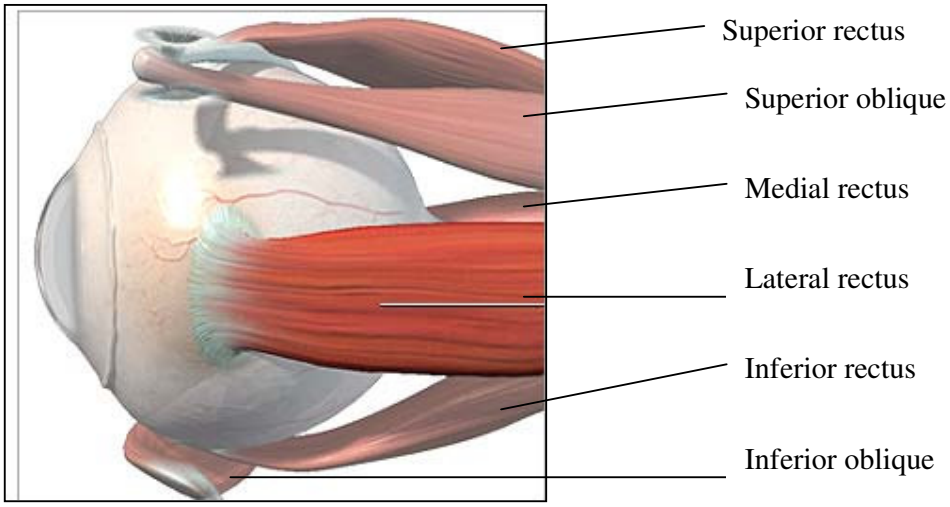

Figure 4.4 Lateral view of eye muscles (Medical Encyclopedia A.D.A.M)

5. OVERVIEW OF EYE REMOVAL

The removal of an eye is a major event in the life of any individual. However, many people have adapted to the loss of their eye and succeed in living a normal life following their surgery. The main reasons for removing an eye are:

- to provide relief from a painful blind eye.
- to create a better cosmetic appearance following an injury or a trauma to an eye.
- to remove a tumour.

There are two methods in an attempt to remove the eye, to provide pain relief and to prepare for reconstruction of the anophthalmic socket. These methods are evisceration and enucleation. Each method has their own benefits.

5.1 Enucleation

Enucleation is the removal of the globe from the orbit, involving the separation of all connections between the globe and the patient (including transection of the optic nerve). Enucleation may be performed to treat a variety of conditions including intraocular malignancy and severe ocular trauma as well as blind, painful, or disfigured eyes [34, 37]. The goals of enucleation are to remove the diseased globe and create a functional socket that facilitates the fitting and retention of an ocular implants.

5.2 Eviscreation

Evisceration involves removal of the contents of the eye, while maintaining an intact scleral shell attached to the extraocular muscles. Enucleation is the treatment of choice when there is a possibility of intraocular malignancy or the chance of developing sympathetic eye inflammation. Evisceration offers several distinct

advantages over enucleation, including ease of the procedure, better anatomic preservation of orbital structures, and superior cosmetic outcome [34,35].

5.3 Exenteration

Exenteration involves removal of the globe along with all the soft tissues of the orbit. It is most commonly performed to control orbital cancers and ocular cancers with orbital invasion [34].

5.4 Anopthalmia

Anopthalmia may be congenital (existing from birth) or acquired. Congenital anopthalmia refers to any orbit that contains a severely incomplete development of eye at birth (microphthalmia), or a complete absence of the globe due to failure of optic vesicle formation. In both those cases the aim of surgery is to stimulate adequate orbital growth. Acquired anophthalmic orbit may be due to trauma or tumor [36]. In acquired forms the goal is restoration of orbital volume with adequate replacement of orbital contents.

6. ORBITAL IMPLANTS

6.1 History and Overview of Orbital Implants

In managing the anophthalmic socket after enucleation and evisceration, attention must be directed toward replacing orbital volume, maximizing prosthetic motility, and providing comfort and aesthetic appearance, through an orbital implant and artificial eye (ocular prosthesis) (Figure 6.1).

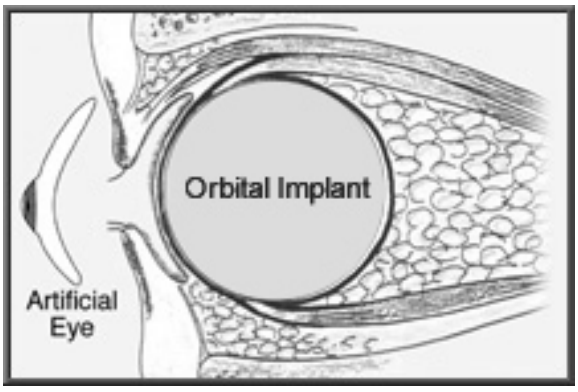

Figure 6.1 Orbital implant and arificial eye [38]

During the last century, numerous orbital implants have been developed and used in an attempt to achieve these goals. The search for the ideal orbital implant first began with Mules in 1885 when an eviscreation a glass sphere is implanted. Subsequently numerous materials like gold, cartilage, silver, aluminum, silicone and glass beads were used to fill irregular cavities in the orbit [34,36]. Most of the implants composed of these materials were found unsuitable due to various reasons and were discarded one after another.

In 1941, an acrylic based, partially exposed orbital implant was introduced by Ruedemann. Implants made of alloplastic materials, such as acrylic, silicone or glass were well tolerated by the host and induced little inflammatory reaction. However their solid nature precluded the direct attachment of extraocular muscles or coupling to the

ocular prosthesis. There have been many variations in the designs of orbital implants after the Ruedemann eye. The partially exposed implants imparted good motility to the artificial eye, but were prone to infection and extrusion.

Over the past ten years implants have been developed to allow for the in-growth of naturally occurring tissues and blood vessels termed as porous integrated. This reduces the risk of the body rejecting (extrusion) the implant at a later stage, which has, in the past, been a problem because of introducing artificial material into the body. It also provides better implant motility by means of anchoring extraocular eye muscles to the implant [36]. Porous enucleation implants currently are fabricated from a variety of materials including natural and synthetic hydroxyapatite, aluminum oxide, and polyethylene. Hydroxyapatite implants are spherical and made in a variety of sizes. Aluminum oxide and porous polyethylene implants can be obtained in spherical and nonspherical shapes and in different sizes. Among porous integrated implants HA is the most widely preferred implant after enucleation [38].

The advantage of using porous implants is that in some cases better artificial eye movement can be achieved. This is achieved by ‘drilling’ a hole into the implant in which a peg can be inserted. The protruding end of the peg is fashioned to form a rounded head, which in turn is fitted to a specially modified artificial eye (Figure 6.2) [40]. The cosmetic outcome can be particularly successful. The drilling process is not always necessary and some patients achieve excellent results through the insertion of the implant alone. If it is judged to be necessary, the drilling procedure takes place from up to 6-12 months following the initial operation to remove the eye [35].

In the past, spherical nonporous implants were placed in the intraconal space and the extraocular muscles were either left unattached or were tied over the implant. Wrapping these implants allows attachment of the muscles to the covering material, a technique that seems to improve implant movement and reduce the incidence of implant migration[39,40]. Because the brittle nature of hydroxyapatite prevents direct suturing of the muscles to the implant, these implants are usually covered with some form of wrapping material [38].

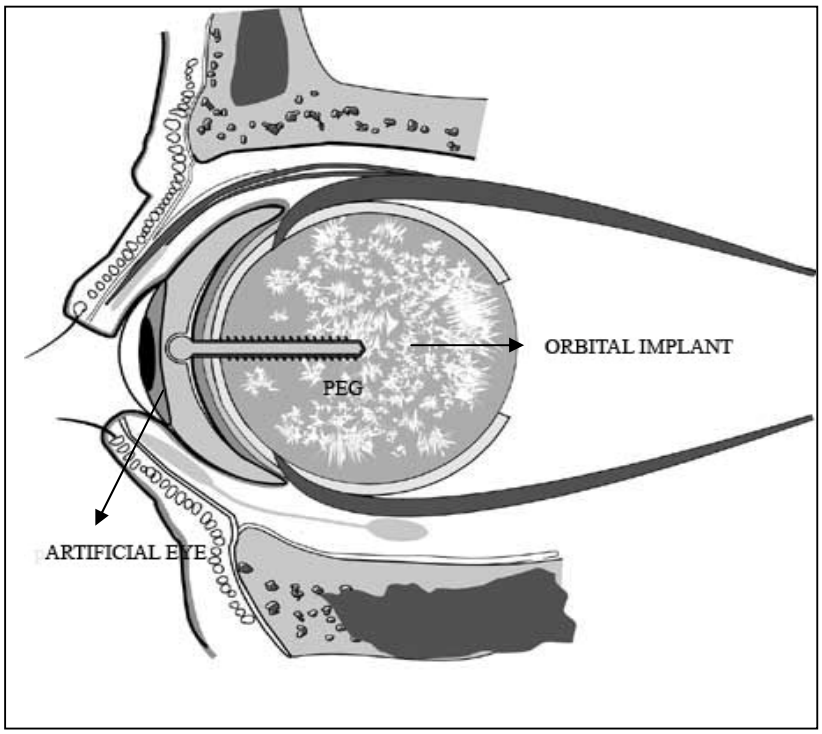

Figure 6.2 Schematic diagram of artificial eye, peg and orbital implant [40]

Enucleation can be performed without implant placement, but this is unusual and will yield a poor cosmetic result. In general, implants replace the volume lost by the enucleated eye, impart motility to the prosthesis, and maintain cosmetic symmetry with the fellow eye. There are two major groups of orbital implants: 1) nonintegrated 2) integrated.

6.2. Nonintegrated Implants

Nonintegrated implants contain no unique apparatus for attachments to the extraocular muscles and do not allow ingrowth of organic tissue into their inorganic substance (Figure 6.3) [35]. Such implants have no direct attachment to the ocular prosthesis. Materials used as nonintegrated implants include glass, rubber, silicone, steel, gold, silver, acrylic, and polymethylmethacrylate (PMMA) [37,40]. Compared to no implant, these devices provide both volume replacement and improved cosmetics.

Imbrication of the rectus muscles in front of a spherical implant imparts motility to the implant and prosthesis. Like a ball-and-socket joint, when the implant moves, the

prosthesis moves. Because the ball and socket are separated by layers of Tenon's fascia, imbricated muscles, and conjunctiva, nonpegged implants offer less motility than pegged implants. Since the late 19th century, many clinical case series have reported the use of a variety of implant materials in the form of nonintegrated and quasi-integrated implants. In 1989, Hornblass et al reported that silicone and glass spheres were the implants of choice for approximately 60% of the members of the American Society of Ophthalmic Plastic and Reconstructive Surgeons who responded to their survey [40].

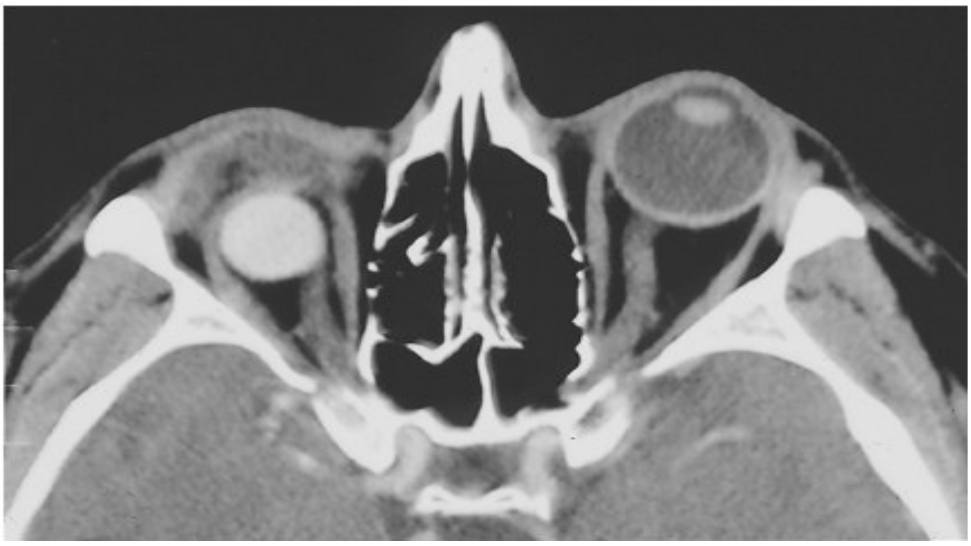

Figure 6.3 Computed tomography of a PMMA (nonintegrated) implant within the muscle cone. Note the small volume of the 16-mm implant as compared to the left globe [35].

6.3. Integrated Implants

6.3.1 Hydroxyapatite Orbital Implants

Hydroxyapatite orbital implants of different varieties have become popular implants worldwide and are used after enucleation, evisceration, or during secondary implantation surgery.

The hydroxyapatite orbital implant is commonly used during enucleation surgery [38]. It is formed from a salt of calcium phosphate that is present in the mineralized portion of human bone (Figure 6.4). It is reported to be nontoxic, nonallergenic, and biocompatible. Its porous structure allows integration of fibrovascular tissues into the stroma of the implant. The common types of the hydroxyapatite implant are the Bio-Eye hydroxyapatite implant (Integrated Orbital Implants, Inc., San Diego, CA), the M-Sphere cancellous bone implant (IOP, Inc., Costa Mesa, CA) and the FCI_3 synthetic hydroxyapatite implant (FCI Inc., France) [35].

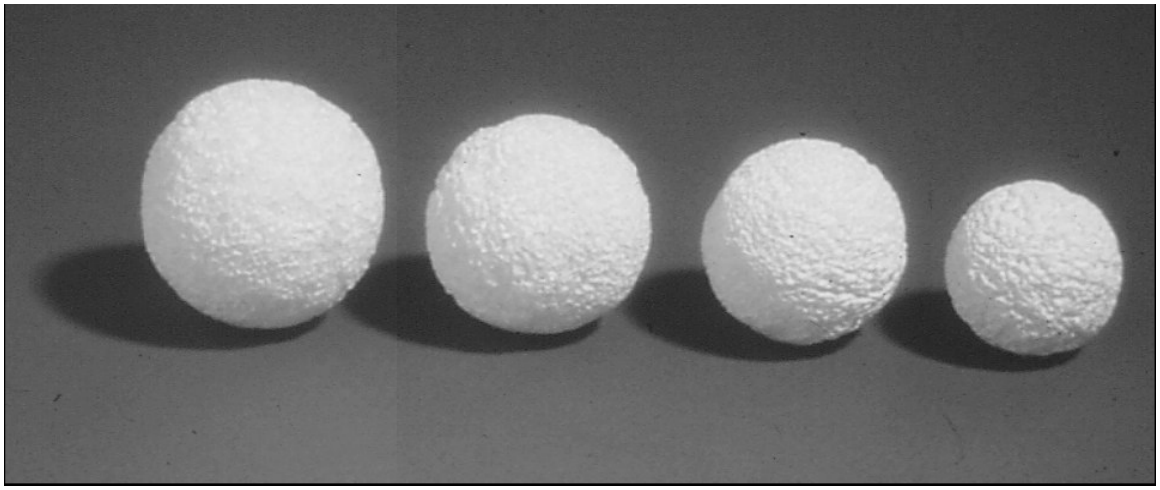

Figure 6.4 Hydroxyapatite implants of various sizes can be shaped at the time of implantation. Their pores allow for fibrovascular ingrowth. (photograph courtesy of Innovative Ophthalmic Products, Inc., Costa Mesa, CA) [35].

Fibrovascular ingrowth and density changes have been assessed by a variety of radiographic techniques, but contrast-enhanced magnetic resonance imaging with surface coil appears to be the modality of choice. Fibrovascular coupling between host

tissue and the hydroxyapatite implant is said to aid in preventing migration and extrusion [43].

It is believed that the rough surface of these implants may induce the abrasion of overlying conjunctiva and Tenon's capsule and resulting in exposure. Consequently hydroxyapatite implant is usually wrapped with donor sclera or other material [41,42,35]. These materials are also used to anchor the extraocular muscles to the implant. Pegging of hydroxyapatite implants is typically performed 6 months or more after the initial surgery to allow fibrovascularization within the implant and only in patients who desire to have the increased motility that can be associated with coupled systems (Figure 6.5).

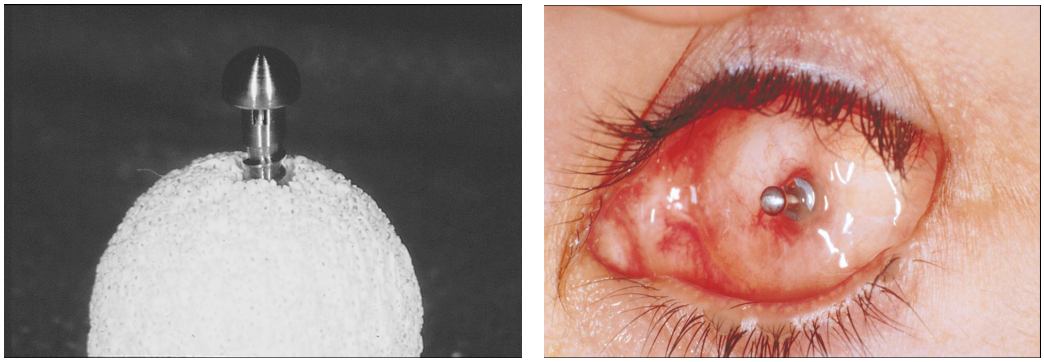

Figure 6.5 Left: A pegged hydroxyapatite orbital implant photographed to demonstrate how the peg is inserted into the device. Actual pegging is done in vivo. **Right***:* A peg is seen emanating from the implant within the orbit of a patient after enucleation. The prosthesis is placed on top of the peg in order to improve motility [35].

6.3.1.1 Coralline Hydroxyapatite Orbital Implants Since United States Food and Drug Administration approval in 1989, the coralline hydroxyapatite (HA) orbital implant (BioEye; Integrated Orbital Implants, Inc., San Diego, CA, U.S.A.) has been in widespread use by ophthalmic plastic surgeons in North America after enucleation, evisceration, or during secondary implantation [38].

The implant is derived from sea coral (coralline). The aragonite ($CaCO_3$) skeletal structure of the common reef-building coral (genus Porites) is converted hydrothermically to calcium phosphate (HA) [$Ca_{10}(PO_4)_6(OH)_2$], without deforming the interconnected pore architecture that resemble the normal haversian system of bone

(Figure 6.6) [18,42]. In a 1992 survey of members of the American Society of Ophthalmic Plastic and Reconstructive Surgeons, coralline HA was the most frequently used implant after primary enucleation [35].

Bio-Eye orbital implants show multiple interconnected, uniformly formed pores within the range of 300-700 μm. According to MRI histopathology of 12mm implants employed, central tissue enhancement was acquired by 4 weeks. Table 6.1 reviews the main characteristics of corralline hydroxyapatite orbital implant.

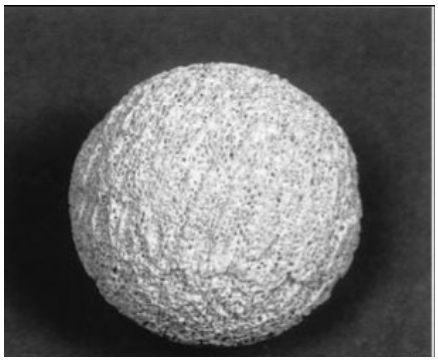

Figure 6.6 20 mm coralline hydroxyapatite orbital implant [42]

Table 6.1 Some of the main characteristics of corraline HA orbital implant [44,52]

	Bio-Eye (coralline hydroxyapatite)
Gross Inspection	Multiple interconnected pores
Penetration with 20 gauge needle	Relatively easy
Pinch Test (Fragility)	Noncrushable, strong
Pore Size (SEM) (μm)	300-700
Solid areas between pores (SEM)	1/3 unit area
Pore Uniformity (SEM)	Excellent
Pore interconnectivity (SEM)	Excellent
MRI (12mm)	Central enhancement by 4 weeks
Histopathology (12mm)	Uniformly throughout by 4 weeks

6.3.1.2 Bovine Hydroxyapatite Orbital Implant Although coralline hydroxyapatite has gained recent popularity as an orbital implantation material, other hydroxyapatite substances have been used as orbital implants for decades.

The M-Sphere (IOP Inc.,Costa Mesa, California) is a commercially available, natural hydroxyapatite implant derived from the cancellous bone of calf fibulae (Figure 6.7). It is fully deproteinized through a process of acetone treatment and immersion in 5% sodium hypochlorite solution [45]. Electron microscopic studies show that the pore size of this anorganic bovine hydroxyapatite varies from approximately 300 to 600 microns. The M-sphere is approximately 50% less dense than coralline hydroxyapatite. The antigen-free nature of this material suggests that it should be biocompatible, nontoxic, and nonallergenic. The material should allow for fibrovascular integration and placement of a motility peg.

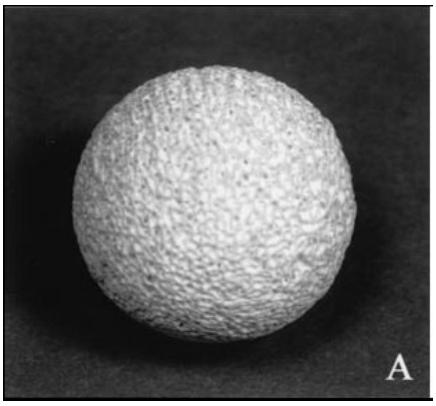

Figure 6.7 Photographs depict a 20-mm bovine Hydroxyapatite sphere [42]

Chemical analysis of the M-Sphere implant by X-ray powder and X-ray fluorescence techniques reveal the implant to be pure HA without contaminants [46]. Magnetic resonance imaging scanning of the implanted 12-mm M-Sphere spheres showed central enhancement by 4 weeks. However, the M-Sphere can be readily crushed between the index and thumb (failed pinch test) and found to be fragile (Figure 6.8) [47].

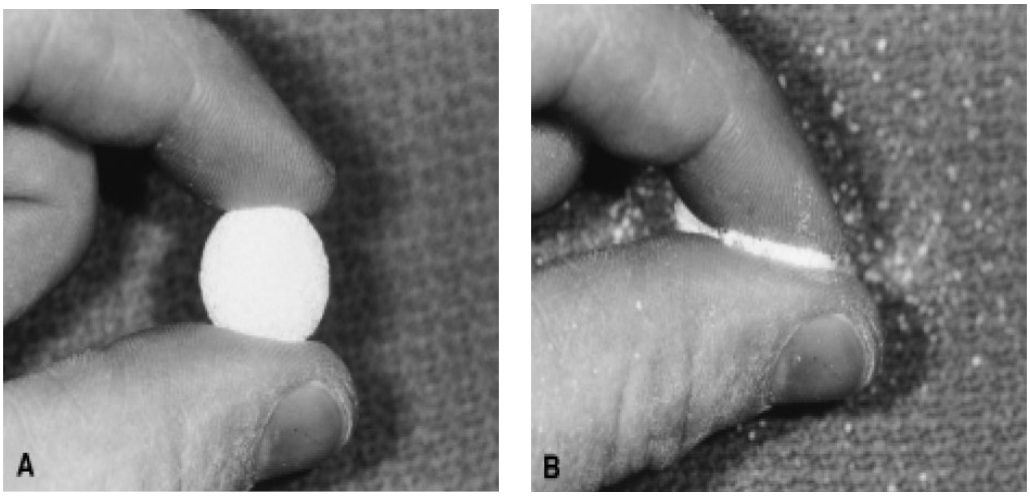

Figure 6.8 Molteno M-Sphere hydroxyapatite (HA) being held between thumb and index finger. B. M-Sphere HA easily crushed (pinch test) [47].

In summary, the Molteno M-sphere is another HA implant available for use after enucleation, evisceration, or as a secondary implant. It is similar in appearance to the BioEye and FCI_3 synthetic HA, has multiple interconnected pores throughout its framework, and is made of pure HA. It allows central vascularization to occur (in a rabbit model) similar to the BioEye and FCI_3 synthetic HA.

6.3.1.3 Synthetic Hydroxyapatite Obviously, the ideal bone implant would be antigen-free to minimize tissue response, provide a hydroxyapatite scaffold to allow fibrovascular ingrowth, and come from an easily replenished resource. To meet these criteria, FCI_3 synthetic hydroxyapatite orbital implants have been used recently (Figure 6.9). HAp required to fabricate FCI_3 orbital implants, was chemically synthesized [47].

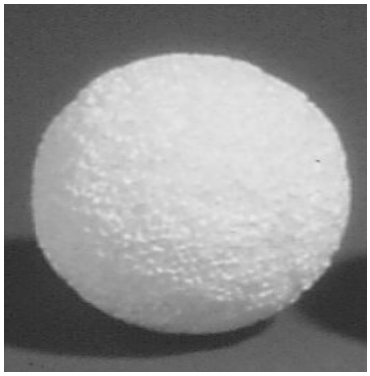

Figure 6.9 Photograph shows 20mm FCI_3 synthetic hydroxyapatite sphere [35].

The synthetic FCI HA implant is similar in appearance to the BioEye, with multiple interconnected pores. These pores allow fibrovascular ingrowth into the implant center by 4 weeks in a rabbit model as does the BioEye [42]. The implant is without contaminants, nonfragile, chemically identical to the BioEye, and easy to work with. Experience in more than 65 patients has shown this implant to be easy to work with [41].

Advantages over the BioEye include the following: 1) drilling of this implant is easier than the BioEye and can be accomplished without the use of motorized drills; 2) the FCI implant is less expensive; and 3) the manufacture of the synthetic HA does not require harvesting of coral with potential disruption to marine ecosystems. The FCI synthetic HA

implant was given Health and Welfare approval in Canada (February 1997) and currently is used throughout Europe and several other countries around the world [44].

Electron microscopic studies show that the pore size of this synthetic hydroxyapatite orbital implant varies from approximately 300 to 500 microns. Some of the main characteristics of FCI_3 are given in Table 6.2.

Table 6.2 Some of the main characteristics of FCI_3 synthetic HA orbital implant [44,52]

	FCI_3 (synthetic hydroxyapatite)
Gross Inspection	Multiple interconnected pores, some blind pouches
Penetration with 20 gauge needle	Easier than Bio-Eye
Pinch Test (Fragility)	Noncrushable, strong
Pore Size (SEM) (μm)	300-500 (fewer pores than Bio-Eye or alumina)
Solid areas between pores (SEM)	1/2 unit area
Pore Uniformity (SEM)	Good (less than alumina or Bio-Eye)
Pore interconnectivity (SEM)	Good (but less than alumina or Bio-Eye)
MRI (12mm)	Central enhancement by 4 weeks
Histopathology (12mm)	Uniformly throughout by 4 weeks

6.3.1.4 Brazilian Hydroxyapatite The Brazilian implant is another form of HA. It is a manmade synthetic HA currently being used as an orbital implant in Brazil. Considering the reported experience, Brazilian HA orbital implants give the impression that the implant is comparable to coralline HA implants [37]. The HA ceramic is obtained from commercially available calcium phosphate powder synthesized in a

nitrogen/water vapor atmosphere at a temperature between 1200ºC and 1300ºC, for 3 hours. The external layer of the sphere is composed of fine particles with 5µm to 10 µm micropores and 50 µm to 100 µm macropores between the particles. The interior of the sphere is made of denser HA, for increased mechanical strength [49].

One of the obvious differences is readily apparent on gross inspection: the Brazilian HA implant appears to be a more solid implant without the visible uniform porous architecture seen in other HA implants (Figure 6.10). However, electron microscopy reveals that extensive microporous architecture exists in those areas that grossly appear to be solid (Figure 6.11) [49]. Biochemically, the Brazilian implant is pure HA.

Histopathologically, the Brazilian HA showed central fibrovascular ingrowth at 4, 8 and 12 weeks. The extensive fibrovascularization indicates that the fibrovascular tissue was able to gain entry through the channels (250–1000 µm) as well as the micropores (5–10 µm).

The Brazilian HA is also a heavier implant than other HA implants on the market. Although the implant is less expensive and does not require a costly manufacturing process, the structural characteristics do not appear to offer any theoretical or clinical advantages over other currently available HA materials.

In summary, the Brazilian implant is a less costly alternative form of HA with a microporous architecture that allows central vascularization.

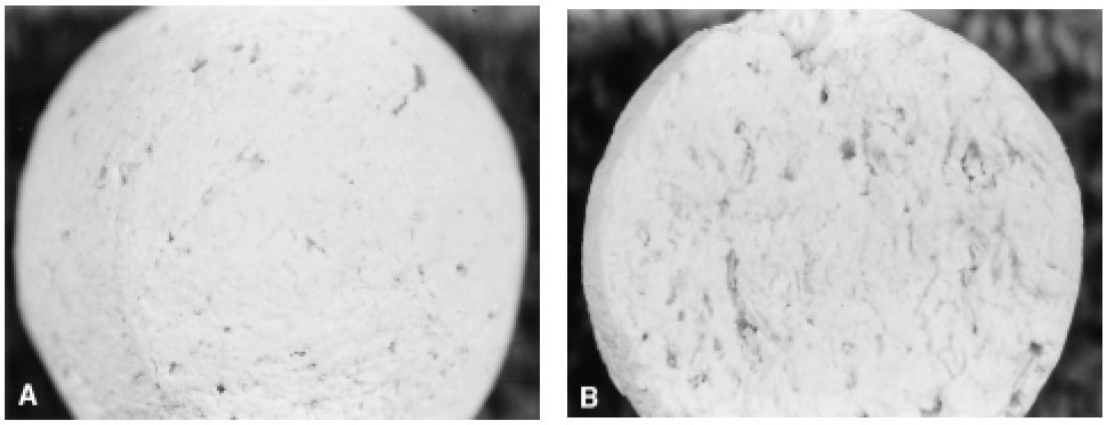

Figure 6.10 A. External surface of the Brazilian implant **B**. Internal surface of the Brazilian implant [49].

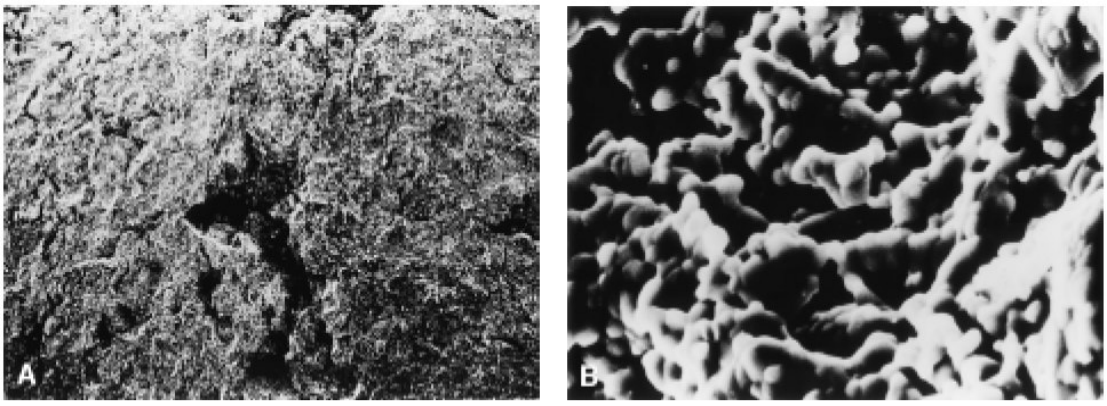

Figure 6.11 A. Scanning electron microscopy of the Brazilian implant B. High-power scanning electron microscopy photograph of the internal architecture of the Brazilian implant [49]

6.3.2 Porous Polyethylene

Polyethylene is a high-density, straight-chain hydrocarbon formed by the polymerization of ethylene molecules under high temperature and pressure. It is a stable polymer that has been used for reconstruction of bone and soft tissue for over 50 years.

Porous polyethylene (PP) is recently used as an integrated implant material (Figure 6.12). This spherical implant was approved by the Food and Drug

Administration for use in reconstructive surgery in 1985 [51]. Like hydroxyapatite, porous polyethylene allows fibrovascular ingrowth, albeit not as quickly as hydroxyapatite. The standard pore size of the current PP spherical implant is approximately 400 µm.

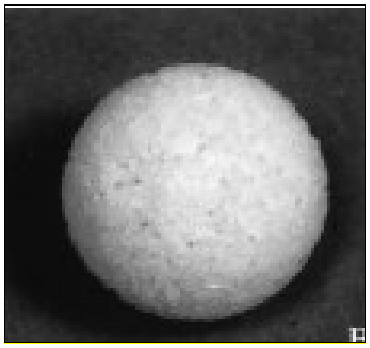

Figure 6.12 20-mm porous polyethylene sphere [42]

Advantages of the porous polyethylene device are that it does not require donor sclera or other type of wrapping material, its cost is low in comparison to hydroxyapatite, the PP structure is not brittle and the extraocular muscles may be sutured directly to the implant [50]. Porous polyethylene implants are smooth and malleable, which makes implantation easier (Figure 6.13). The device can be implanted in the standard fashion followed by attachment of the extraocular muscles [51].

A new titanium post coupling system (Porous Polyethylene Coupling Post; Porex Surgical, Inc., College Park, GA) was recently approved by the Food and Drug Administration. The coupling device consists of a medical- grade, inert titanium screw, available in various lengths, that is attached to the porous polyethylene implant 6 to 12 months after implantation [51].

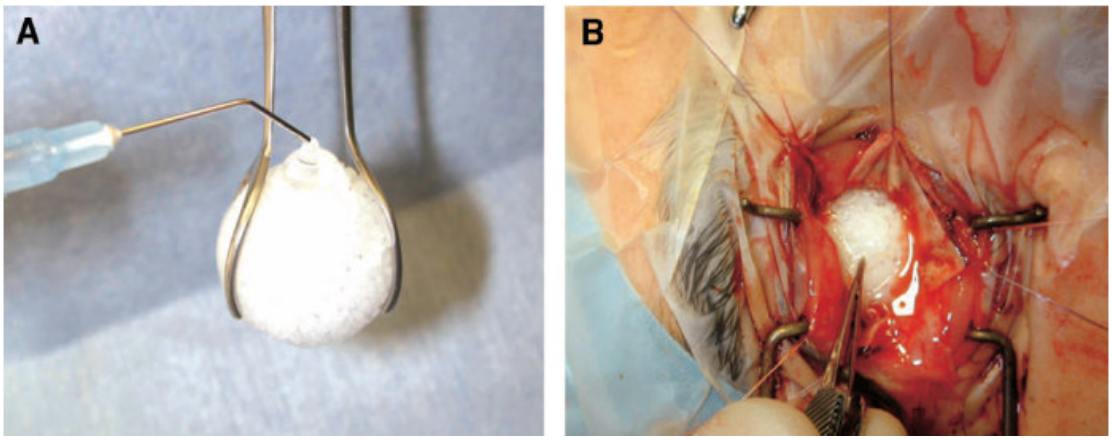

Figure 6.13 A Hydroxymethylcellulose (HPMC) being applied to the 20-mm porous polyethylene orbital implant for lubrication **B** Implant is placed well within the eviscerated scleral remnant [56].

6.3.3 Aluminum oxide (Al_2O_3)

Ceramics are substances made of inorganic minerals processed at high temperatures. Aluminum oxide (Al_2O_3) (also known as alumina) is a ceramic biomaterial that has been used for more than 30 years in orthopedics and dentistry. Alumina is in a highly oxidized state and thus degrades slowly with minimal biologic response in vivo. High-purity alumina (Al_2O_3) ceramic is considered to be the prototype of a truly bioinert material [8]. It does not dissolve in body fluids, and there is strong evidence that it is coated with protein molecules immediately after insertion into the body. As a result, it escapes recognition as a foreign body and is immunologically camouflaged [10].

Aluminum oxide orbital implants are easy to work with, simple to manufacture, and less expensive than other HA implants. It received U.S. Food and Drug Administration approval in April 2000 (Figure 6.14) [52]. Scanning electron microscopy also demonstrated alumina pores to be the most uniform in their distribution. The standard pore size of porous alumina orbital implant is 500µm. Some of the main characteristics of alumina orbital implants are also given in Table 6.3.

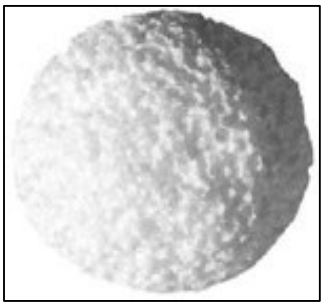

Figure 6.14 20mm porous alumina sphere [52].

Table 6.3 Some of the main characteristics of Al_2O_3 (alumina) orbital implant [44,52]

	Bioceramic implant (alumina)
Gross Inspection	Multiple interconnected pores, some blind pouches
Penetration with 20 gauge needle	Easy (easier than Bio-Eye)
Pinch Test (Fragility)	Noncrushable, strong
Pore Size (SEM) (µm)	500
Solid areas between pores (SEM)	<1/5 unit area
Pore Uniformity (SEM)	Excellent (more uniform than Bio-Eye, FCI HA)
Pore interconnectivity (SEM)	Excellent
MRI (12mm)	Central enhancement by 4 weeks
Histopathology (12mm)	Uniformly throughout by 4 weeks

In summary, the Bioceramic orbital implant (aluminum oxide, Al_2O_3, alumina) represents a new generation of porous orbital implant. It is straightforward to manufacture, structurally strong, free of contaminants, and easy to work with [37].

6.3.4 Other Implants

Many substances have been considered for use in orbital implants. Polytetrafluoroethylene, which was previously investigated for use as wrapping material for hydroxyapatite implants, has recently been investigated for use in spherical orbital implants in a rabbit model [35].

6.4 Evaluation of Fibrovascular Ingrowth

Over the past 12, years there has been increasing interest in the use of porous orbital implants in anophthalmic socket surgery. These implants provide a porous scaffold that permits ingrowth of fibrovascular tissue, which improves fixation to orbital soft tissues and thereby decreases the risk of migration or extrusion and theoretically decreases the risk of infection. Attachment of the extraocular muscles directly to the implant has been shown to facilitate vascularization and improve motility [35,38].

The fibrovascular ingrowth provides an orbital implant with biological anchoring and blood supply deep inside the implant. With completion of blood flow, the porous orbital implant reduces the incidence of complications that might occur with the use of nonporous orbital implants. The porous orbital implant is biologically fixed to orbital soft tissues so that it prevents escape or migration of the implant, and induces regeneration of epithelium on insertion of a peg when attaching an ocular prosthesis to the implant, thereby reducing complications associated with it [53]. The implant also improves the immune defense mechanism through blood vessels, thus decreasing the incidence of infection.

The methods used in clinical practice to estimate an extent of fibrovascular ingrowth of an orbital implant are bone scan using radioisotope, color Doppler, CT, MRI and etc [54]. With bone scan it is difficult to capture a site of increased absorption

of radioisotopes as it cannot provide three-dimensional information with high resolution on intraorbital structures and orbital implants due to the limit of tissue specificity. And it is also hard to distinguish whether increase in movement of an orbital implant implies fibrovascular ingrowth into the implant or a vascularized scar after surgery around the implant. CT and color Doppler were used to measure fibrovascular ingrowth of an orbital implant, but now rarely used because of its low usefulness.

Contrast-enhanced magnetic resonance imaging with surface coil appears to be the modality of choice for distinguishing the presence of fibrovascular ingrowth due to its high resolution and capacity to attain three-dimensional images. MR imaging and bone scan techniques have both been advocated by orbital surgeons to assess the degree of HA orbital implant fibrovascularization in situ before drilling of the implant and motility peg placement [55]. A prospective study of 10 patients directly comparing technetium- 99m-diethylenetriamine pentaacetic acid and gadolinium-enhanced T1-weighted MR imaging with fat suppression demonstrated that MR imaging may be more specific in determining which patients have complete vascularization of their implant (Figure 6.15, Figure 6.16).

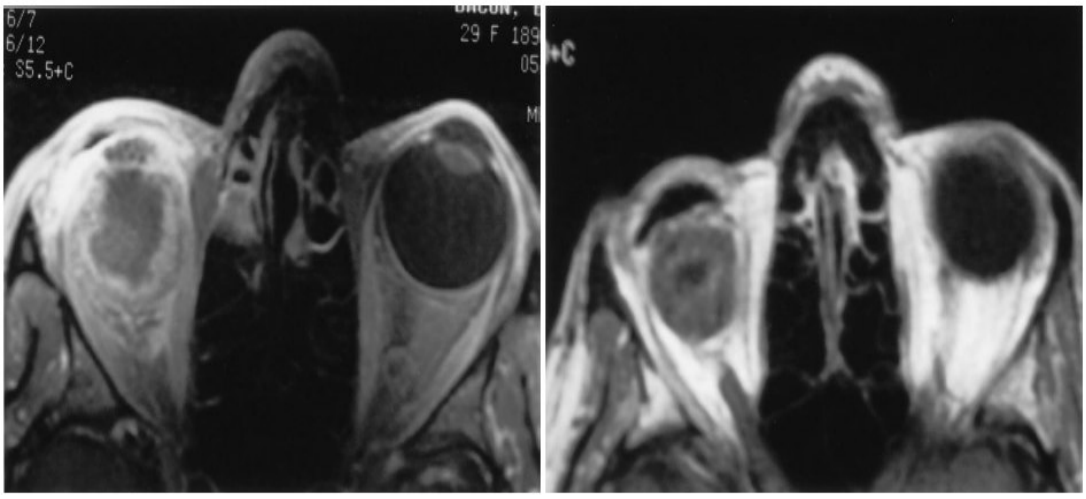

Figure 6.15 Left; MR image after injection of gadolinium-DPTA demonstrates a typical example of early (4 weeks after surgery) peripheral enhancement, suggesting peripheral fibrovascular ingrowth. **Right;** MR image after injection of gadolinium-DPTA demonstrates late (4-7 months after surgery) subtotal enhancement suggesting a lack of central fibrovascular ingrowth [55].

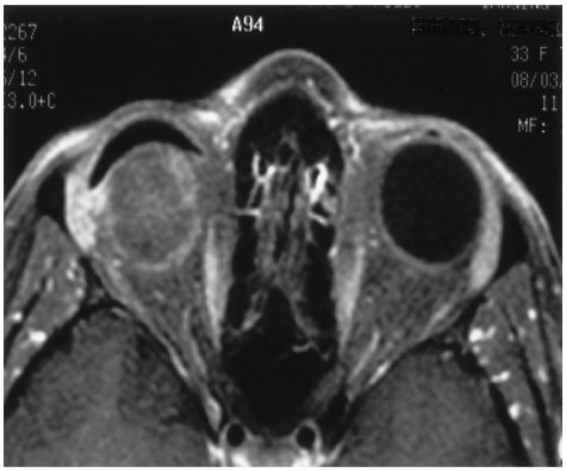

Figure 6.16 MR image after injection of gadolinium-DPTA demonstrates a typical example of late (4-12 months after surgery) homogeneous enhancement, suggesting complete fibrovascular ingrowth [55].

7. WRAPPING MATERIALS

7.1 Overview of Wrapping Materials

The goal of wrapping implants is to allow precise attachment of the rectus muscles to the wrapped HA and closely simulate the normal anatomic muscle positions (Figure 7.1). Another reason for using a wrapping technique is to to add an extra layer of tissue as a protective barrier between the implant and the conjunctiva. It is intended to decrease the risk of conjunctival erosion and exposure [57]. The third goal of wrapping HA orbital implants are to make the insertion of the implant easier. Hydroxyapatite is difficult to work with because it tends to adhere to the surrounding tissues. Wrapping the implants decreases tissue drag and facilitates more posterior implant placement.

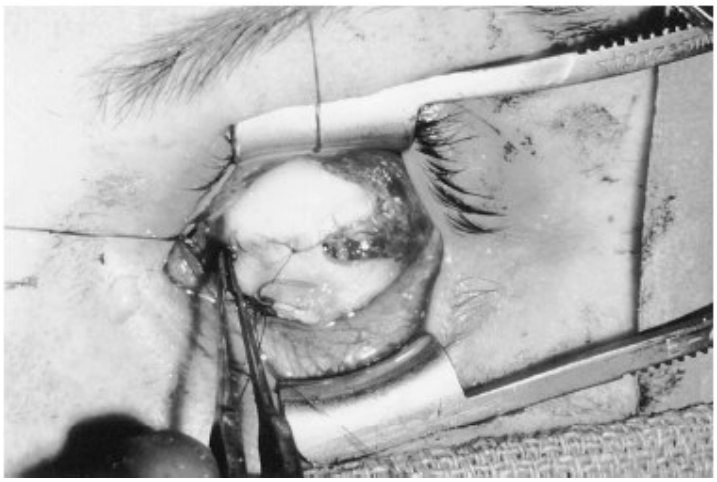

Figure 7.1 Meticulous placement of extraocular muscles on wrapped HA simulates original location of muscles [58].

Various wrapping materials have been proposed in the literature. An ideal graft for wrapping HA should be easily obtained; it should be strong yet easily shaped and sutured; it should have low antigenicity and tissue toxicity and no potential for spread of disease; and it should be inexpensive. Homologous donor sclera, autologous tissues, synthetic mesh and bovine pericardium are the most common wrapping materials for orbital implants

[35]. If the donor sclera or fascia is not screened properly and processed carefully, disease transmission is possible. Therefore, alternative wrapping materials for orbital implants have certain potential advantages.

While the wrapping material does provide some protection against conjunctival erosion, it also tends to slow vascularization of the implant to varying degrees. Attempts to encourage vascularization through this barrier tissue can be made by cutting rectangular windows in the wrapping at the sites of rectus muscle reattachment and leaving an opening at the posterior aspect of the implant [35,37]. Imaging and histopathologic studies have shown that when these openings are made, vascularization with central progression occurs more rapidly at these sites.

The advantage of unwrapped technique is that there is no barrier to the vascularization of the sphere. The vascularization of the implant progress more rapidly. The unwrapped technique is cost-effective because the cost of a wrap is avoided and the operating room time is shortened [61]. The theoretical risk of transmitting disease through nonautogenous wrapping material is also eliminated with the unwrapped technique. However, most agree that the benefits of a wrapping, such as ease of insertion and providing a site for extraocular muscle attachment, outweigh the risks of delayed fibrovascularization.

7.1.1 Donor Sclera

Human donor sclera has been the most widely used implant wrapping material. Perry recommends using fresh frozen donor sclera [38]. After thawing, the appropriate cultures of the donor sclera can be taken. The sclera is trimmed and wrapped to fit the implant, with the use of 4-0 or 5-0 nonabsorbable suture. Although donor sclera is readily available, it is expensive and the theoretical risk of transmissible disease exists. No case of human immunodeficiency virus transmission as a result of implanting donor sclera has ever been documented.

7.1.2 Autologous Tissue

Autologous materials for wrapping implants include muscles, dermis, pericardium, auricular muscle complex, and the membrane covering the skull. The advantages of these materials in enucleation surgery are that autologous tissues are a living graft, will not elicit a foreign body response, and vascularize rapidly [58]. Drawbacks to autologous tissue grafts are that harvesting the graft requires additional surgical time. Autologous tissue remains a good alternative to banked sclera in selected patients.

7.1.3 Synthetic Mesh

Vicryl (polyglactin 910) is a synthetic knitted mesh that is identical to the material found in Vicryl absorbable suture. Vicryl mesh, noting its ease of insertion and attachment of extraocular muscles. An advantage of synthetic mesh is that it eliminates the possibility of disease transmission. Wrapping a spherical implant with Vicryl mesh does not require time-consuming suturing or window formation and permits 360° fibrovascularization of porous implants [59]. Vicryl mesh is easy to place around the implant, inexpensive, readily available, and eliminates the risk of transmissible diseases.

7.1.4 Bovine Pericardium

Pericardium is the fibrous tissue covering the heart. Bovine derived pericardium as a wrapping material for orbital implants was reported to produce satisfactory results and found to be comparable to the other traditionally used materials. It is generally used for wrapping ceramic implants like HA (Figure 7.2) [60]. It is available as a sterilized sealed prepared wrapping material, making its use very easy. It is sterilized using glutaraldehyde, ethanol, and propylene oxide and has to be immersed and agitated in 500 ml of sterile physiological saline after removal from non-pyrogenic water with propylene oxide in the supply container before wrapping the orbital implant.

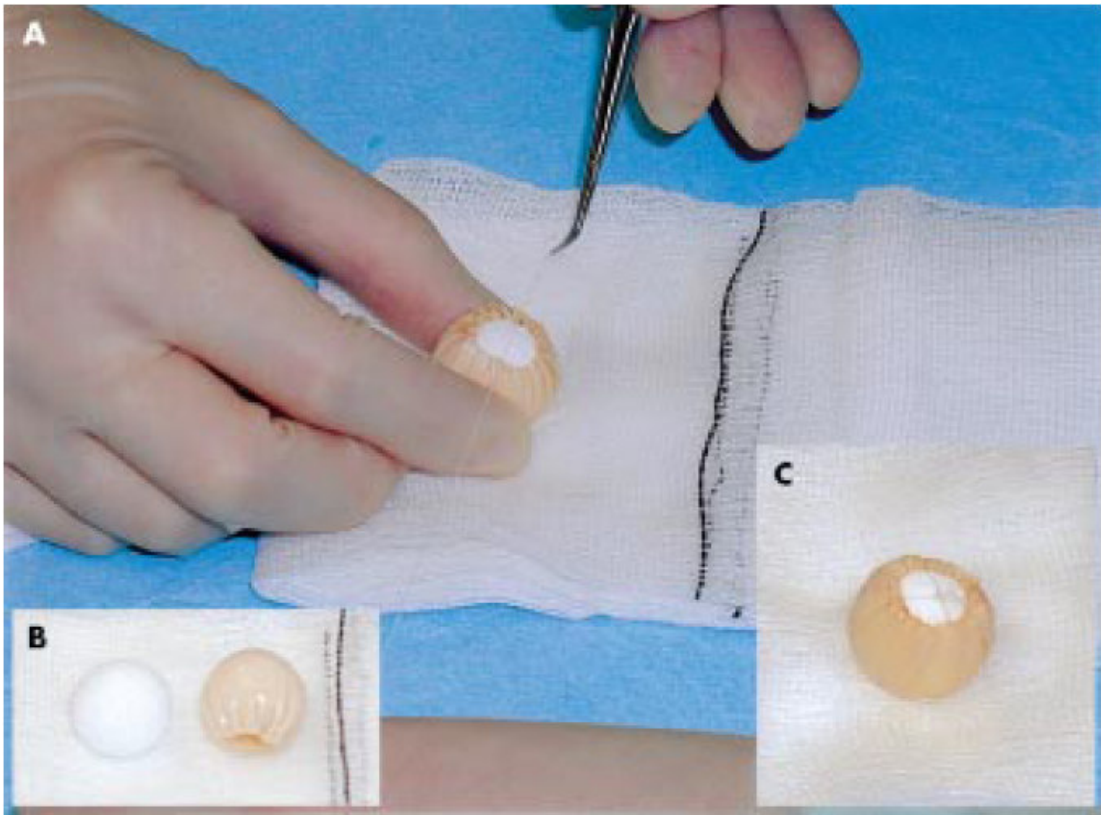

Figure 7.2 (A) Hydroxyapatite implant wrapped in bovine pericardium with ends of the wrap being anchored with suture. **(B)** The hydroxyapatite implant and the bovine pericardium wrap shown separately. **(C)** The wrapped implant ready for implantation [60].

8. PEG & SLEEVE

8.1 Overview of Peg and Sleeve

A benefit of using porous orbital implants is the extensive porous system permitting fibrovascular ingrowth, which theoretically may help decrease the risk of implant extrusion and infection. Additionally, with drilling and peg insertion, this implant can be directly coupled to the prosthesis, allowing a wide range of prosthetic movement, especially fine darting eye movements commonly seen during conversational speech. These movements impart a more lifelike quality to the prosthetic eye.

Peg placement, however, is usually delayed (usually 6 months) until the implant shows a high degree of fibrovascularization ingrowths, as established by objective imaging studies, such as a bone scan or magnetic resonance imaging scan [62]. MRI scanning appears to be the more accurate way of assessing vascularization. Pegging entails a second surgical procedure as seen in Figure 8.1. Many individuals are pleased with their prosthetic movement, electing to avoid the additional surgery, expense, and potential risks involved with implant drilling and peg insertion. Furthermore, complications associated with secondary pegging have gradually emerged in successive period [63].

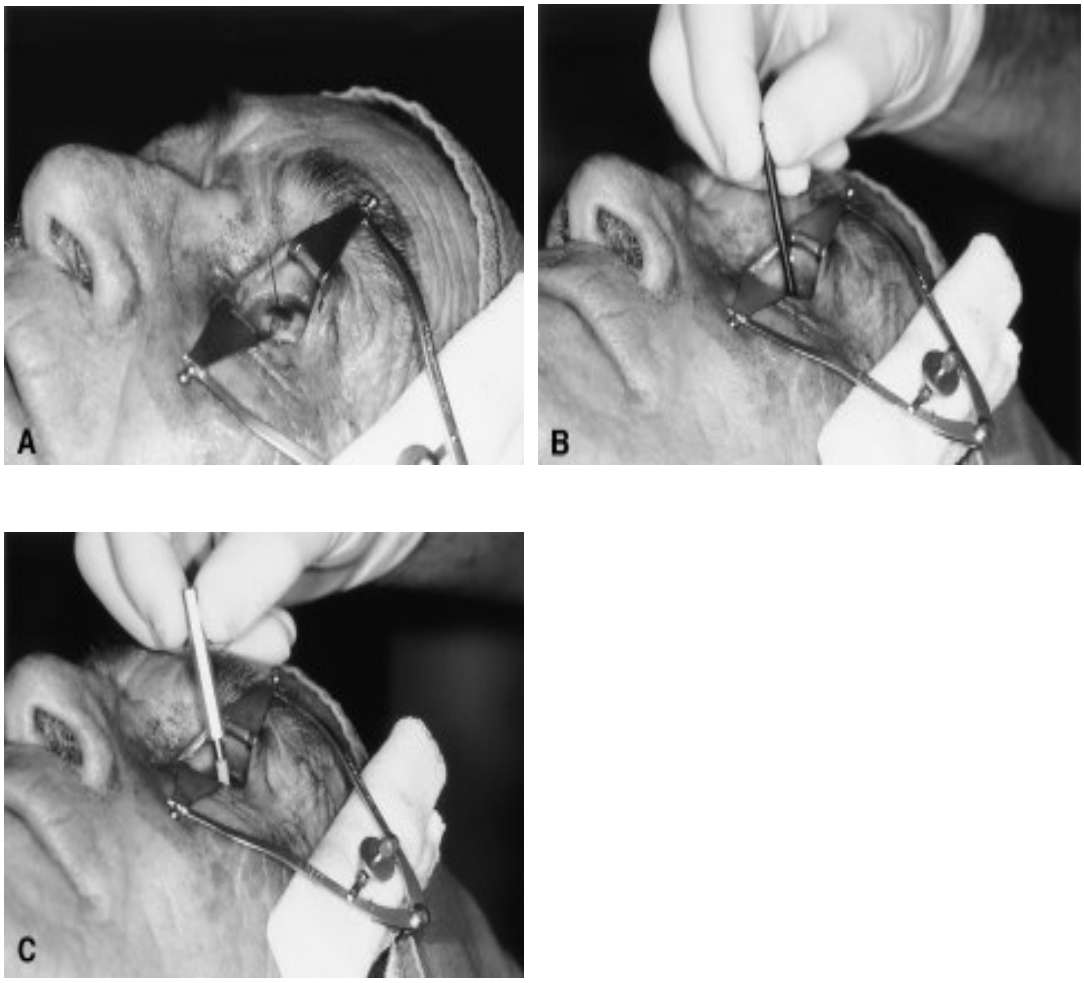

Figure 8.1 A. A pilot hole is made into the implant with a needle. **B.** The pilot hole is enlarged with a handheld drill bit. **C.** Hydroxyapatite- coated sleeve is screwed into the implant [62].

Pegging HA implants may be performed to improve motility. The peg system most commonly used over the past few years involves a polycarbonate peg by itself or a polycarbonate peg and sleeve system. Problems with this peg included difficulty inserting and removing it from healed conjunctival tissue and discomfort for the patient [62]. To obtain a more secure fit of the orbital implant and peg to the prosthesis, a modification of the ball-insocket peg design resulted in a peg-and-sleeve system (Figure 8.2). After drilling of the hydroxyapatite implant, a sleeve is screwed into the implant in an attempt to better fitting of the peg. Afterwards ball headed peg is inserted into the sleeve in a way that ball headed portion of the peg remained protruding above the conjunctiva [63].

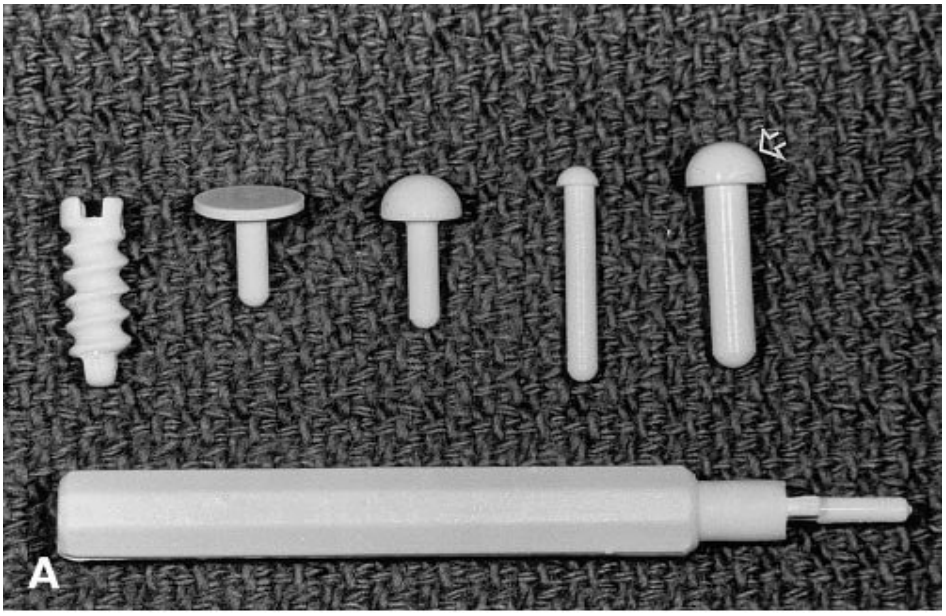

Figure 8.2 The original polycarbonate peg (arrow) is shown adjacent to the more commonly used pegs and sleeve system [62].

Complications associated with pegging HA orbital implants using a polycarbonate peg were thought to be result of a tissue response to the polycarbonate peg material. This fact stimulated the investigation of new peg materials that may be more biotolerant with human tissue. The search for an ideal peg is still ongoing, and new peg designs are continually being developed in an attempt to improve motility, improve host tolerance, and decrease problems encountered. A new hydroxyapatite-coated titanium sleeve with corresponding titanium peg was produced for this purpose (Figure 8.3) (FCI, Cedex, France) [62].

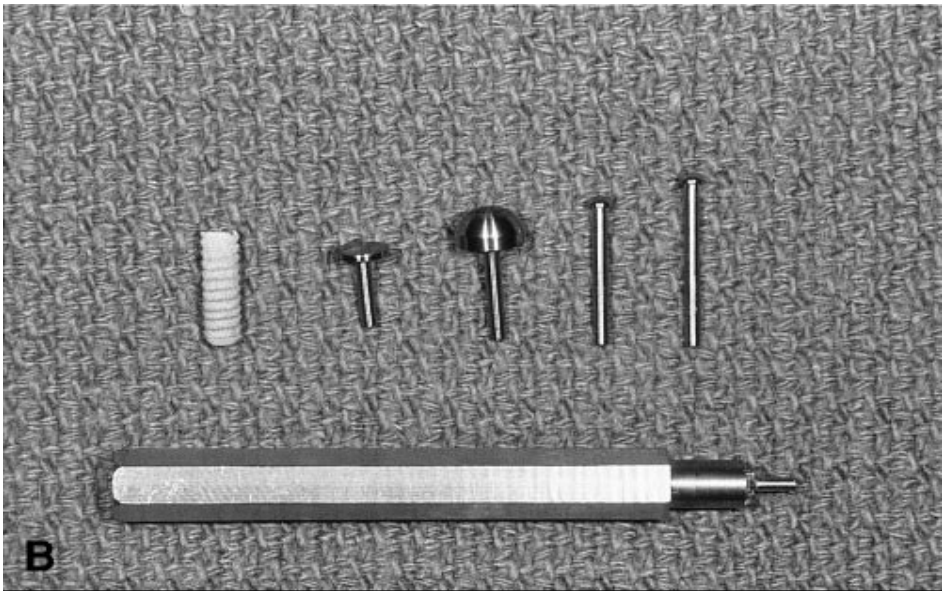

Figure 8.3 Hydroxyapatite coated titanium sleeve and titanium pegs [62].

9. ARTIFICIAL EYE & CONFORMER

9.1 Overview of Artificial Eye and Conformer

An artificial eye (ocular prosthesis) is used to restore the natural appearance of the eye and surrounding tissues, and is the visible part of the surgical changes to the socket (Figure 9.1 .A). It is molded to fit between the eyelids over the conjunctiva that covers the orbital implant. The prosthesis can be removed and polished on a regular basis. Artificial eyes are usually made of acrylic or glass. Custom artificial eyes are hand-crafted by highly skilled ocularists (eye makers) to precisely match the look of the natural eye [34].

This prosthesis is generally placed two to six weeks after enucleation, in order to allow the socket tissues time to heal adequately. Prior to that time, a thin plastic plate (conformer) is usually worn in place of the prosthesis (Figure 9.1.B). This conformer helps to prevent shrinkage of the space between the inner surface of the lids and the conjunctival covering of the ball implant. Until the ocular prosthesis is fitted, the upper eyelid may be droopy. The prosthesis supports the eyelid and generally allows the lids to open and close normally [36,62].

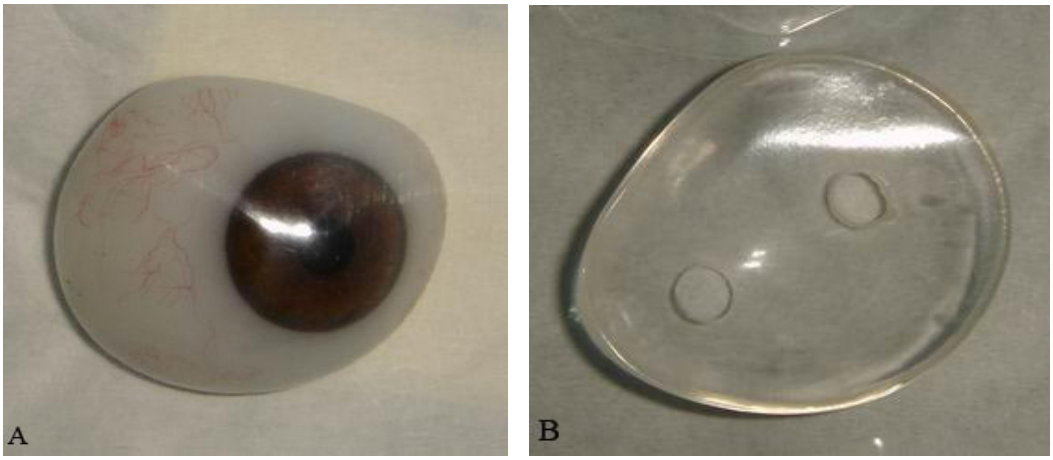

Figure 9.1 A. Artificial eye (ocular prosthesis), B. Conformer

10. COMPLICATIONS

10.1 Postoperative Complications

10.1.1 Exposure

Due to several causes, the anterior surface of the implant under the conjunctiva and tenon's layer becomes visible (Figure10.1). Exposure is most widely encountered complication after implantation of orbital implants [37, 65, 66].

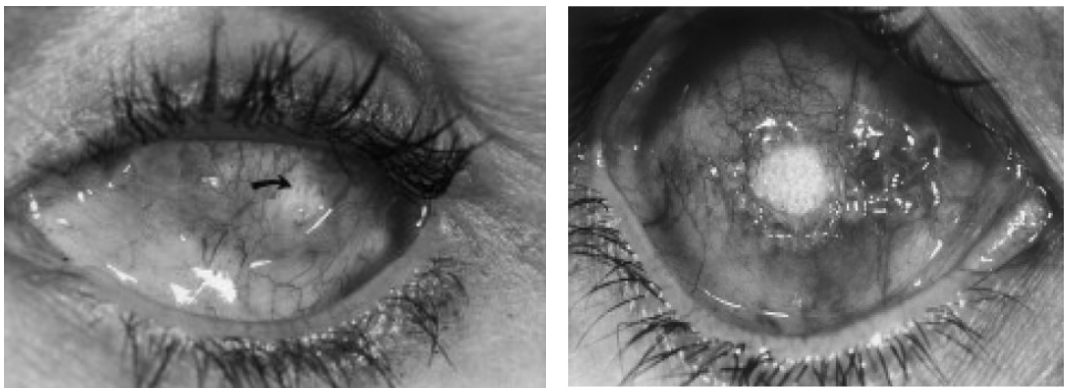

Figure 10.1 Left; Small exposure noted 3 months after enucleation. **Right;** Large exposure noted 7 months after evisceration. Temporalis fascia graft was required.

Predisposing factors to exposure include closing the wound under tension, inadequate or poor wound closure technique, infection, mechanical or inflammatory irritation from the speculated surface of the porous implants like HA [66,67]. Several of these factors are technique-related rather than implant-related. It is believed that appropriate implant placement and proper tissue closure are of primary importance in preventing porous implant exposure. When properly placed in the orbit, the HA (or any implant) must sit in the socket with no tendency to spontaneously move forward. If it does, it must be repositioned and seated within the socket tissue.

Rosner et al and Nunery et al have documented an orbital inflammatory response to hydroxyapatite implants, which is characterized by a foreign body giant cell reaction. This inflammatory response may lead to increased implant exposure [64].They hypothesize that

this reaction may be more abundant in children. For exposures of less than 3 mm, observation may suffice; however, in larger exposures, the use of free autogenous tissue grafts is recommended [67].

Wrapping of the orbital implant, especially autologous tissue, and a multilayer closure reduce the possibility of implant exposure. Exposure problems are not limited to the porous implants [35,37].

10.1.2 Orbital Infection

Orbital infection is a rare complication of enucleation, but it can lead to wound dehiscence. It can be characterized by edema and persistent pain [65]. Meticulous handling of tissues and clean surgical technique combined with systemic and topical antibiotics for at least 5 to 7 days postoperatively will minimize the possibility of infection. Infection may require removal of the implant, local and systemic antibiotics, and then implant replacement.

10.1.3 Superior Sulcus Deformity

A superior sulcus deformity, which is caused by loss of orbital volume and relaxation of tissues within the orbit, manifests as a deep groove or space between the upper eyelid and orbital rim, giving the appearance of dropped eye lid (ptosis) and sunken eye (Figure 10.2). It could be treated with the choice of larger implants or surgical operation [65, 66].

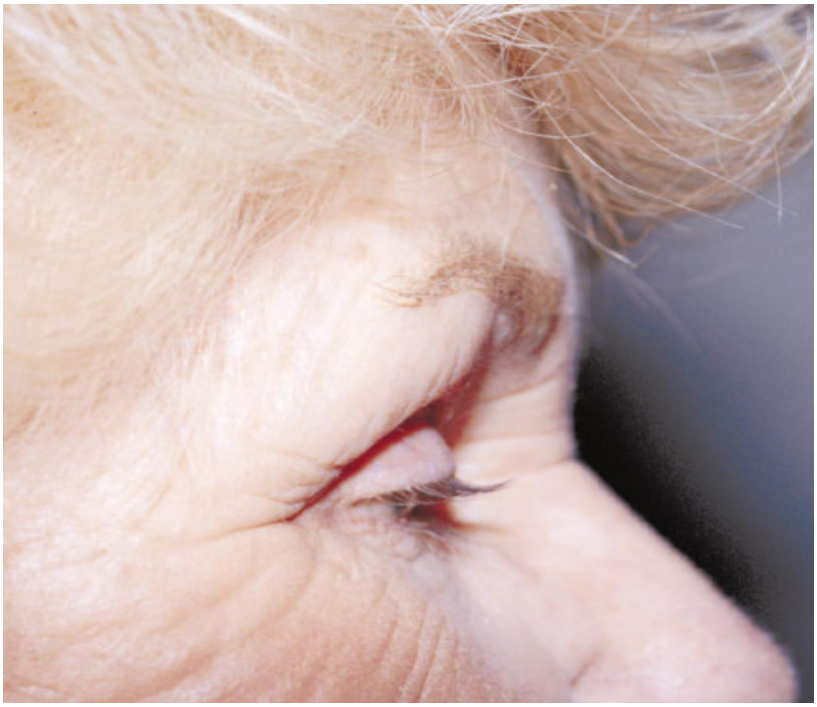

Figure 10.2 A side view of the right eye demonstrates a superior sulcus deformity [65]

10.1.4 Pyogenic Granuloma

Pyogenic granuloma is a disorder that may involve the skin and mucous membranes. Histopathologically, it is composed of a vascularized overproliferation of granulation tissue. It could be observed due to variety of reasons such as inflammatory response to foreign material [66].

10.1.5 Wound Dehiscence

Because of low tissue strength and poor wound healing wound dehiscences may occur after implantation. Goldberg and associates described six cases of conjunctival dehiscence overlying the hydroxyapatite implant and hypothesized that spicules of the implant inhibited epithelialization. The rough surface of the hydroxyapatite implant can make insertion slightly more difficult and may be implicated in conjunctival dehiscence [35,66]. Moreover, unlike silicone or PMMA spheres, exposure of Hydroxyapatite implants did not imply eventual extrusion or infection. Conservative therapies, such as

topical antibiotics, conjunctival edge freshening, high posterior vaulting of the prosthesis, and scleral patch grafting, resulted in satisfactory outcomes.

10.1.6 Extrusion

The orbital implant may come out due to excessive scarring or infection. Surgical correction with replacement of the implant can be carried out when the infection resolves. Extrusion may require the loss of orbital implant [40].

10.2 Complications After Pegging

Although pegging the porous orbital implants improve the range of prosthetic movement and gives a lifelike quality to the prosthetic eye, pegs have their own set of problems and complications [62]. Most peg problems and complications are minor but may require either drops, prosthetic adjustment, or a minor surgical procedure. Some peg problems are recurrent and occasionally serious (implant infection) and require either peg removal, implant removal, or both. The implant exposure rate after peg placement, considering all types of pegs, is much higher than the exposure rate in unpegged implants [68].

Reported peg complications include granulation tissue in the peg hole pushing the peg out, peg falling out spontaneously, peg hole drilled on an angle, tissue overgrowth of the peg, conjunctiva overgrowing the peg hole, clicking with prosthesis movement, sleeve positioned on an angle, sleeve sitting above the conjunctival layer, hydroxyapatite exposure around the peg hole, nonspecific infection of conjuctiva, conjunctival edema, postoperative pain, and a broken peg. (Figure 10.3) demonstrates some of the common peg problems encountered in Ti peg system for HA porous orbital implants [69].

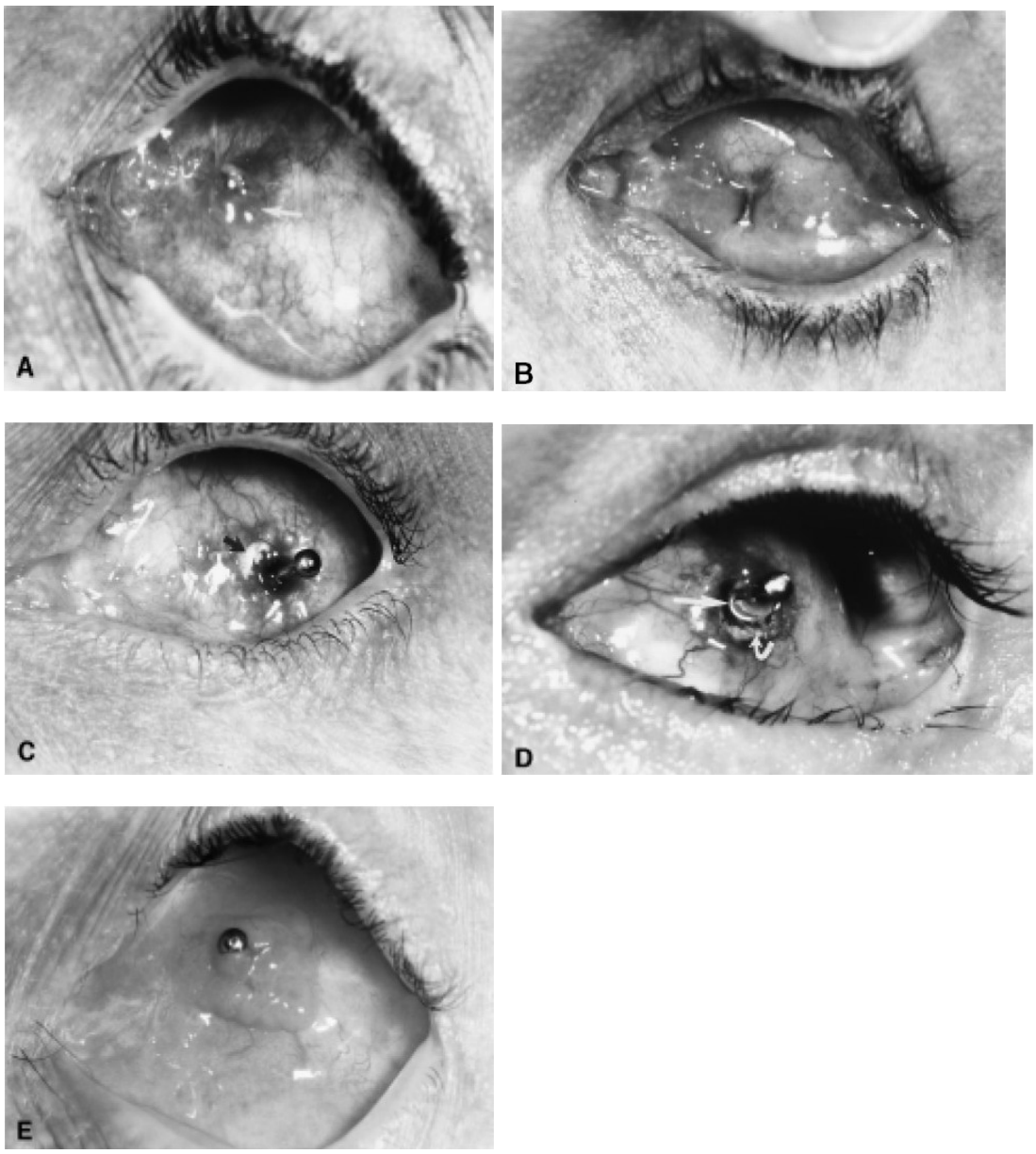

Figure 10.3 A. Titanium peg came out with removal of prosthesis and conjunctiva grew over titanium sleeve (arrow). **B.** Titanium peg is angled downward preventing proper coupling to artificial eye (patient is looking straight ahead). **C.** Hydroxyapatite (HA) implant is exposed adjacent to titanium peg system (arrow). **D.** Sleeve shaft visible (straight arrow), HA visible (curved arrow). Entire sleeve was loose. **E.** Pyogenic granuloma around titanium peg [62].

11. EXPERIMENTAL STUDY

11.1 Fabrication of Specimen Orbital Implants

Hydroxyapatite (HAp) powder required for this study was provided by synthetically derived HAp powder produced by Alfa Aesar Comp. HAp powder with a particle size of 1-15 µm and appropriate quantity of naphthalene powder (300 µm size) were mixed by repeated sieving. In order to have varying amounts of porosity and pore size, naphthalene was added with different ratios as seen in (Table 11.1). Measurements were performed by precision balance (Soehnle, Germany). Ceramic binder composed of distilled water and polythylene glycole was than added to mixture and the blend was mixed on a glass surface by means of a spatula.

Table 11.1 Composition of the specimens

	Weight of Hydroxyapatite (g)	**Weight of Naphthalene(g)**
%20 Naphthalene	5	1
%30 Naphthalene	6,9	2,1
%40 Naphthalene	5,4	3,6
%45 Naphthalene	4,95	4,05
%60 Naphthalene	3,6	5,4

%20 naphthalene supplemented specimen was shaped separately by hand (Figure 11.1). The diameter of this specimen was 22 mm and it was sintered at 1180 °C for 2 hours in the chamber furnace (Carbolite HTF 17). The specimen was heated from room temprature to 1180 °C as seen in Figure 11.2. Here, the contraction and porosity formation characteristics of the sphere were determined. On the basis of data collected, the mould made of gypsum plaster was fabricated.

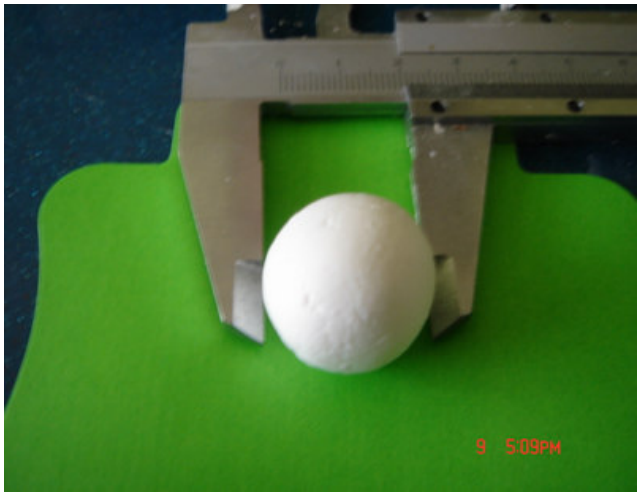

Figure 11.1: %20 naphthalene added HAp specimen implant before sintering

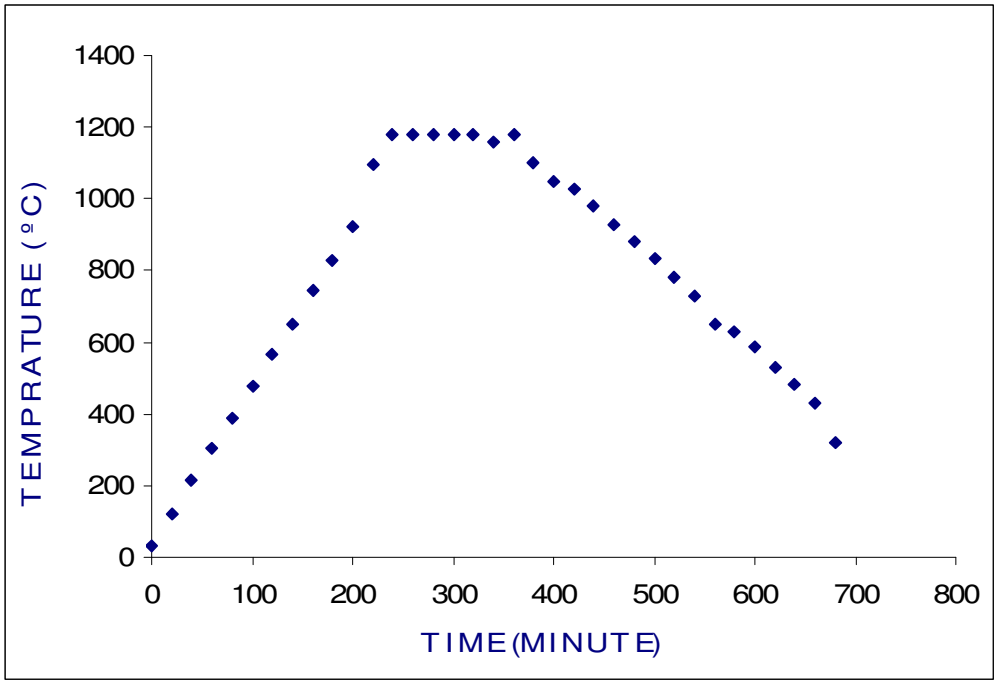

Figure 11.2 Temprature time curve of %20 naphthalene added specimen

%30, %40, %45 and %60 naphthalene supplemented specimens were shaped by the mould. Four implant specimens having a diameter of 26,5 mm were sintered at 1200 °C for 3 hours in the chamber furnace (Carbolite HTF 17) (Figure 11.3). After sintering the specimens were cooled in the furnace.

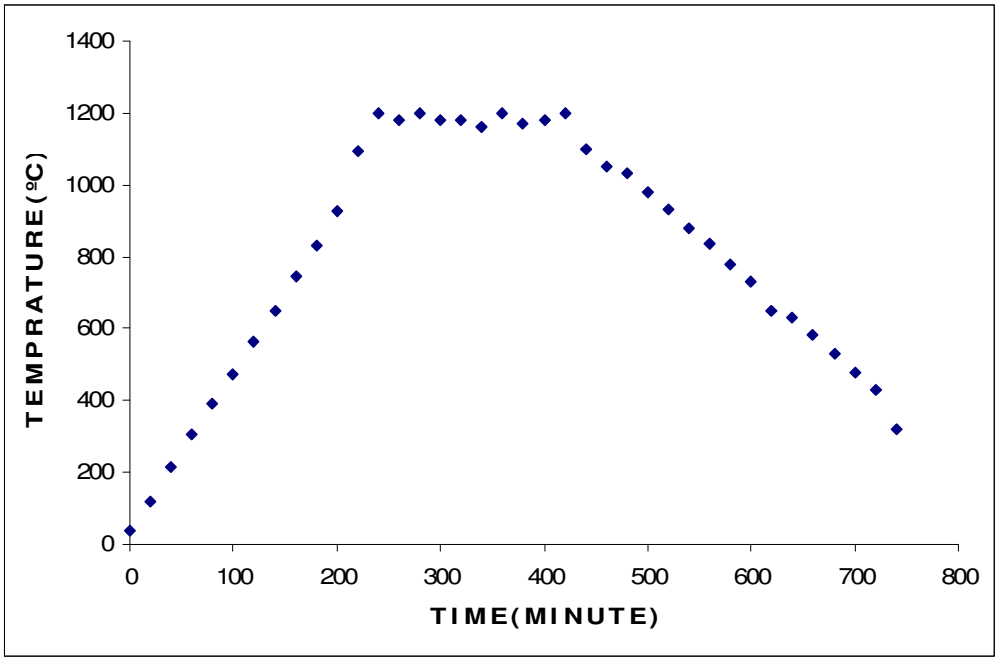

Figure 11.3 Temprature time curve of %30, %40, %45, %60 naphthalene added specimens

11.1.1 Mould Design & Shaping Specimen Implants

A simple mould made of gypsy plaster has been designed to shape the sample implants more precisely and smoothly. After sintering, the volume contraction rate of %20 naphthalene supplemented specimen was approximately found to be % 45. In order to have 20 mm sample implant in diameter, the inner diameter of the mould was foreseen to be between 25-27 mm. In this way, the diameter of the spheres to be fabricated was expected to be 20mm after sintering.

In order to shape the mould, a marble having a diameter of 26,5 mm was used. Gypsy plaster mixture was casted into cylindrically shaped, one side open container and the marble was than embedded in the gypsy plaster (Figure 11.4).

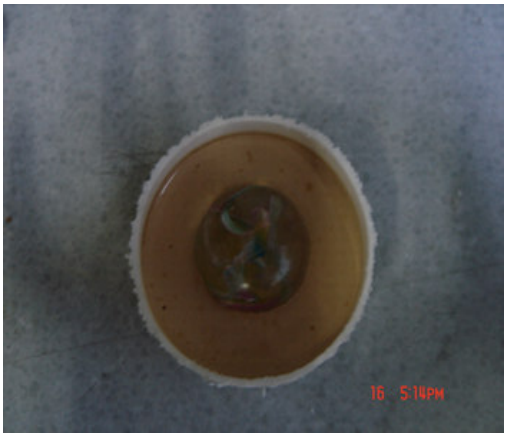

Figure 11.4 Embedded marble in the gypsum plaster

The same process was repeated for the other part of the mould and two pieces of the mould were dried about 3 hours for hardening. After the hardening process, the notches were formed in order to clamp two pieces (Figure 11.5).

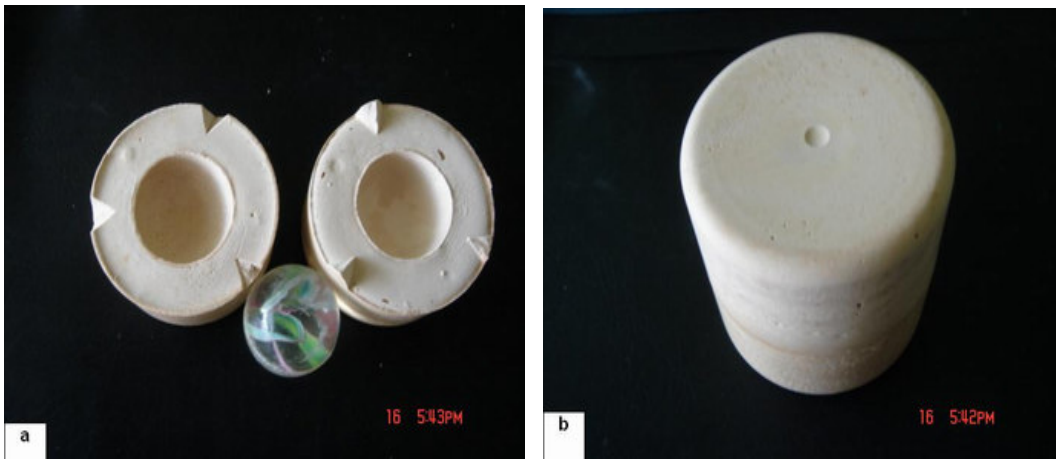

Figure 11.5 a) Gypsum plaster mould made up of two pieces **b)** Closed view of mould

The specimen implants supplemented with %30, %40, %45, %60 naphthalene, were shaped by means of mould. The mould was put in water so as to saturate the mould to water. The inner surfaces of mould pieces were polished so as to facilitate

the come out of the samples. In order to let the excessive ceramic go out, channels were formed on the surface of the mould. The ceramic mixture was than compressed and the excessive ceramic was forced out (Figure 11.6). Consequently, four specimen implants having a diameter of 26,5mm and having varying amounts of naphthalene were formed.

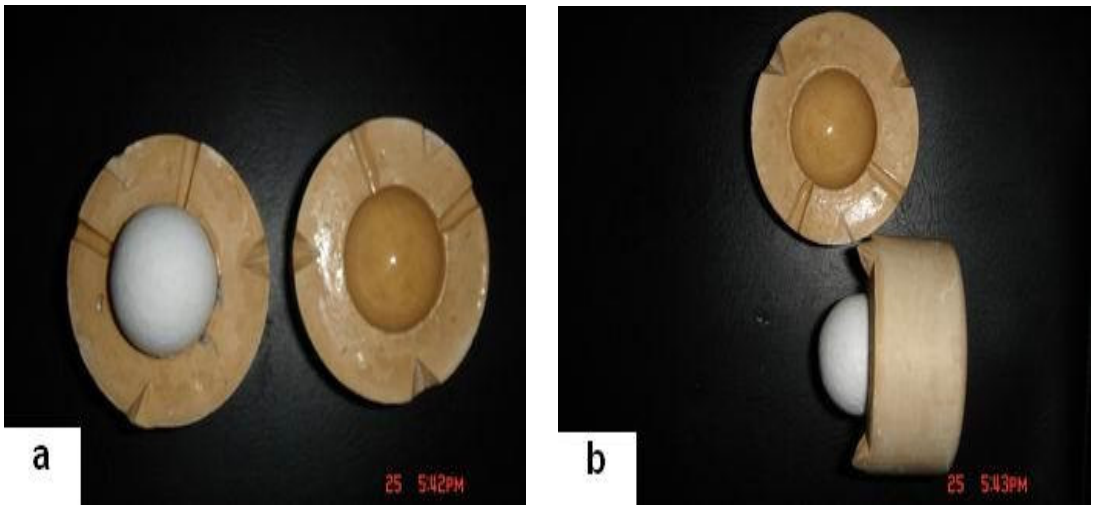

Figure 11.6 a,b) HAp specimen implant shaped by mould

11.2 Implant Characterization

X-ray diffraction analysis and IR spectra analysis were performed to evaluate chemical composition and phase purity of sample implants. The pore morphology and pore size distribution of the samples were investigated by scanning electron microscope (SEM). Besides, physical properties of sample implants like weight, bulk density, volume contraction and percent of porosity were measured. As a mechanical test compressive strength of the specimens were examined.

X-ray diffraction analysis (Bruker D8 Advanced Diffractiometer) was performed using monochromatic Cu $K_{\alpha\,1}$ radiation at 55 mA and 40 kV. The sintered specimens were crushed and the powders were compared with respect to starting powder to find out whether there is a phase change after sintering process.

IR spectrum analysis (Mattson Instruments FT-IR 3020) was performed by KBr pellet method. The infrared spectrum of the samples were recorded within the range of 400-4000 cm^{-1}. The sintered samples were crushed and the powders obtained were analyzed with regard to starting powder to compare these characteristics of the final product to that of the starting material.

The pore morphology and pore size distribution were examined by SEM (JEOL JSM 6060LW). Prior to taking SEM images, the sample implants were broken in order to observe the pore morphology and pore size distribution properly. The samples were ultrasonically cleaned in acetone for about 1 min and then the infrared dried samples were sputter coated (SC 7620, Polaron) with gold for 3 min to get a coating thickness of ~ 50nm. Thereafter, the inner parts of the sample implant surfaces were investigated by SEM.

Physical properties of sample implants were examined. For density and porosity measurements, dry weights of sample implants were measured. The sample implants were then put in distilled water for 10 hrs and wet weights were measured. Weight measurements were performed by precision balance (Soehnle, Germany). Bulk density, porosity and contraction rate were calculated by using below formulas.

V_T (Total Volume) = $4/3 \times \pi \times r^3$ (1)

Vp (Volume of Porosity) = (W-D) (2)

% Amount of Porosity = $(Vp/V_T)x100$ (3)

Bulk Density = $D/(V_T-V_P)$ (4)

Volume Contraction = $(r_1^3-r_2^3)/r_1^3$ (5)

(where W is the wet weight, D is the dry weight, r_1- r_2 are radii before and after sintering)

As a mechanical property, compressive strength of the specimens produced, was investigated. To be able to measure the compressive strength, four cylindrically shaped HAp specimens supplemented with %30, %40, %45 and %60 naphthalene were formed (Figure 11.7). Apart from these specimens, in order to investigate the structural integrity of a spherical implant under the axial force to be applied, a new HAp specimen implant having %55 naphthalene was produced. During the manufacturing process, all of these specimens, similar to those produced for investigating the stability of chemical composition and phases present, were sintered at 1200°C for 3 hours.

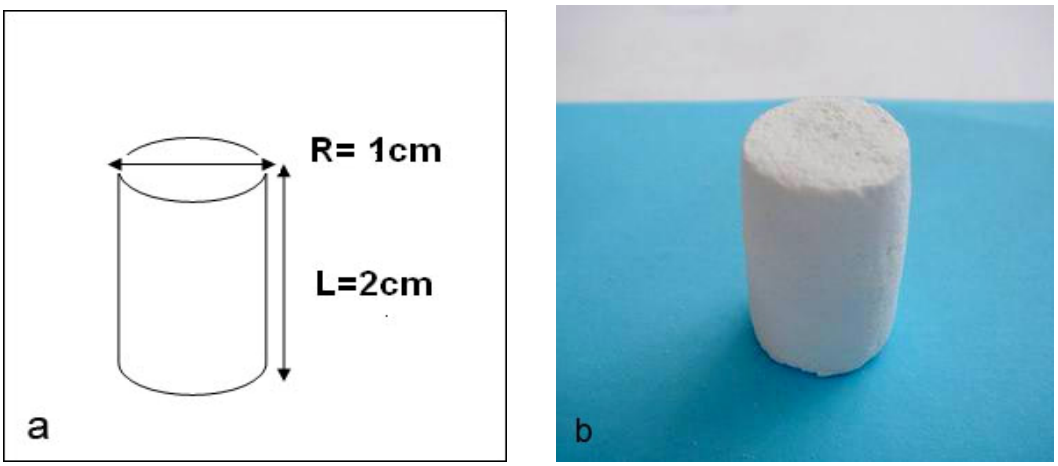

Figure 11.7 a The approximate dimensions of cylindrical specimens. **b.** %40 naphthalene added cylindrical specimen

Compression tests were carried out by using a servo-electrical universal testing system (Instron 4302, Canton, MA, U.S.A) (Figure 11.8). This device could be used for tension compression, and/or fatigue measurements on different materials. The device operates in connection with a computer. Instron Series Software was used for controlling the compression force applied, data acquisition and data analysis. Each specimen tested was compressed at a rate of 0.5 mm per minute. Samples were placed on a plate and a cylindrical apparatus applied vertical force in accordance with the adjustments. Force (Newtons) versus deflection (millimeters) was measured and plotted on a graph.

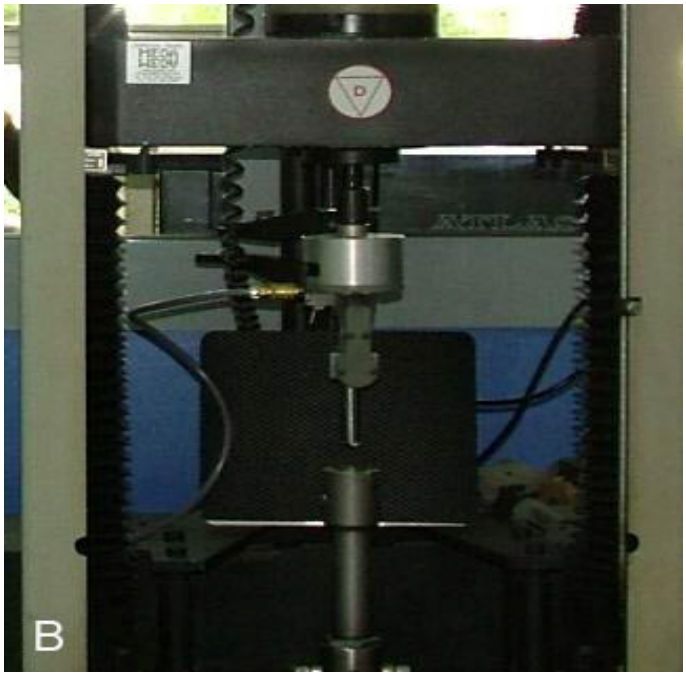

Figure 11.8 A. Specimen compression tests were carried out by using a servo-electrical universal testing system (Instron) **B.** Part of the compression test device on which the specimens placed and the force applied.

12. RESULTS AND DISCUSSION

12.1 Sintering Sample Implants

Sintering temprature is a critical factor influencing the phase stability, densification behaviour, sintered microstructure and hence the mechanical properties of hydroxyapatite ceramics. Thermal stability of hydroxyapatite depends on a number of factors which may, but do not necessarily have to, cause its decomposition. Decomposition of HAp results in the changes in physicochemical properties of the final material as well. It affects the performance of an implant in a living body by changing its solubility, resorption rate and even biocompatibility. Therefore, it is significant to determine accurate sintering parameters.

Calcium phosphate can be crystallized into salts, HAp and tricalcium phosphate $Ca_3(PO_4)_2$, or ß-whitlockite depending on the Ca/P ratio, presence of water, impurities, and temprature. In wet environment and at lower temprature (<900 ºC) it is more likely that the (hydroxyl or hydroxy) apatite will form, whereas in a dry atmosphere and higher temprature the tricalcium phosphate (TCP) will be formed [12,13]. The main difference between these two materials is that (TCP) degrades much faster than HAp. HAp is thermodynamically stable in body fluid, whereas TCP is not stable and resorbed by biochemical reactions under such conditions [15].

Decomposition of HAp to anhydrous calcium phosphate such as TCP, is expected to occur at ~ 1200-1450 ºC [20,23]. Decomposition results from dehydroxylation beyond a critical point. For temperatures below the critical point (1300 ºC) HAp crystal structure retained despite dehydroxylation, and HAp rehydrates on cooling. If the critical point is exceeded, complete irreversible dehydroxylation occurs, resulting in collapse of the HAp structure and decomposition. After the critical point, α-TCP and β-TCP are often formed. In particular, the molecular volume increase that occurs in the β-TCP→ α-TCP transformation seems to be the most deleterious phenomenon for mechanical properties [22].

Rate of temperature increase is another parameter that must be taken into consideration when sintering HAp ceramics. In case of supplement addition like naphthalene is required, the high pace of temperature increase becomes more significant, since high temperature rates results in fast evaporation of the additives and causes cracks in the sintered bodies [24]. During preliminary studies made for determining optimum sintering parameters, the pace of sintering temperature was chosen to be 12-13 ºC min^{-1} and HAp specimen was sintered at 1150 ºC for 4 hours. Due to the high pace of temperature increase and high thermal gradient difference within the specimen, the specimen was broken (Figure 12.2). However the structure of broken pieces were observed to be hard, that is to say after sintering process the broken pieces of HAp were acquired sufficient strength.

Figure 12.2 The pieces of broken specimen due to the high pace of temperature increase and high thermal geradient within the specimen

Regarding the long sintering durations, in order to prevent HAp from decomposition and provide sufficient strength to specimen implants, the sintering temperature was chosen to be between 1150-1200 ºC. The pace of temperature increase was chosen to be 4-6 ºC. To be able to practice sintering conditions preferred, little specimen made of HAp was shaped regardless of paying attention to specifications and sintered at 1150 ºC for 4 hours. After sintering, the sample was come out without any defect and achieved sufficient strength (Figure12.3a). A little hole having a diameter of 2 mm, was drilled by a hand drill to examine the resistance to penetration (Figure12.3b). The hole did not cause any deformation on the surface of the sample.

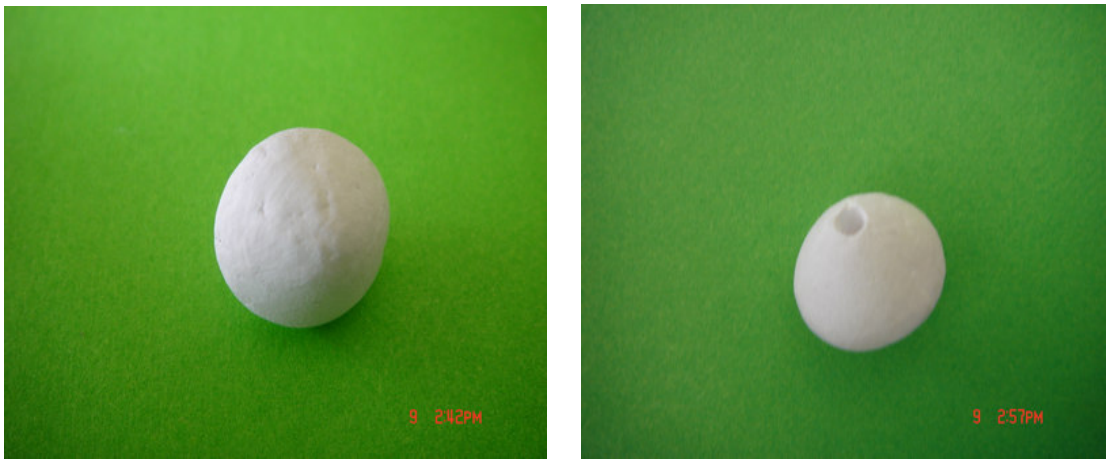

Figure 12.3 a) Sintered HAp sample without any defect **b)** A little hole was drilled by a hand drill on the sample

%20 naphthalene added specimen implant, having a diameter of 21mm, was spherically shaped by hand and sintered at 1180 ºC for 2 hours. After sintering, the diameter of the sintered sample was found to be 16 mm and achieved sufficient strength (Figure 12.4). Depending on the data obtained, the contraction and porosity formation characteristics of the specimen were determined and the mould was designed.

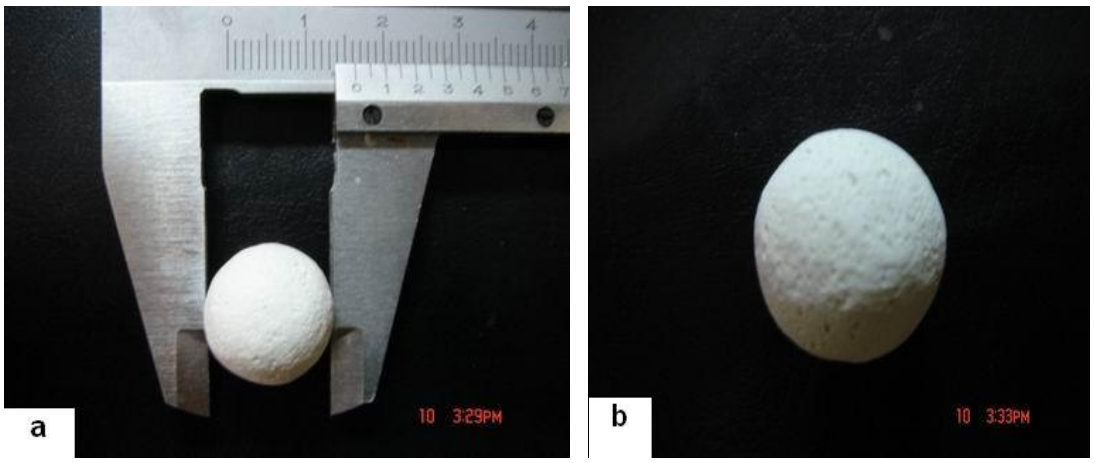

Figure 12.4 a,b) Image of a %20 naphthalene added specimen implant sintered at 1180 ºC for 2 hours

The specimens supplemented with %30, %40, %45 and %60 naphthalene, were spherically shaped by mould and sintered at 1200 ºC for 3 hours. %30, %40 and %45 naphthalene added specimen implants were sintered without any defect as seen in Figure 12.5 (a)-(c) respectively. All three specimens have achieved sufficient strength after sintering.

Figure 12.5 a,b,c) Image of a %30, %40 and %45 naphthalene added specimen implants respectively **d**) All three specimen implants are together

However, %60 naphthalene added specimen implant has deformed and spherical shape couldn't be preserved after sintering. Due to the high amount of naphthalene addition sufficient strength couldn't be obtained (Figure 12.6). The structure of the specimen implant was prone to be dissipated and was found to be fragile.

Figure 12.6 %60 naphthalene added, deformed specimen implant sintered at 1200 ºC for 3 hours

12.2 Physical Properties

Bulk densities, weight, amount of porosity and contraction rate of implant specimens were examined. In general, the weight and the bulk density of the samples were decreased with increasing rate of naphthalene. On the contrary, the contraction rate and the amount of porosity were increased with increasing rate of naphthalene (Table 12.1).

Since %60 naphthalene added specimen was deformed after sintering, the volume of this specimen was measured by water displacement method i.e. by Archimedes' principle. Amount of porosity, bulk density and contraction rate of the specimens were calculated by the formulas given in section 11.2.

Table 12.1 Physical properties of specimen implants

	Weight (gr)	**Bulk Density ($grcm^{-3}$)**	**Volume Contraction (%)**	**Amount of Porosity (%)**
%30 naphthalene	5,9	1,82	50,3	%35
%40 naphthalene	4,3	1,63	53,7	%47
%45 naphthalene	3,9	1,56	57,1	%54
%60 naphthalene	2,5	1,13	68,6	%72

Compared to theoretical density (3.16 gr cm^{-3}) of HAp, bulk densities of specimen implants were found to be lower. These lower values were attributed to high porosity (%35-%72) of the specimens.

There was an inverse proportion between the porosity and the mechanical strength. Increasing the amount of naphthalene added resulted in mechanically weak and fragile structure. Therefore, this factor restricted further naphthalene addition.

12.3 Mechanical Properties

Compressive strengths of the cylindrical specimens prepared, were investigated. Besides the specimen orbital implant produced for this purpose was tested so as to investigate the structural integrity under axial force. %30 naphthalene added specimen was broken while determining the appropriate force range to be applied. %40, %45, %60 naphthalene added specimens and %55 naphthalene added specimen orbital implant were tested without a problem. The specimens both cylindrical and spherical were placed on a flat surface and they are subjected to

compressive force, applied gradually through the cylindrical rod like apparatus of the device (Figure 12.7, 12.8). Although axial compression as tested in this study is not a force that orbital implants are subjected to in real life, we used axial compression testing as a measure of implant's structural integrity. Besides the results achieved through these tests, could be beneficial to evaluate the capability of these kind of implants to hold a peg.

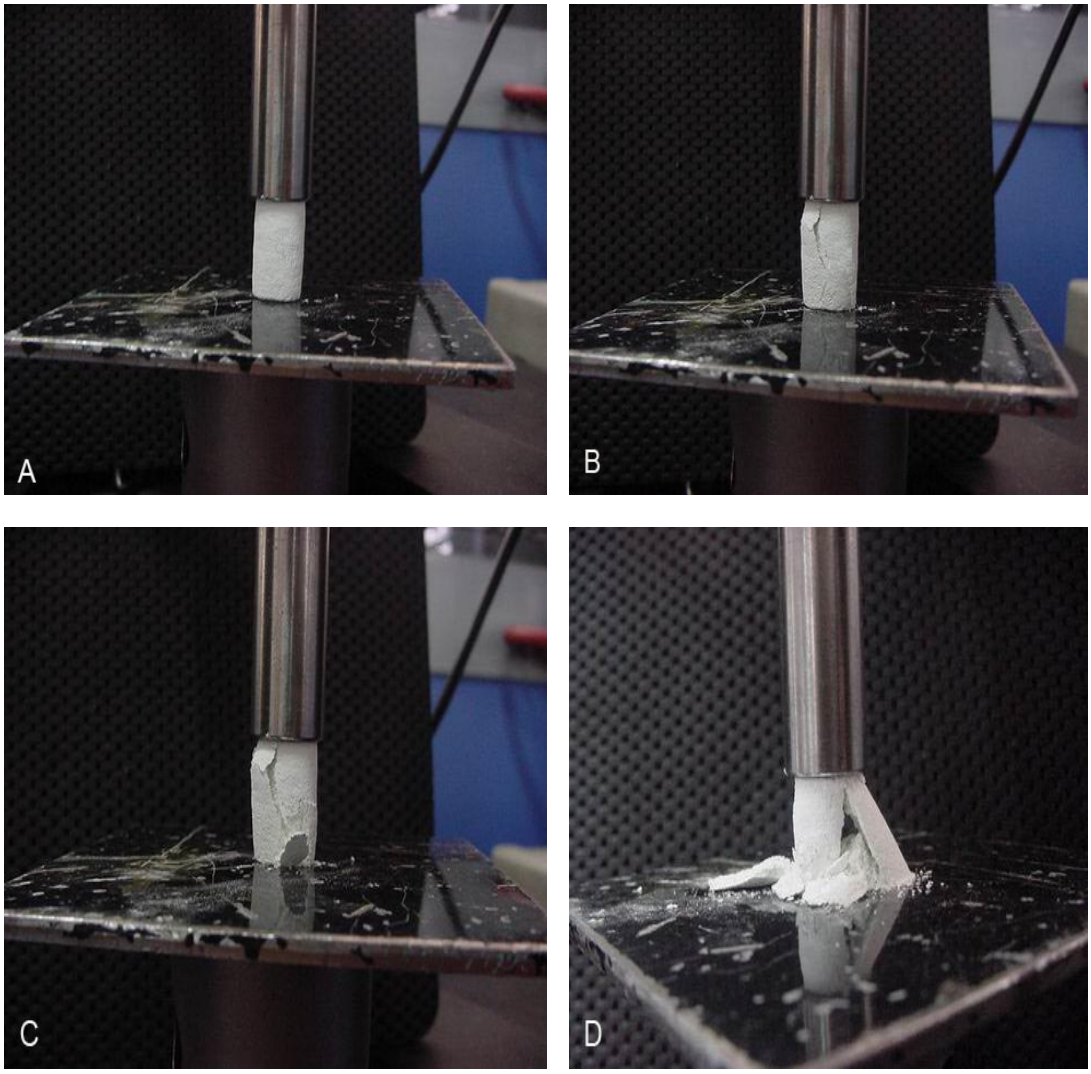

Figure 12.7 A,B,C,D. Compression force is gradually applied until the cylindrical specimens were broken and maximum stress value was determined.

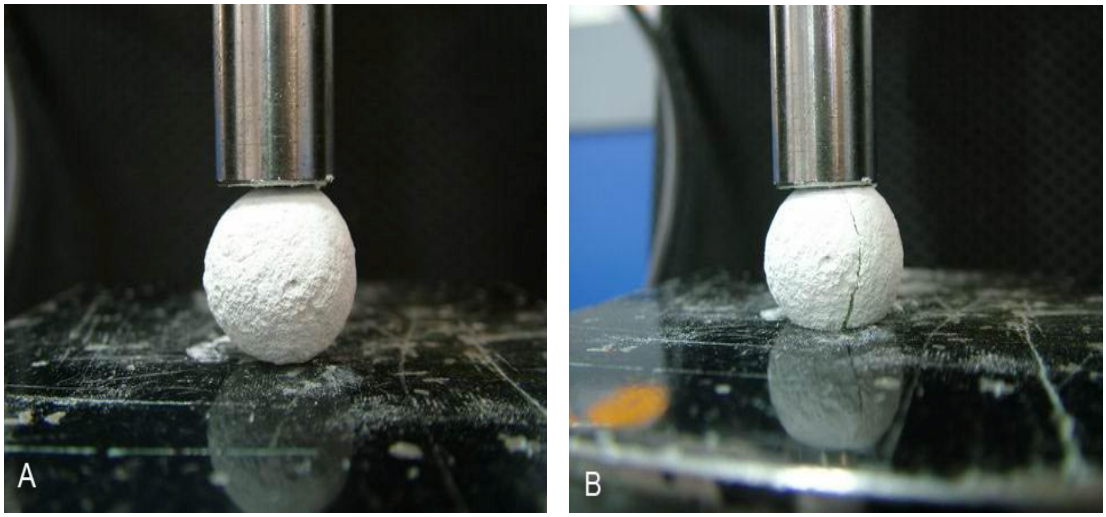

Figure 12.8 %55 Naphtalene added specimen implant was subjected to compressive force until the structural integrity completely lost.

Stress versus strain graphs and force versus deflection graph were plotted for the cylindrical specimens and the specimen implant respectively (Figure 12.9-12.12). The compression device automatically discerns the deformities through the sensors attached on the cylindrical apparatus and once the deformity detected, the device reduces the force being applied gradually so as to clarify the critical point at which the structural integrity completely lost. The highest peaks observed on the graphs referring to the specimens supplemented with %40, %45 and %60 naphthalene, corresponds to the ultimate compressive stress at which the structural integrity completely lost. At this critical point the cracks were observed and the specimens were collapsed. Before that point the specimens preserved their structure except a few minor deformities on their outer surface. Since it was not possible to find out the compressive strength of the %55 naphthalene added specimen orbital implant, the compressive force required to overcome structural integrity was investigated.

The multiple tiny peaks seen with the collapsible specimens are referred to as “pop ins” and represent the early disruption of trabeculae within porous specimens [73]. As the amount of naphthalene added to specimens augmented, the “pop ins”seen on the graph, were observed to be more prominent as expected.

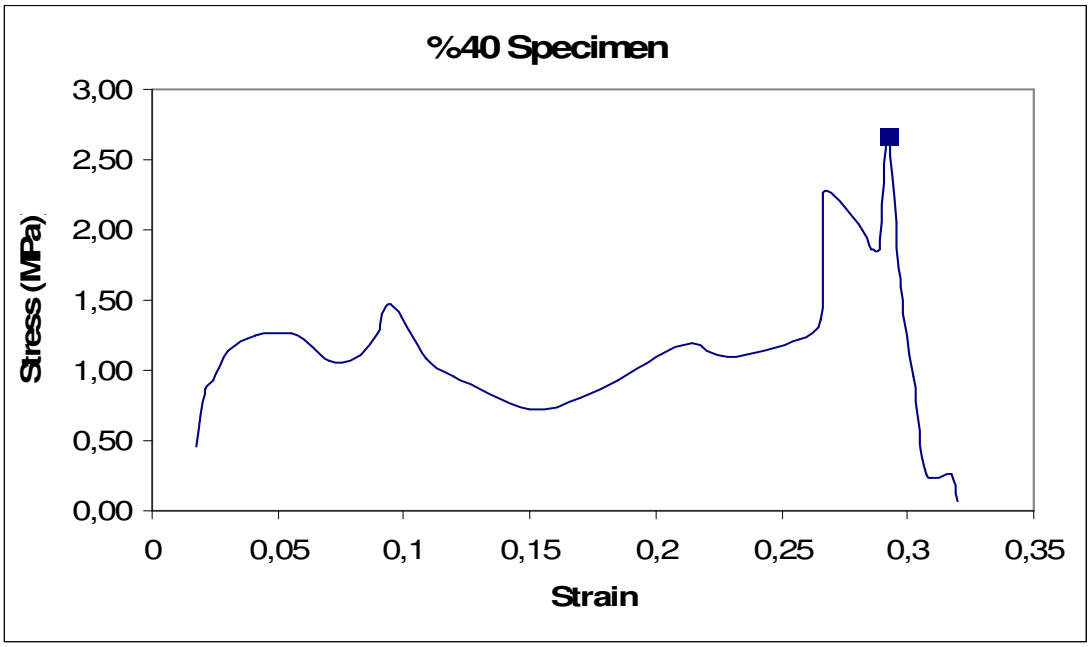

Figure 12.9 Stress versus strain graph of %40 naphthalene added cylindrical specimen.

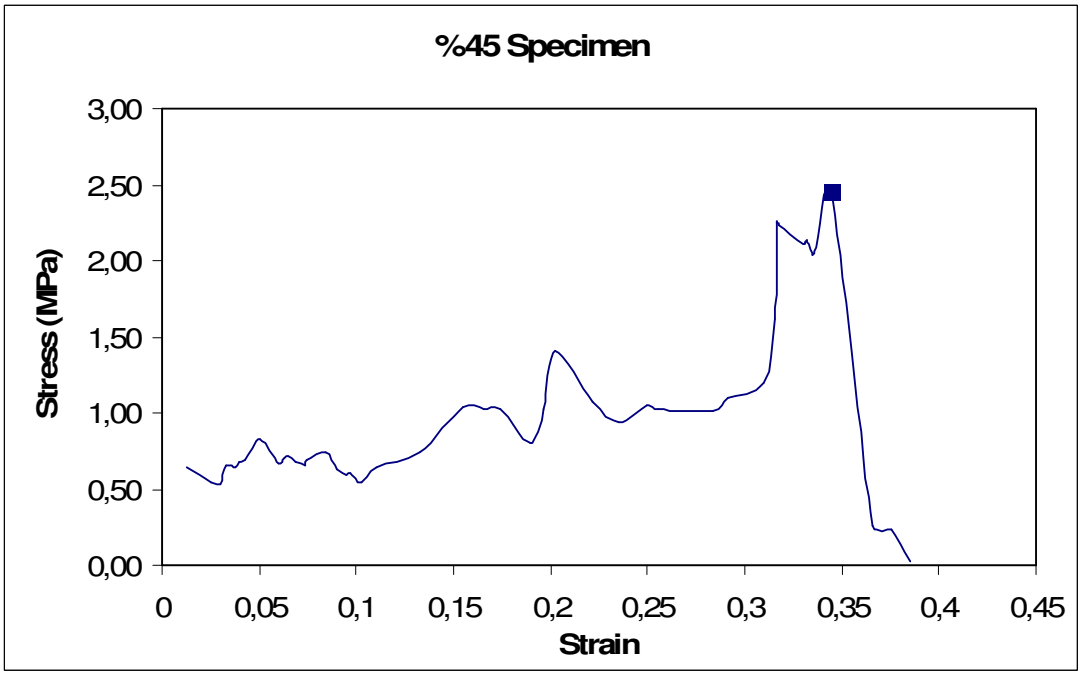

Figure 12.10 Stress versus strain graph of %45 naphthalene added cylindrical specimen

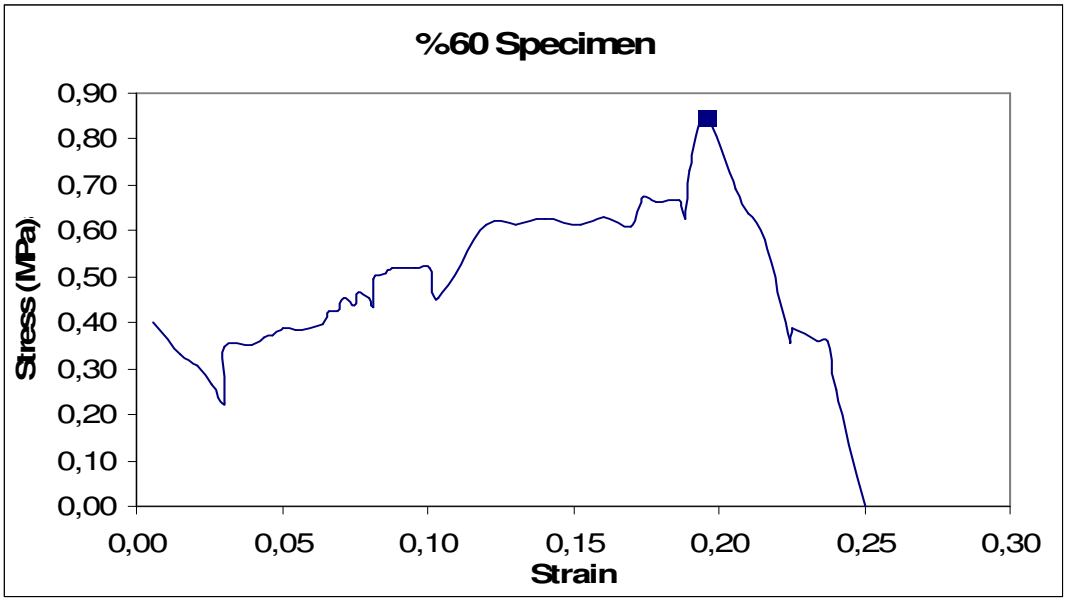

Figure 12.11 Stress versus strain graph of %60 naphthalene added cylindrical specimen

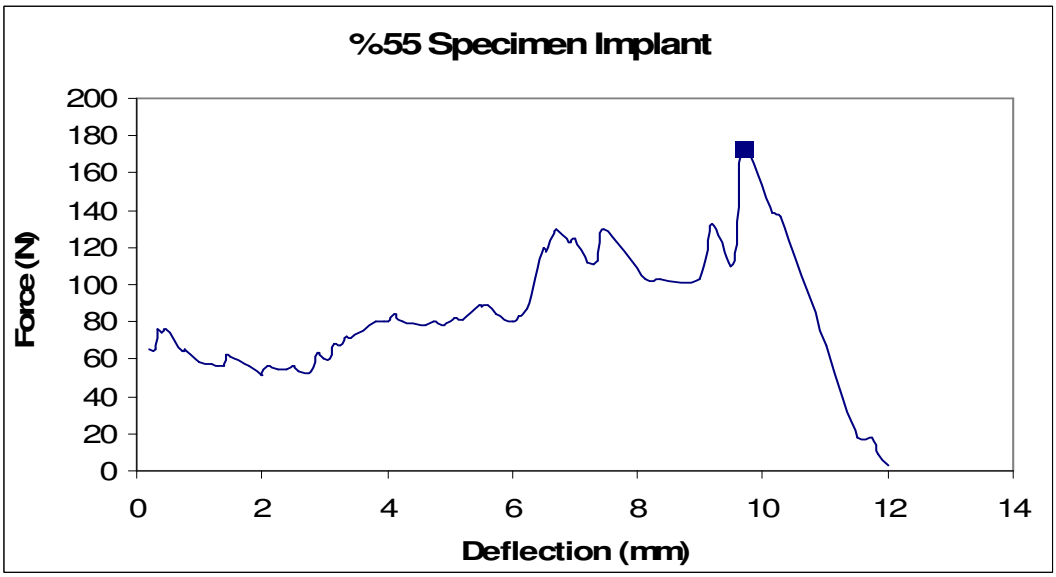

Figure 12.12 Force versus deflection graph of %55 naphthalene added specimen orbital implant

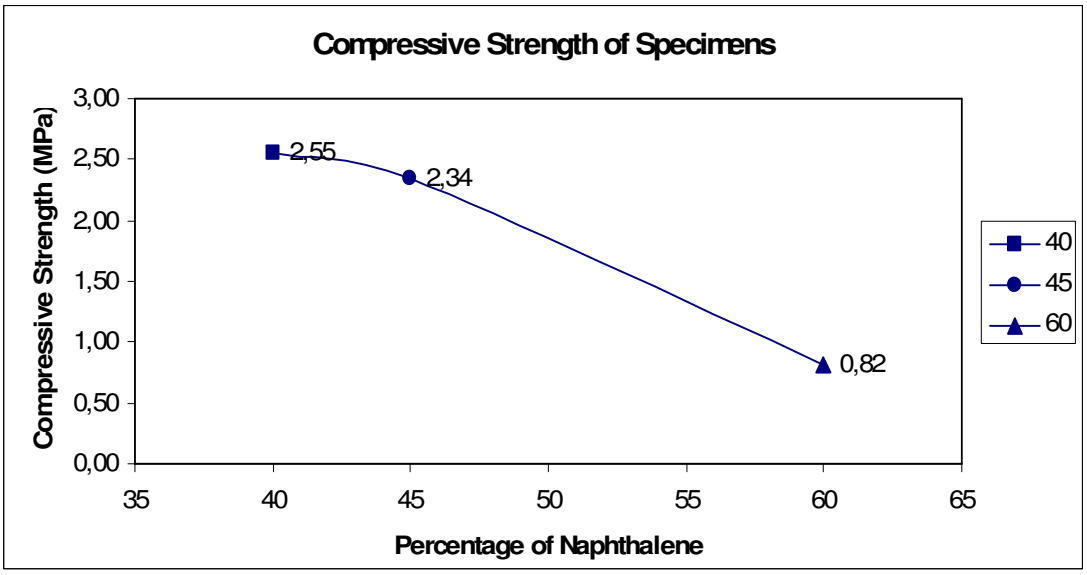

Figure 12.13 Compressive strength of cylindrical specimens (R=10mm,L=20mm, R/L=0,5) supplemented with %40, %45 and %60 naphthalene.

It was clearly observed that increasing the amount of naphthalene added resulted in the decrease on the compressive strength (Figure 12.13). In particular, the compressive strength of %60 naphthalene added specimen dropped considerably. Apart from cylindrical specimens, %55 naphthalene added specimen orbital implant preserved its structural integrity up to the force of 175N (17,8 kgf). When the amount of naphthalene added and the function of the implant in the socket considered, these values were found to be sufficient.

12.4 Powder Characterization

12.4.1 X-Ray Diffraction Analysis

Decomposition of HAp, negatively affects the mechanical properties of the implant. Decomposition products like α tricalcium phosphate (α-TCP), β tricalcium phosphate (β-TCP) and tetra tricalcium phosphate (TTCP) degrades in body fluids whereas HAp is thermodynamically stable within the body [15]. Therefore the presence of these products influences the performance of an implant in a living body

by changing its solubility, resorption rate and even biocompatibility. It is an important problem, both from scientific and application points of view

Both the commercial HAp powder and the HAp samples grinded after sintering, were analyzed by X-ray diffraction so as to compare the phase purity of sintered samples to that of starting powder. Based on the XRD patterns as seen in Figure 12.14 and Figure 12.15, both the sintered HAp and the commercial one, have clear and sharp reflections corresponding to hydroxyapatite, which confirm the phase purity and high crystallinity degree of the samples. The peak broadening on the XRD pattern of starting HAp powder is an indication of the presence of submicron crystallite in the powder [71].

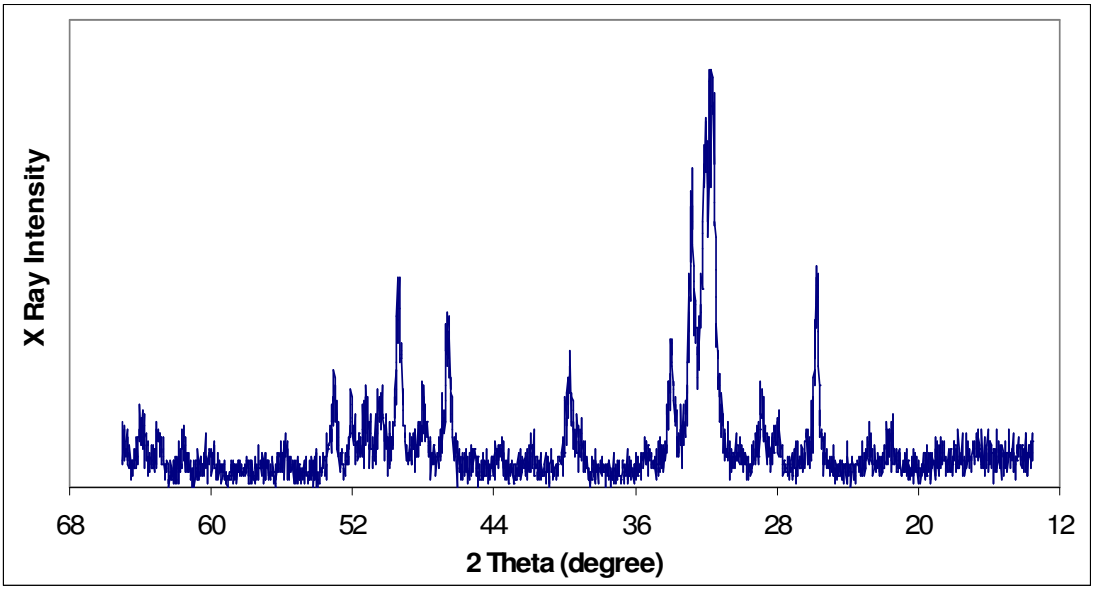

Figure 12.14 XRD pattern of commercial HAp powder

On the XRD pattern of HAp, when certain temperature threshold was exceeded deformation of HAp starts with the reflection peak of α-TCP. As the temperature further increased, reflection peaks indicating the presence of β-TCP and TTCP appear [71]. All these decomposition phases appear between 28-31 theta degree. Apart from these phases, CaO could appear between 35-40 2 theta degree.

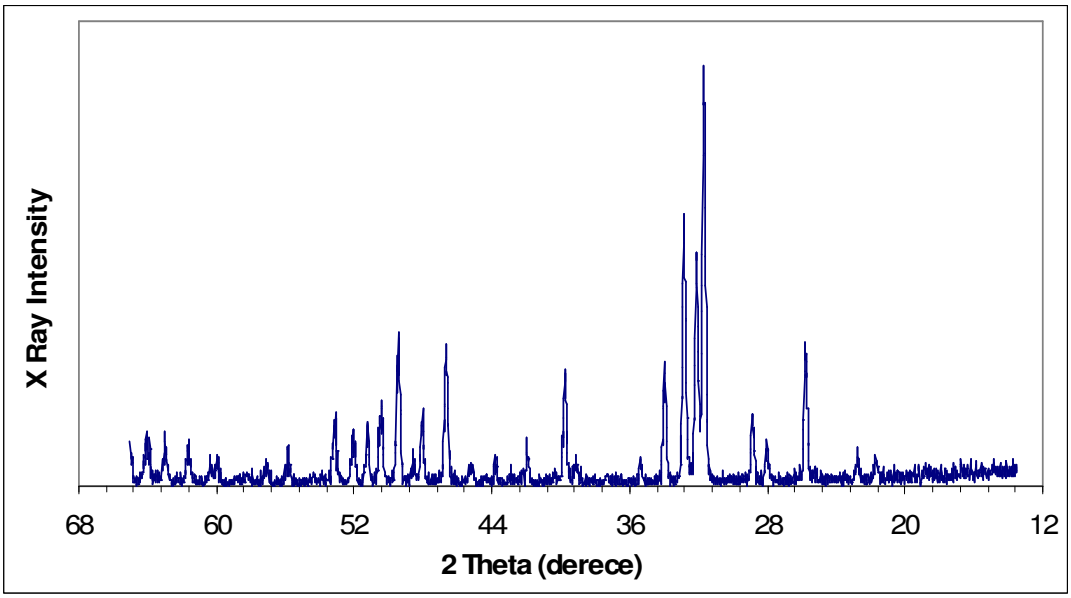

Figure 12.15 XRD pattern of sintered HAp sample

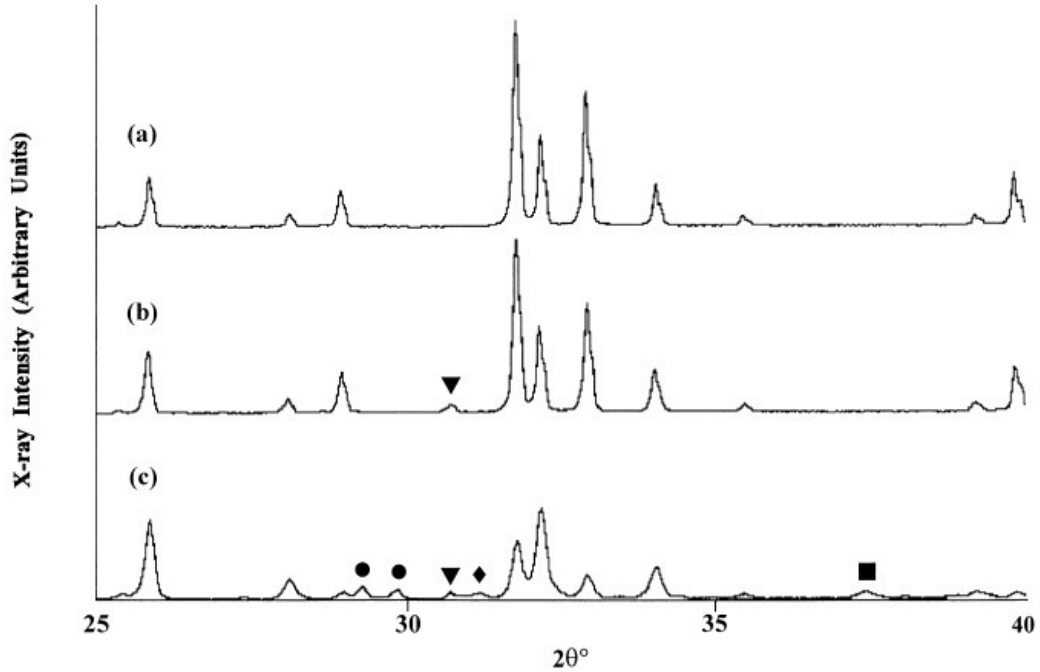

Figure 12.16 a) Normal XRD pattern of HAp **b) Over** critical temperature α-TCP appears **c)** Further temperature increase result in the formation of β-TCP, TTCP and CaO (Key: ●= TTCP, ♦=β-TCP;▼=α-TCP and ■ =CaO) [71].

The formation of decomposition phases in connection with increasing temperature were shown in Figure 12.16. As far as the Figure 12.16 (b) and (c) concerned, triangles above the reflection peaks refer to the formation of α-TCP, circles refer to the β-TCP, rhombus refers to TTCP and the square refers to CaO presence in the phase composition.

In order to find out whether the indication of these decomposition phases found in the sintered sample, XRD pattern was analysed within the appropriate range as shown in Figure 12.17. As it was clearly seen, there was no diffracted peak of α-TCP, β-TCP and TTCP in the specified region.

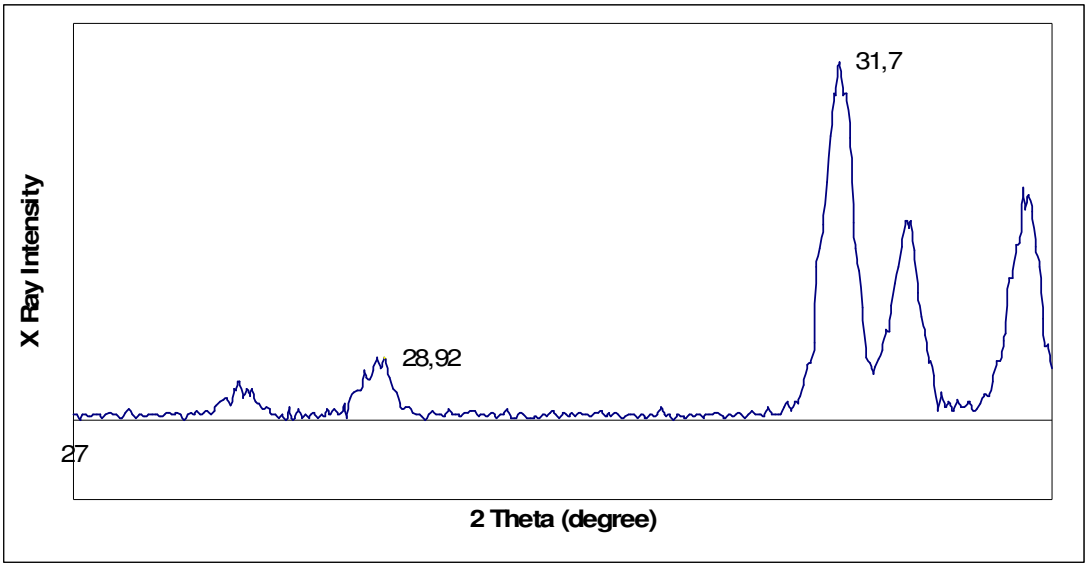

Figure 12.17 A part of XRD pattern referring to sintered HAp

The decomposition of HAp to CaO takes place according to the following reaction.

$$Ca_{10}(PO_4)_6(OH)_2 \rightarrow 3Ca_3(PO_4)_2 + CaO + H_2O \qquad (1)$$

The presence of CaO in the sintered sample was examined within the appropriate region of XRD pattern (Figure 12.18). Similar to the other decomposition phases investigated above, there was no diffracted peak indicating the presence of CaO in the specified XRD range.

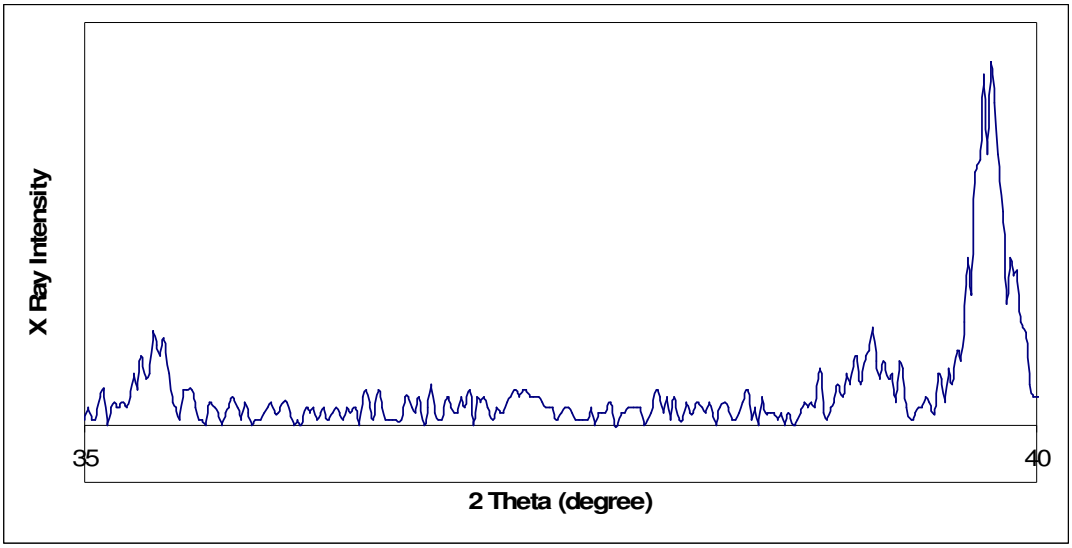

Figure 12.18 A part of XRD pattern referring to sintered HAp

Based on the XRD measurements it can be concluded that sintering process employed to the specimen implants caused no HAp decomposition. Since there were no other phases other than HAp, Ca/P ratio was preserved after sintering.

12.4.2 FTIR Spectrum Analysis

After grinding sintered samples, the infrared spectrum of the resulting powder and the commercial HAp powder (Alfa Aesar) were taken and compared. Figure 12.19 and Figure 12.20 are characterizing the IR spectra of commercial powder and the sintered sample respectively. In Figure 12.19, the absorption peaks observed at 631, 3427 and 3568 cm^{-1} corresponding to OH^- ion of the apatite. The absorption bands observed around 565, 604, 962, 1034, 1093 cm^{-1} result from PO_4^{3-} ion in the composition. The peak around 1637 cm^{-1} is due to the presence of H_2O in the sample [71,72]. As seen in Figure 12.20, the sintered sample showed the absorption peaks observed at around 633, 3446 and 3566 cm^{-1} corresponding to the presence of OH^- ion and the peaks at around 571, 602, 1047 ve 1089 cm^{-1} result from PO_4^{3-} ion. The FT-IR of the sintered HAp powder revealed only reflections corresponding to characteristic bands of HAp. The presence of vibrations due to other impurity phases

like $CaCO_3$, CaO was not detected. Besides, based on the FT-IR spectra of sintered samples no trace of naphthalene presence was observed. The drop observed at about 3446 cm^{-1} result from gradual loss of OH^- ion in the composition. This fact is known as dehydroxylation and result in the formation of oxyapatite (OAp) or oxyhydroxyapatite (OHAp). These two phases are stable and do not undergo any reverse phase transformation [71].

The phenomena of the hydroxyapatite decomposition should be distinguished from the dehydroxylation process. When HAp is heated above 900 ºC, HAp tend to lose H_2O and the formation of oxyapatite occurs according to the following equation. [72]

$$2\ OH \rightarrow O + H_2O \uparrow \quad (1)$$

$$Ca_{10}(PO_4)_6(OH)_2 \rightarrow Ca_{10}(PO_4)_6O.\Delta + H2O \quad (2)$$

where Δ is a non-charged vacancy and the hydroxyl- ion-deficient product $Ca_{10}(PO_4)_6O$. Δ is known as oxyapatite [24]. Accordingly, one of the lattice sites which was originally occupied by two OH groups in a HA unit cell, is now occupied by an oxygen atom while leaving the other vacant. [71] Further heating may lead to HA decomposition to form tricalcium phosphate and tetracalcium phosphate through the following process:

$$Ca_{10}(PO_4)_6(OH)_2 \rightarrow 2Ca_3(PO_4)_2 + Ca_4P_2O_9 + H_2O \quad (3)$$

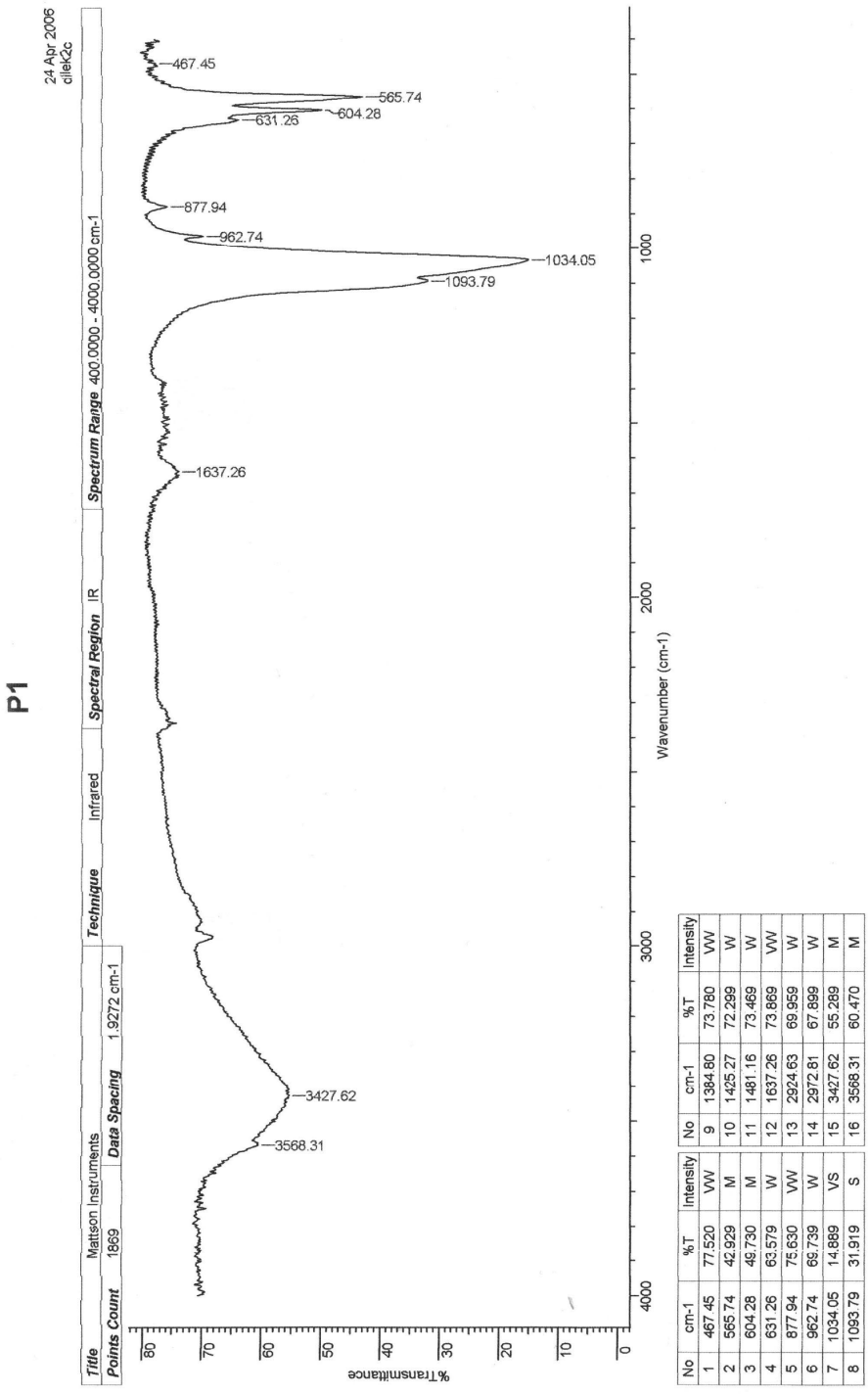

No	cm-1	%T	Intensity
1	467.45	77.520	VW
2	565.74	42.929	M
3	604.28	49.730	M
4	631.26	63.579	W
5	877.94	75.630	VW
6	962.74	66.739	W
7	1034.05	14.889	VS
8	1093.79	31.919	S

No	cm-1	%T	Intensity
9	1384.80	73.780	VW
10	1425.27	72.299	W
11	1481.16	73.469	W
12	1637.26	73.869	VW
13	2924.63	69.959	W
14	2972.81	67.899	W
15	3427.62	55.289	M
16	3568.31	60.470	M

Figure 12.19 Infrared Spectrum of commercial HAp powder before sintering

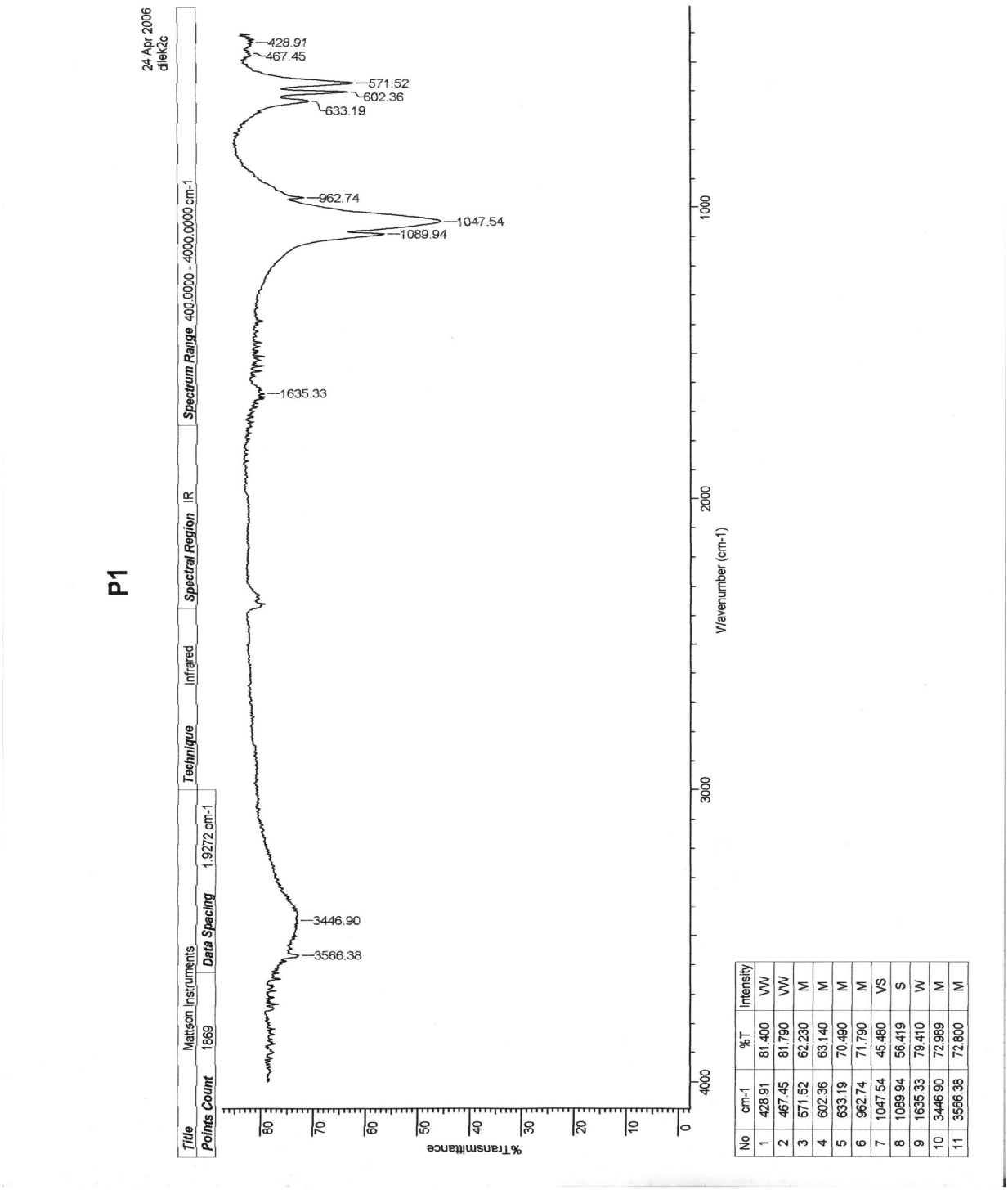

No	cm-1	%T	Intensity
1	428.91	81.400	VW
2	467.45	81.790	VW
3	571.52	62.230	M
4	602.36	63.140	M
5	633.19	70.490	M
6	962.74	71.790	M
7	1047.54	45.480	VS
8	1089.94	56.419	S
9	1635.33	79.410	W
10	3446.90	72.989	M
11	3566.38	72.800	M

Figure 12.20 Infrared Spectrum of HAp sample implant

12.4.3 ESEM Analysis

Pore morphology and pore size distribution of the sample implants formed by varying amounts of naphthalene addition were investigated by SEM analysis (Figure 12.21-12.28). Prior to SEM analysis, the samples were broken, ultrasonically cleaned in acetone and then the dried samples were sputter coated with gold. Afterwards the inner surfaces of sample implants were investigated by SEM.

The amount of porosity and pore size distribution as micro and macro pores, play a significant role in terms of the time required for the complete fibrovascular ingrowth. There is no specific macro pore size range, but pore sizes between 100μ-250μ were known to be adequate for rapid fibrovascularization [35,37]. However even having sufficient amount of micropores (5-15 μ) within the implant, might result in the complete fibrovascularization [49]. Brazilian HAp orbital implant is a good example when considered from that aspect. Brazilian HAp orbital implant has microporous architecture as well as randomly arranged channels. This structure was observed to be sufficient to allow the recipient blood vessels and fibrous tissues to grow into the implant [49]. However time required for fibrovascular ingrowth is more when compared to the other orbital implants used (Bio-Eye, FCI, M-Sphere) [53].

Another factor needed to be taken into consideration is the interconnectivity of pores within the implant structure. Similar to the pore size in the implant, interconnectivity of the pores affects the time required for fibrovascular ingrowth as well. Therefore, in order to lessen the time needed for the implant to be accepted as a living portion of body and the healing process, it is significant to have interconnected pore architecture.

%30 naphthalene added specimen was observed to be solid and having insufficient amount of micro and macropores distributed in the structure. As the rate of naphthalene increased as %40, %45, %60, the amount and the intensity of micro and macropores augmented as expected. The macropores were observed particularly on the specimens supplemented with % 45 and %60 naphthalene. The size of

macropores was in the range of 100µ-500µ. There were both spherically and lamellarly shaped pores within the SEM images obtained from sample implants; however the majority of macropores observed in the structure were lamellarly shaped. Except a few closed pores, the majority of the pores, in particular on the specimens supplemented with %45 and %60, were interconnected.

As far as the interconnectivity and pore size distribution as micro and macropores concerned, the best results were achieved from %45 and %60 naphthalene added specimens. However %60 naphthalene added specimen was mechanically insufficient and deformed during sintering process.

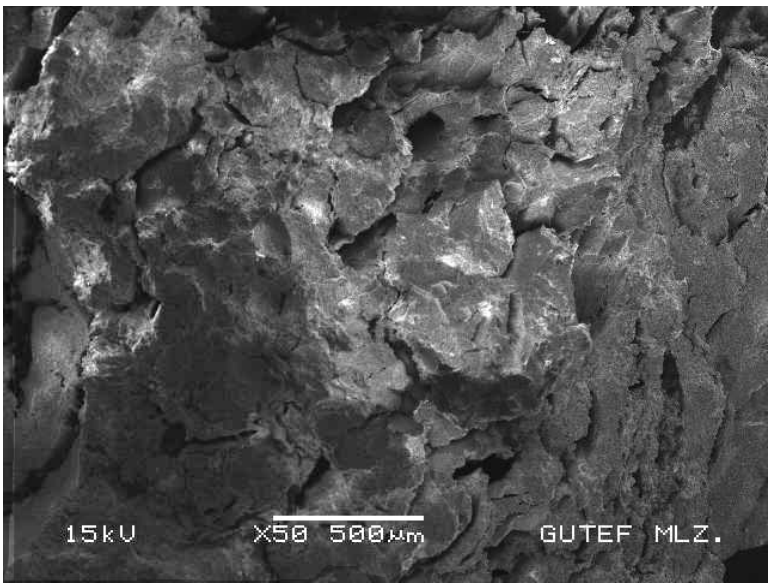

Figure 12.21 Scanning electron micrograph of %30 naphthalene added specimen implant (secondary electron mode with magnification ×50)

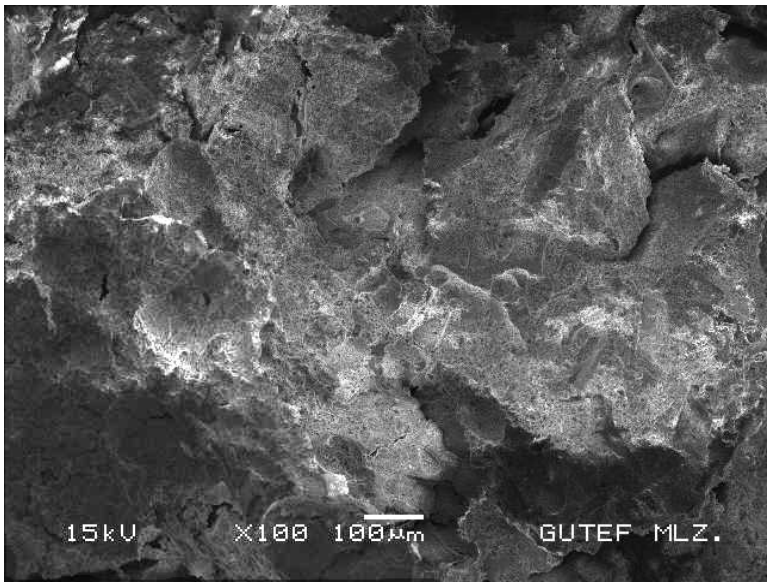

Figure 12.22 Scanning electron micrograph of %30 naphthalene added specimen implant (secondary electron mode with magnification ×100)

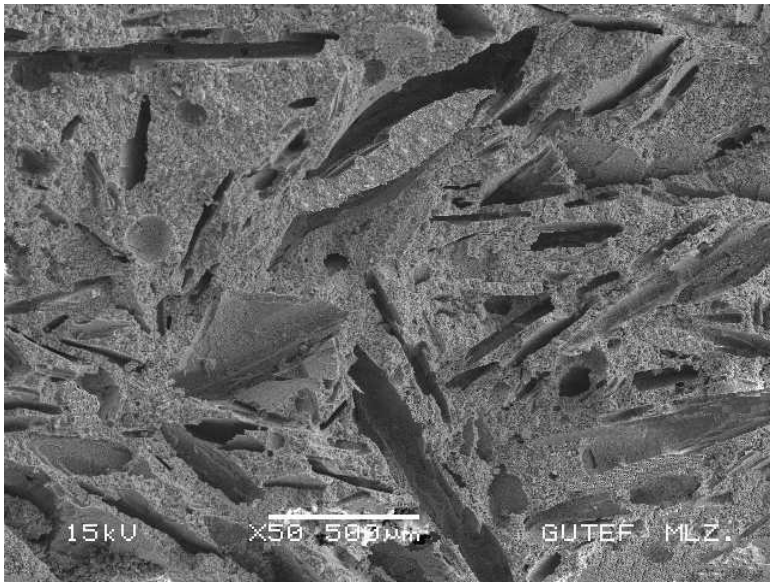

Figure 12.23 Scanning electron micrograph of %40 naphthalene added specimen implant (secondary electron mode with magnification ×50)

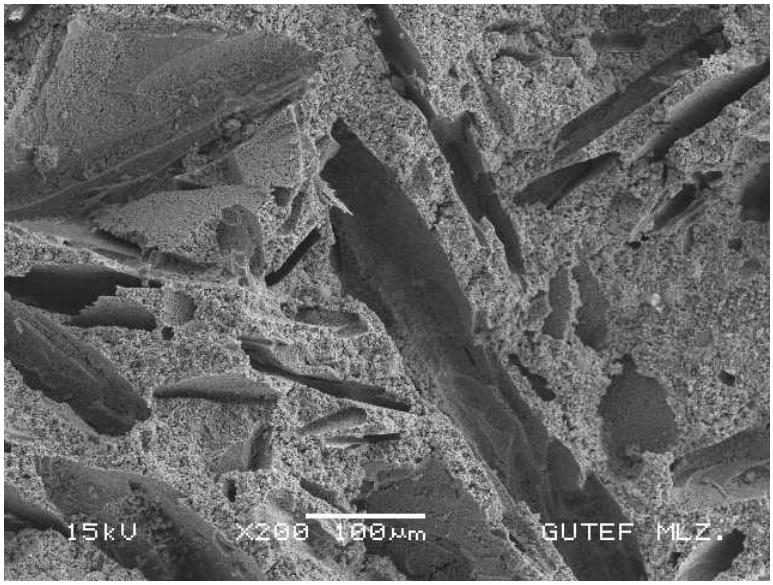

Figure 12.24 Scanning electron micrograph of %40 naphthalene added specimen implant (secondary electron mode with magnification ×200)

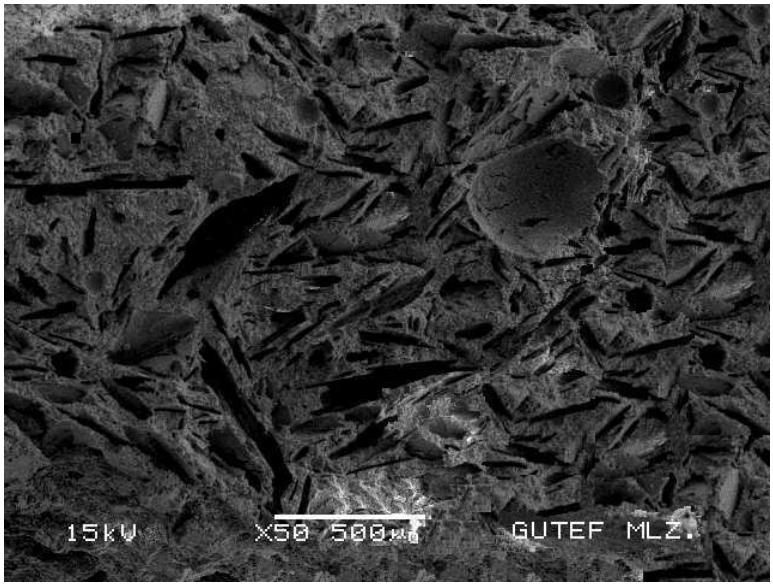

Figure 12.25 Scanning electron micrograph of %45 naphthalene added specimen implant (secondary electron mode with magnification ×50)

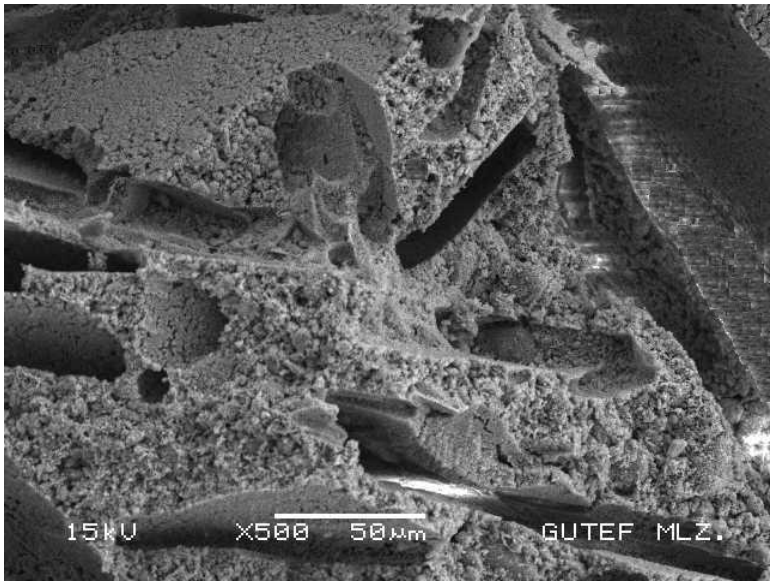

Figure 12.26 Scanning electron micrograph of %45 naphthalene added specimen implant (secondary electron mode with magnification ×500)

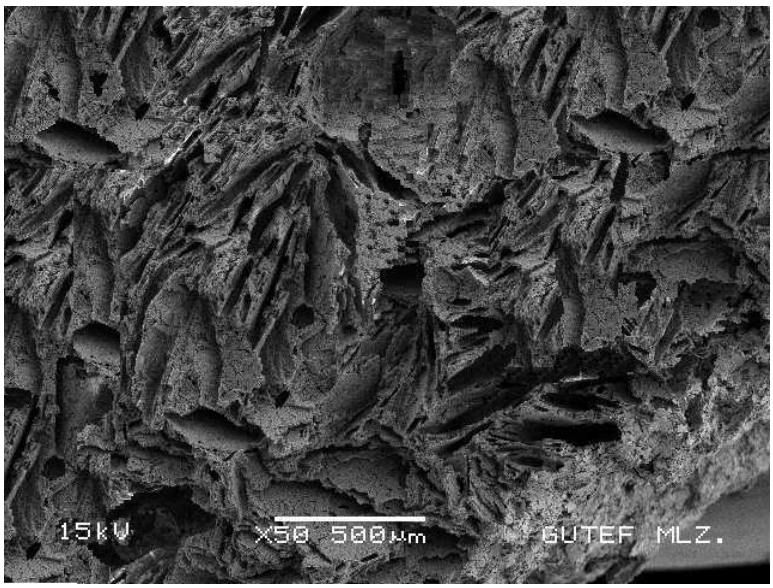

Figure 12.27 Scanning electron micrograph of %60 naphthalene added specimen implant (secondary electron mode with magnification ×50)

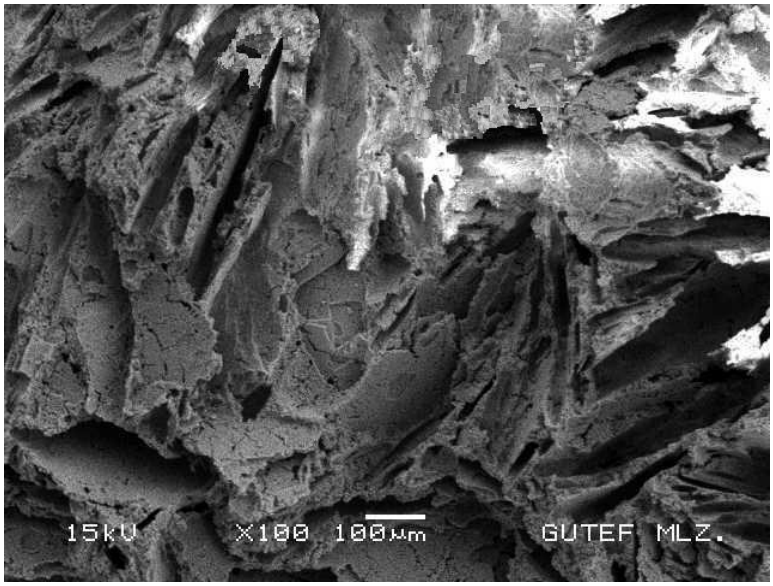

Figure 12.28 Scanning electron micrograph of %60 naphthalene added specimen implant (secondary electron mode with magnification ×100)

13. CONCLUSIONS

In this thesis project, a novel and simple process was employed so as to fabricate porous orbital implants from hydroxyapatite. In order to control the amount of porosity and pore size of the implants, varying amounts of naphthalene as %30, %40, %45 and %60 were added and sintered. After sintering, %60 naphthalene added specimen implant could not achieve sufficient strength and deformed. The other three sample implants were sintered without any defect.

Characterization of the sample implants with respect to phase purity and chemical composition were performed by X- Ray diffraction (XRD) and Infra-red spectrometer (IR) so as to compare this characteristic of the final product to that of starting material. Based on the XRD analysis, no signs of HAp decomposition were detected after sintering, that is to say phase purity of HAp was preserved. The FTIR analysis of the sintered sample was in agreement with XRD result which revealed that characteristic peaks corresponding to PO_4^{-3} and OH^- ions were conserved. The presence of vibrations due to other impurity phases like calcium carbonate, calcium oxide was not detected. Besides, based on the FT-IR spectra of sintered sample no trace of naphthalene presence was observed. However due to long sintering period and high temperature (>900 ºC) gradual loss of OH^- ions was detected in the FTIR spectrum of sintered sample.

Physical properties like bulk density, weight, amount of porosity and contraction rate of the specimen implants were examined. As expected, the weight and the bulk density of the samples were decreased with increasing rate of naphthalene. On the contrary, the contraction rate and the amount of porosity were increased with increasing rate of naphthalene. Moreover increasing the amount of naphthalene added, led to mechanically weak and more fragile structure. As a result, compressive strength of the specimens tested was decreased with regard to the amount of naphthalene added. Although axial compression as tested in this study is not a force that orbital implants are subjected to in real life, we used axial

compression testing as a measure of implant structural integrity. Considering the data obtained by compressive strength tests it could be concluded that the %45-%50 naphthalene addition may provide sufficient mechanical strength which could be required to be able to preserve their structural integrity in the body and to evaluate the ability of these implants to hold a motility peg.

Pore morphology and pore size distribution of the sample implants formed by varying amounts of naphthalene addition were investigated by SEM analysis. %30 naphthalene added sample implant was appeared to be more solid. As the amount of naphthalene supplement was increased as %40, %45 and %60, the amount and intensity of micro and macropores enhanced as expected. There were both spherical and lamellar pores; however the majority of macropores were lamellar. The sizes of macropores were in the range of 100µ -500µ. Except a few closed pores, the majority of the pores, in particular on the specimens supplemented with %45 and %60, were interconnected. On the basis of results achieved, the amount and intensity of micro and macropores distributed within the implant specimen having %45 naphthalene, was found to be sufficient for fibrovascularization.

As far as the mechanical strength, weight, pore size distribution in terms of micro macropores and interconnectivity concerned, the best results were achieved from %45 naphthalene added specimen implant.

REFERENCES

1. Hench, L.L., and E.C. Ethridge. 1982. Biomaterials. An Interfacial Approach, Academic Press, New York, London

2. Williams, D.F. 1990. Biocompatibility: an overview, p.52. In D.F.Williams (ed.) Concise Encyclopedia of Medical & Dental Materials. Pergamon Press: Oxford etc.

3. G. Heness and B. Ben-Nissan Innovative Bioceramic Materials Forum Vol. 27 (2004) 104 – 114

4. Robert B. Heimann Materials Science of Crystalline Bioceramics: A Review of Basic Properties and Applications CMU. Journal (2002) Vol. 1(1)

5. Willmann, G. 1995. In G. Fishman, A. Clare and L. Hench (eds.) Bioceramics. Materials and application. Ceramic Transactions 48, The American Ceramic Soc.: Westerville, p. 83.

6. T. Yuhta, Y.Kikuta, Y.Mitamura, K.Nakagane, S.Murabayashi, I.Nishimura, Journal of Biomedical Materials Research, 28(2), 217-224 (1994

7. T. V. Thamaraiselvi and S. Rajeswari Biological Evaluation of Bioceramic Materials - A Review Trends Biomater. Artif. Organs, Vol 18 (1), pp 9-17 (2004)

8. A. Marti Dr Robert Mathys Foundation, Bischmattstr. 12, CH-2544 Bettlach Inert bioceramics (Al2O3 ZrO2) for medical application Injury, Int. J. Care Injured 31 (2000) S-D33-36

9. V .A.Dubok, Powder Metallurgy and Metal Ceramics, 39(7-8), 381-394 (2000).

10. Biological Evaluation of Bioceramic Materials - A Review Trends Biomater. Artif. Organs, Vol 18 (1), pp 9-17 (2004)

11. S.Kannan, A.Balamurugan, S.Rajeswari, M.Subbaiyan, Corrosion Reviews, Vol 16 (1), pp 20-52 (2002)

12. Hench, L.L., Molecular Design of Bioactive Glasses and Ceramics for Implants. In Ceramics: Towards the 21st Century, eds. W. Soga and A. Kato, (Ceram. Soc. of Japan, 1991) pp. 519-34.

13. Park J. B. and R. S. Lakes, Biomaterials: An Introduction, Plenum Pres, New York, 1992

14. H.Yuan, J.D.De Bruijin, X.Zhang, C.A. Van Blitterswijk, K.Degroot, Journal of Biomedical Materials Research, 58(3), 270-276 (2001).

15. Hulbert SF, Bokros JC, Hench LL, Wilson J, Heimke G. Ceramics in clinical investigations: Past, present, and future. High Tech Ceramics. Amsterdam: Elsevier, 1987:189-213.

16. H.Y. Yasuda, S. Mahara, Y. Umakoshi, S. Imazato, S. Ebisu Microstructure and mechanical property of synthesized hydroxyapatite prepared by colloidal process Biomaterials 21 (2000) 2045}2049

17. E. Damien, P.A. Revell Coralline hydroxyapatite bone graft substitute: A review of experimental studies and biomedical applications Journal of Applied Biomaterials & Biomechanics 2004; 2: 65-73

18. L. Le Guehennec, P. Layrolle and G. Daculsi A Review of Boceramics and Fibrin Sealent European Cells and Materials Volume 8. (pages 1-11)

19. T.M. Sridhar, U. Kamachi Mudali, M. Subbaiyan Sintering atmosphere and temperature effects on hydroxyapatite coated type 316L stainless steel Corrosion Science 45 (2003) 2337–2359

20. Nasser Y. Mostafa Characterization, thermal stability and sintering of Hydroxyapatite powders prepared by different routes Materials Chemistry and Physics 94 (2005) 333–341

21. Anna Slosarczyk, Jan Piekarczyk Ceramic materials on the basis of hydroxyapatite and tricalcium phosphate Ceramics International 25 (1999) 561±565

22. S. Raynaud, E. Champion, D. Bernache-Assollant Calcium phosphate apatites with variable Ca/P atomic ratio II. Calcination and sintering Biomaterials 23 (2002) 1073–1080

23. D. Bernache-Assollanta, A. Ababoua, E. Championa, M. Heughebaertb Sintering of calcium phosphate hydroxyapatite Ca10(PO4)6(OH)2 I. Calcination and particle growth Journal of the European Ceramic Society 23 (2003) 229–241

24. Gökbayrak, H., "Production of Hydroxyapatite Ceramics," MS Thesis, Boğaziçi University, 1996.

25. Gören, Ş., "Optimization of the Production Conditions of Hyroxylapatite from Animal Bone" MS. Thesis, Boğaziçi University, 2004

26. Oktar, F., N., Characterization of Processed Tooth Hydroxyapatite and Bioglass for Potential Applications in Dentistry, MS. Thesis, Boğaziçi University

27. S. Madhavi_, C. Ferraris, T.J. White Synthesis and crystallization of macroporous Hydroxyapatite Journal of Solid State Chemistry 178 (2005) 2838–2845

28. Nasser Y. Mostafa Characterization, thermal stability and sintering of Hydroxyapatite powders prepared by different routes Materials Chemistry and Physics 94 (2005) 333–341

29. A. Afshar , M. Ghorbani , N. Ehsani , M.R. Saeri,C.C. Sorrell Some important factors in the wet precipitation process of Hydroxyapatite Materials and Design 24 (2003) 197–202

30. Shekhar Nath, Bikramjit Basu, Arvind Sinha A Comparative Study of Conventional Sintering with Microwave Sintering of Hydroxyapatite Synthesized by Chemical Route Trends Biomater Artif organs, Vol 19(2), pp 93-98 (2006)

31. Sang-Hoon Rhee Synthesis of hydroxyapatite via mechanochemical treatment Biomaterials 23 (2002) 1147–1152

32. J. Gua, M. Menga, A. Cookb, M.G. Faulkner c A study on natural movement of artificial eye implant Robotics and Autonomous Systems 32 (2000) 153–161

33. E.R. Kandel, J.H. Schwartz, T.M. Jessell, Essentials of Neural Science and Behavior, Appleton & Lange, Norwalk, CT, 1997, pp. 660–677.

34. Grant W. Su, and Michael T. Yen, Current Trends in Managing the Anophthalmic Socket After Primary Enucleation and Evisceration Ophthalmic Plastic and Reconstructive Surgery Vol. 20, No. 4, pp 274–280

35. Darius M. Moshfeghi, Andrew A. Moshfeghi, and Paul T. Finger, Enucleation Survey of Opthalmology Volume 44 Number 4 January–February 2000

36. Philip L. Custer, Enucleation: Past, Present, and Future Ophthalmic Plastic and Reconstructive Surgery Vol. 16, No. 5, pp 316–321

37. Hornblass A, Biesman BS, Eviatar JA: Current techniques of enucleation: a survey of 5,439 intraorbital implants and a review of the literature. Ophthalmic Plast Reconstr Surg 11: 77–86; discussion 87–8, 1995

38. Perry AC. Integrated orbital implants. Adv Ophthal PlastReconstr Surg 1990;8:75–81.

39. Marcelo Coelho Goiato, Daniela Nardi Mancuso, Maria Lucia Mar¸ al Mazza Sundefeld, Marcelo Basilio Da Motta Gabriel, Ana Cristina Murakawa, Aime´e Maria Guiotti, Aesthetic and functional ocular rehabilitation Oral Oncology Extra (2005) 41, 162–164

40. Philip L. Custer, Robert H. Kennedy, John J. Woog, Sara A. Kaltreider, Dale R. Meyer, Orbital Implants in Enucleation Surgery Ophthalmology 2003;110:2054–2061, 2003

41. Silvana Artioli Schellini, Mariangela E.A. Marques, Carlos Roberto Padovani, Eulazio M. Taga, Comparison of Synthetic Hydroxyapatite and Porous Polyethylene Implants in Eviscerated Rabbit Eyes Ophthalmic Plastic and Reconstructive Surgery Vol. 19, No. 2, pp 136–139

42. Perry AC, Hydroxyapatite; the vascularizing integrated orbital implant, in Stephenson CM (ed): Ophthalmic, Plastic, Reconstructive, and Orbital Surgery. Boston, Butterworth-Heinemann, 1997, pp 463–79

43. Sang Woo Park, Hae Young Seol, Suk Joo Hong, Kyeong Ah Kim, Jeong Chul Choi, In Ho Cha, Magnetic resonance evaluation of fibrovascular ingrowth Journal of Clinical Imaging 27 (2003) 377– 381

44. David R. Jordan, Steven Gilberg, and Ahmed Bawazeer, Coralline Hydroxyapatite Orbital Implant (Bio-Eye): Experiencewith 158 Patients Ophthalmic Plastic and Reconstructive Surgery Vol. 20, No. 1, pp 69–74

45. Julian D. Perry, Robert Alan Goldberg, John D. McCann, Norman Shorr, Robert Engstrom, and John Tong Bovine Hydroxyapatite Orbital Implant Ophthalmic Plastic and Reconstructive Surgery Vol. 18, No. 4, pp 268–274

46. David R. Jordan, Ivan Hwang, Seymour Brownstein, Todd McEachren, Steve Gilberg, Steve Grahovac, and Louise Mawn, The Molteno M-Sphere Ophthalmic Plastic and Reconstructive Surgery Vol. 16, No. 5, pp 356–362

47. Jordan DR, Gilberg S, Mawn L, et al. The synthetic Hydroxyapatite implant: a report of 65 patients. Ophthal Plast Reconstr Surg 1998;14:4:250–5.

48. Shields CL, Shields JA, Potter P. Hydroxyapatite orbital implant after enucleation. Arch Ophthamol 1992;110:333–8

49. David R. Jordan, Ivan Hwang, Todd McEachren, Seymour Brownstein, Steve Gilberg, Steve Grahovac and Louise Mawn, Brazilian Hydroxyapatite Implant Ophthalmic Plastic and Reconstructive Surgery Vol. 16, No. 5, pp 363–369

50. Sean M. Blaydon, Todd R. Shepler, Russell W. Neuhaus, William L. White, and John W. Shore, The Porous Polyethylene (Medpor) Spherical Orbital Implant Ophthalmic Plastic and Reconstructive Surgery Vol. 19, No. 5, pp 364–371

51. Karesh JW, Dresner SC. High-density porous polyethylene (Medpor) as a successful anophthalmic socket implant. Ophthalmology 1994;101:1688–95.

52. David R. Jordan, Louise A. Mawn, Seymour Brownstein, Todd M. McEachren, Steven M. Gilberg, Vivian Hill, Steve Z. Grahovac, and J.-P. Adenis, The Bioceramic Orbital Implant: A New Generation of Porous Implants Ophthalmic Plastic and Reconstructive Surgery Vol. 16, No. 5, pp 347–355

53. Rubin PAD, Popham JK, Bilyk JR, Shore JW. Comparison of fibrovascular ingrowth into hydroxyapatite and porous polyethylene orbital implants. Ophthal Plast Reconstr Surg 1994;10:96–103.

54. Sang Woo Park, Hae Young Seol, Suk Joo Hong, Kyeong Ah Kim, Jeong Chul Choi, In Ho Cha Magnetic resonance evaluation of fibrovascular ingrowth into porous orbital implants Journal of Clinical Imaging 27 (2003) 377– 381

55. Jamell GA, Hollsten DA, Hawes MJ, Griffin DJ, Klingensmith WC, White WL, Spirnak J. Magnetic resonance imaging versus bone scan for assessment of vascularization of the hydroxyapatite orbital implant. Ophthalmic Plast Reconstr Surg 1996;12:127–30.

56. D. Julian de Silva,and Jane M. Olver, F.R.C.Ophth Hydroxypropyl Methylcellulose (HPMC) Lubricant Facilitates Insertion of Porous Spherical Orbital Implants Ophthalmic Plastic and Reconstructive Surgery Vol. 21, No. 4, pp 301–322

57. Jordan DR, Klapper SR. Wrapping hydroxyapatite implants. Ophthalmic Surg Lasers 1999;30:403–7.

58. Stephen R. Klapper, David R. Jordan, Karim Punja, Seymour Brownstein, Steven M. Gilberg, Louise A. Mawn, and Steven Z. Grahovac, Hydroxyapatite Implant Wrapping Materials: Analysis of Fibrovascular Ingrowth in an Animal Model Ophthalmic Plastic and Reconstructive Surgery Vol. 16, No. 4, pp 278–285

59. Jordan DR, Allen L, Ells A, et al. The use of Vicryl mesh (polyglactin 910) for implantation of hydroxyapatite orbital implants. Ophthal Plast Reconstr Surg 1995; 11:95–9.

60. M Gupta, P Puri and I G Rennie Use of bovine pericardium as a wrapping material for hydroxyapatite orbital implants Br. J. Ophthalmol. 2002;86;288-289

61. John A. Long, Thomas M. Tann , William H. Bearden and Michael A. Callahan, Enucleation: Is Wrapping the Implant Necessary for Optimal Motility? Ophthalmic Plastic and Reconstructive Surgery Vol. 19, No. 3, pp 194–197

62. David R. Jordan, and Stephen R. Klapper, A New Titanium Peg System for Hydroxyapatite Orbital Implants Ophthalmic Plastic and Reconstructive Surgery Vol. 16, No. 5, pp 380–387

63. Cook SD, Thomas KA, Kay JF, Jarcho M. Hydroxyapatite– coated porous titanium for use as an orthopedic biologic attachment system. Clin Orthop 1988;230:303– 12.

64. Cook SD, Dalton JE. Biocompatibility and biofunctionality of implanted materials. Alpha Omegan 1992;85:41–7.

65. Remulla HD, Rubin PA, Shore JW, et al. Complications of porous spherical orbital implants. Ophthalmology 1995;102:586–93.

66. Shields CL, Shields JA, De Potter P, et al. Problems with the hydroxyapatite orbital implant: experience with 250 consecutive cases. Br J Ophthalmol 1994;78: 702–6.

67. Buettner H, Bartley GB. Tissue breakdown and exposure associated with orbital hydroxyapatite implants. Am J Ophthalmol 1992; 113:669–73.

68. David R. Jordan, Stanley Chan,Louise Mawn,Steven Gilberg, Tom Dean, Seymour Brownstein, Vivian E. Hill, Complications Associated with Pegging Hydroxyapatite Orbital Implants Ophthalmology 1999;106:505–512

69. C-J Lin, S-L Liao, J-R Jou, S C S Kao, P-K Hou and M-S Chen Complications of motility peg placement for porous hydroxyapatite orbital implants Br. J. Ophthalmol. 2002;86;394-396

70. Gultekin Goller, Faik Nuzhet Oktar Sintering effects on mechanical properties of biologically derived dentine hydroxyapatite Materials Letters 56 (2002) 142–147

71. G. Muralithran, S. Ramesh The effects of sintering temperature on the properties of hydroxyapatite Ceramics International 26 (2000) 221±230

72. A. Rapacz-Kmita, C. Paluszkiewicz, A. Slosarczyk, Z. Paszkiewicz, FTIR and XRD investigations on the thermal stability of Hydroxyapatite during hot pressing and pressureless sintering processes.

73. David R. Jordan, Nina Ahuja, Steven Gilberg and Real Bouchard Behavior of Various Orbital Implants Under Axial Compression Ophthalmic Plastic and Reconstructive Surgery Vol. 21, No. 3, pp 225–229

APPENDIX A

MATERIALS BIOCOMPATIBILITY MATRIX

Device Categories			Biological Effect												
Body Contact		Contact Duration **A - Limited** (≤ 24 hours) **B - Prolonged** (24 hours-30 days) **C - Permanent** (> 30 days)	Initial Evaluation Tests								Supplementary Evaluation Tests			
			Cytotoxicity	Sensitization	Irritation/Intracutaneous Reactivity	Systemic Toxicity (acute)	Subchronic Toxicity	Genotoxicity	Implantation	Hemocompatibility	Chronic Toxicity	Carcinogenicity	Reproductive/Developmental[3]	Biodegradation[3]
Surface Devices	Skin	A	X	X	X									
		B	X	X	X									
		C	X	X	X									
	Mucosal Membrane	A	X	X	X									
		B	X	X	X	F	F		F					
		C	X	X	X	F	X	X	F		F			
	Breached or Compromised Surface	A	X	X	X	F								
		B	X	X	X	F	F		F					
		C	X	X	X	F	X	X	F		F			
External Communicating Devices	Blood Path, indirect	A	X	X	X	X				X				
		B	X	X	X	X	F			X				
		C	X	X	F	X	X	X	F	X	X	X		
	Tissue/Bone/Dentin Communicating[1]	A	X	X	X	F								
		B	X	X	F	F	F	X	X					
		C	X	X	F	F	F	X	X		F	X		
	Circulating Blood	A	X	X	X	X		F[2]		X				
		B	X	X	X	X	F	X	F	X				
		C	X	X	X	X	X	X	F	X	X	X		
Implant Devices	Tissue/Bone	A	X	X	X	F								
		B	X	X	F	F	F	X	X					
		C	X	X	F	F	F	X	X		X	X		
	Blood	A	X	X	X	X			X	X				
		B	X	X	X	X	F	X	X	X				
		C	X	X	X	X	X	X	X	X	X	X		

X = ISO Evaluation Tests for Consideration

F = Additional Tests which may be required by FDA

Note [1] Tissue includes tissue fluids and subcutaneous spaces

Note [2] For all devices used in extracorporeal circuits

Note [3] Depends on specific nature of the device and its component materials